BREAKWATERS UNDER CONSTRUCTION EXPOSED TO OBLIQUE WAVES

MSc-Thesis

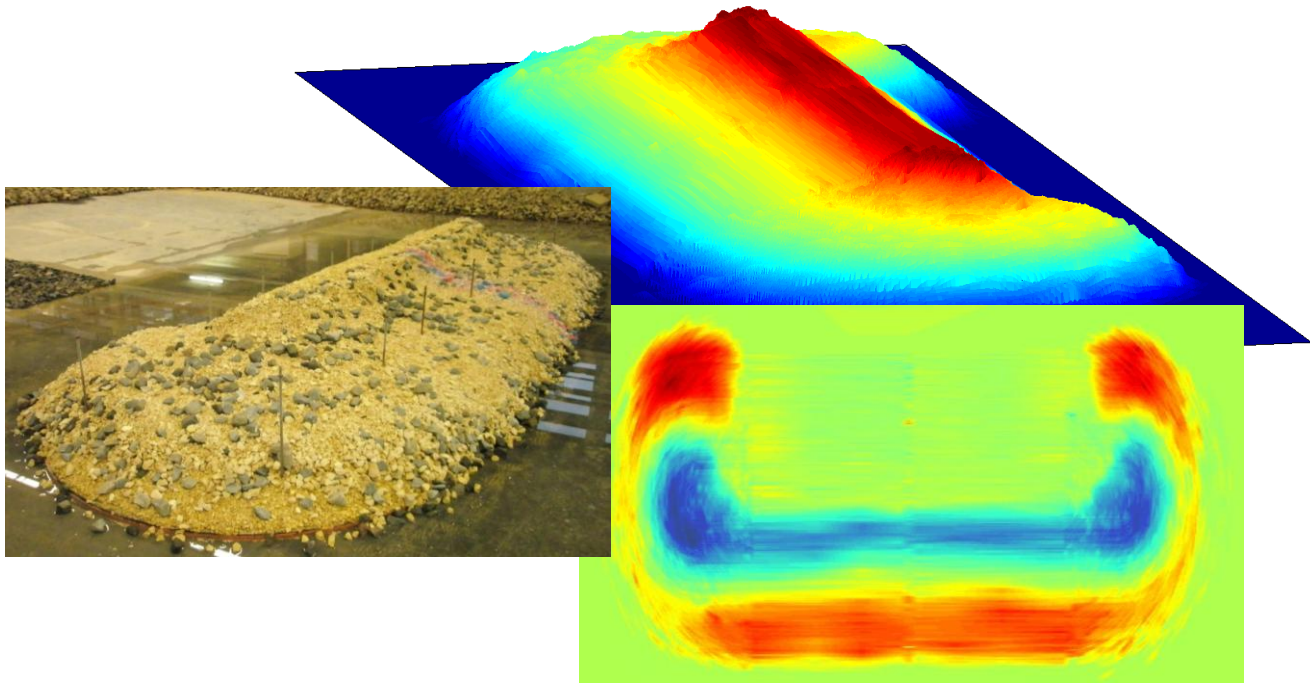

TU Delft

Van Oord

Patrick Mulders
C1153412
Faculty of Civil Engineering and Geosciences

MSc-Thesis
Delft, June 2010

BREAKWATERS UNDER CONSTRUCTION EXPOSED TO OBLIQUE WAVES

MSc-Thesis

Institute
Delft University of Technology
Faculty of Civil Engineering and Geosciences
Department of Hydraulic Engineering

Master thesis author
P.H.M. Mulders
Student number: 1153412
Email: phmmulders@hotmail.com

Graduation committee

Prof.dr.ir. M.J.F. Stive	Hydraulic Engineering, TU Delft
Ir. H.J. Verhagen	Hydraulic Engineering, TU Delft
Prof.dr.ir. W.S.J. Uijttewaal	Environmental Fluid Mechanics, TU Delft
Ir. G.M. Smith	Engineering Department, Van Oord

Patrick Mulders
C1153412
Faculty of Civil Engineering and Geosciences

MSc-Thesis
Delft, June 2010

Preface

When I was a little boy I experienced the floodings of the river Meuse in 1993 and 1995. This and the development of the 'Grensmaas-project' afterwards nourished my fascination of hydraulic engineering. Over the years my fascination grew stronger and eventually led to my study in Civil Engineering at Delft University of Technology. Now, roughly fifteen years after the last flooding, my master thesis in the field of Hydraulic Engineering is completed.

This report contains the MSc-Thesis "Breakwaters under construction exposed to oblique waves". It is part of the curriculum of the MSc study Hydraulic Engineering at the Faculty of Civil Engineering and Geosciences at Delft University of Technology.

First of all I would like to thank my graduation committee for their supervision and dedication. I am grateful for the daily supervision and guidance given by Henk Jan Verhagen, and for the insights and remarks of Professor Marcel Stive. The study was performed in collaboration with the engineering department of Van Oord. Here I was supervised by Greg Smith who was a big inspiration for me during the development of the research. The experiments itself were conducted in the Laboratory of Fluid Mechanics at Delft University of Technology. For allowing me to use the basin and for his sincere interest throughout the research I would like to thank Professor Wim Uijttewaal.

However, without any help of the staff of the laboratory I would not have been able to execute the tests. Therefore special thanks to Arie for his ingenuity and for making the practical designs of the model and measuring frame; Sander for his help with the measuring equipment and wave generators and last but not least Jaap for his help in building the model. Also special thanks to Ruben and Ben of the workshop for building the ground plates with reinforcement, the hoisting frames and measuring frame; and BASF for supplying me with Elastocoast.

Last but not least I would like to thank all others who contributed to my thesis and supported me during the sometimes hard times.

Patrick Mulders

Abstract

During the construction of breakwaters contractors often encounter undesired reshaping of exposed core material. This reshaping is comparable to the deformation process of berm breakwaters in which the outer profile reshapes into a more stable s-curve. In the case of oblique waves this deformation is enhanced by a longshore transport of stones leading to even more loss of material and damage.

Throughout the years few formulas were derived for both processes which describe the behaviour of berm breakwaters as well as gravel beaches reasonably well. These formulas however turned out to be inadequate when it comes to describing the behaviour of core material. In particular the influence of the wide grading of quarry run, commonly used as core material, is to a large extent unknown and generally not described in the available relations.

To investigate this influence of the stone grading on both the two-dimensional deformation and longshore transport new physical model tests were carried out in the wave basin at Delft University of Technology. In total 12 tests were executed in which two different gradings $\left(f_g = 1.3;\ 6 \right)$, three different angles of wave attack $\left(\psi = 0^\circ, 30^\circ, 45^\circ \right)$ and two different wave spectra $\left(H_{m0} = 0.08m;\ 0.10m \right)$ were tested.

Data collected from the tests included wave and profile measurements together with the displacements of stones, originating from two colour beams which were applied in the middle of the trunk. These data along with visual observations eventually led to a conceptual model describing stone movements in both transverse and longshore direction. Using Matlab three-dimensional profile and erosion models were generated from which the different profile parameters were determined. With respect to the distance from origin, for each test an exponential relation was derived to describe the stone displacements. After determination of the area of uniform transport these exponential relations were used to calculate the total longshore transport by means of extrapolation and multiple integrations.

Subsequently all parameters found were compared to the formulas currently available for both processes. Regarding the deformation parameters the test results produced the best fit with the formulas derived in [MERLI 2009]. Still on several occasions a deviant relation was found concerning the influence of wave obliquity. In addition, the formulas became less accurate for the narrow grading used in the tests, which fell outside the range tested by Merli. However, for the crest height of the deformed profile test results deviated completely from the available formula as no influence was found whatsoever for all tested parameters. Here the deviation was contributed to a higher instability of the part above the initial deformation, partly due to the steepness of the slope.

On the subject of the longshore transport clear trends were found describing the influence of the varying parameters. Both a higher wave load and wider grading lead to an increase of the longshore transport. For the wider grading, however, this increase gave a rather distorted image, as not all fractions in the mixture were transported evenly. Due to segregation the coarsest fractions were mostly transported in the transverse direction while the finer fractions were transported further away in the longitudinal direction. Alternatively, computation of the longshore volume transport proved to be more representative. Regarding the effect of wave obliquity an increase in angle of wave attack of 30° to 45° was accompanied by a decrease in longshore transport; though this decrease was less than already available formulas indicated. However despite the fact that it describes a completely different trend concerning this particular influence, the best fit was found after multiplying the relation derived by [ALIKHANI 1996] with a factor 100.

Keywords:

Grading
Breakwater
Wave obliquity
Core
Physical model test
Reshaping
Two-dimensional deformation
Longshore transport
Stone displacement

List of Symbols and abbreviations

A_o	Observed area in mobility formulas	$[m^2]$
B	Crest width	$[m]$
BLc	Blockiness defined as the volume of a stone divided by the Volume of the enclosing XYZ orthogonal box with a minimum volume.	$[\%]$
B_o	Observed width in mobility formulas	$[m]$
c	Wave celerity	$[m/s]$
c_g	Wave group celerity	$[m/s]$
c_{kb}	Characteristic wave celerity	$[m/s]$
c_{0p}	Wave celerity based on T_p in deep water	$[m/s]$
C_D	Drag coefficient	$[-]$
C_k	Ratio H_k/H_s , 1.55 in deep water when Rayleigh distributed	$[-]$
C_L	Lift coefficient	$[-]$
C_N	Coefficient for normal wave force	$[-]$
C_P	Coefficient for parallel wave force	$[-]$
D	Sieve diameter	$[m]$
D_n	Nominal diameter $\left(\frac{W}{\rho_s}\right)^{\frac{1}{3}}$	$[m]$
D_{n15}	Nominal diameter of the 15% value of the sieve curve	$[m]$
D_{n50}	Median nominal diameter	$[m]$
D_{n85}	Nominal diameter of the 85% value of the sieve curve	$[m]$
D_s^{**}	Dimensionless mean displacement length	$[-]$
E	Energy of the wave spectrum	$[N/m]$
$E_{JONSWAP}(f)$	Unidirectional variance density spectrum	$[m^2 s]$
f	Frequency	$[Hz]$
f_g	Stone grading $\left(\frac{D_{n85}}{D_{n15}}\right)$	$[-]$
f_p	Peak frequency	$[Hz]$
F_l	Fetch length	$[m]$
F_N	Force normal to the outer slope	$[N]$
F_P	Force parallel with the outer slope	$[N]$
Fr	Froude's law $\left(\frac{U}{\sqrt{gl}}\right)$	$[-]$
g	Gravitational acceleration	$[m/s^2]$
$G(\theta \mid f)$	Wave directional spreading function	$[1/rad]$
h	Water depth	$[m]$
h_c	Crest height in Van der Meer formulas	$[m]$
h_s	Step height in Van der Meer formulas	$[m]$
h_t	Transition height in Van der Meer formulas	$[m]$
H	Wave height	$[m]$
H_i	Significant wave height of the incident wave spectrum	$[m]$
H_k	Characteristic wave height $(H_{1/50})$	$[m]$

H_{kb}	Characteristic breaking wave height	$[m]$
H_{m_0}	Significant wave height calculated spectrally $\left(4\sqrt{m_0}\right)$	$[m]$
H_s	Significant wave height	$[m]$
H_r	Significant wave height of the reflected wave spectrum	$[m]$
H_0	Dimensionless wave height parameter $\left(\frac{H_s}{\Delta D_{n50}}\right)$	$[-]$
H_0T_0	Combined dimensionless wave height-wave period parameter	$[-]$
k	Wave number $\left(\frac{2\pi}{L}\right)$	$[m^{-1}]$
K_D	Coefficient in Hudson formula	$[-]$
l	Length	$[m]$
l_c	Crest length in Van der Meer formulas	$[m]$
l_d	Mean displacement length	$[m]$
l_s	Step length in Van der Meer formulas	$[m]$
l_r	Run-up length in Van der Meer formulas	$[m]$
L	Wave length	$[m]$
L_0	Wave length in deep water $\left(2\pi/gT^2\right)$	$[m]$
LT	Length to thickness ratio defined as maximum length divided by minimum distance between parallel lines through which the particle would just pass.	$[-]$
m_n	n-th order moment of the variance density spectrum $\left(\int_0^\infty f^n E(f)df\right)$	$[m^2]$
n	Porosity $\left(V_v/V_T\right)$	$[-]$
N	Number of waves	$[-]$
N_d	Number of stones displaced at least once during 1000 waves	$[-]$
N_{od}	Damage index in mobility formulas	$[-]$
N_s^{**}	Modified stability number in mobility formulas	$[-]$
P	Permeability coefficient in the Van der Meer formulas	$[-]$
P_R	Percentage rounded stones in armour material	[%]
r	Reduction factor to describe effect of shallow foreshore	$[-]$
R_c	Freeboard crest	$[m]$
Re	Reynolds number $\left(\frac{Ul}{\nu}\right)$	$[-]$
Rec	Recession length	$[m]$
s	Wave steepness $\left(H/L\right)$	$[-]$
s_m	Mean wave steepness based on T_m	$[-]$
s_{mo}	Mean wave steepness in deep water based on T_m	$[-]$
s_{mk}	Reference wave steepness (0.03)	$[-]$
s_{0p}	Wave steepness based on T_p and in deep water	$[-]$
s_{02}	Wave steepness based on T_{02}	$[-]$
S	Damage parameter in the Van der Meer formulas	$[-]$
S_s	Surface damage level in mobility formulas	$[-]$
S_N	Longshore volume transport	$[stones/wave]$
$S_V(x)$	Longshore volume transport	$[m^3/s]$

$S_V(y)$	Transverse volume transport	$[m^3/s]$
$S(f,\theta)$	Multidirectional wave spectrum	$[m^2 s/rad]$
T_m	Mean period defined as $T_{m01}=\frac{m_0}{m_1}$	$[s]$
T_p	Peak period	$[s]$
T_0	Dimensionless wave period parameter $\left(\sqrt{g/D_{n50}}T_m\right)$	$[-]$
T_{0p}	Dimensionless wave period parameter based on T_p	$[-]$
T_{02}	Mean period defined as $\sqrt{\frac{m_0}{m_2}}$	$[s]$
U	Velocity	$[m/s]$
U_{10}	Wind velocity at 10m elevation above sea surface	$[m/s]$
V_T	Total volume of sample	$[m^3]$
V_v	Volume of voids in sample	$[m^3]$
W_{15}	Weight of the 15% value of the sieve curve	$[kg]$
W_{50}	Median weight	$[kg]$
W_{85}	Weight of the 85% value of the sieve curve	$[kg]$
W'	Buoyant mass $\left((\rho_s-\rho_w)D_{n50}^3\right)$	$[kg]$
α	Angle of outer slope	$[\circ]$
α_f	Energy scale parameter in in formula for Jonswap spectrum	$[-]$
$\alpha_1,\alpha_2,\alpha_3$	Angles of different parts of outer slope in Van der Meer formulas	$[\circ]$
β	Angle used to describe step in Van der Meer formulas	$[\circ]$
β_r	Rear side slope	$[\circ]$
γ	Angle used to describe step in Van der Meer formulas	$[\circ]$
γ_b	Breaker index (1.42)	$[-]$
γ_f	Peak enhancement factor in formula for Jonswap spectrum	$[-]$
Δ	Relative density $\left(\frac{\rho_s}{\rho_w}-1\right)$	$[-]$
θ	Direction of wave propagation	$[rad]$
$\theta_1,\theta_2,\theta_3$	Slopes to describe deformed profile in the formulas of Merli	$[rad]$
φ	Angle of repose	$[\circ]$
ξ	Surf similarity parameter $\left(\frac{\tan\alpha}{\sqrt{s}}\right)$	$[-]$
ξ_m	Surf similarity parameter based on T_m	$[-]$
ξ_{mcrit}	Same as ξ_m at transition between plunging and surging waves	$[-]$
ξ_{0p}	Surf similarity parameter based on s_{0p}	$[-]$
λ_x	Prototype-to-model scale ratio for certain parameter x	$[-]$
μ	Resistance coefficient against rolling and sliding	$[-]$
ν	Kinematic viscosity of water	$[m^2/s]$
ψ	Angle of wave attack	$[\circ]$
ψ_{kb}	Characteristic wave obliquity	$[\circ]$
ρ_w	Density of the water fluid	$[kg/m^3]$
ρ_s	Density of the stone particle	$[kg/m^3]$
σ	Peak width parameter in formula for Jonswap spectrum	$[-]$

AAU	Aalborg University
BDM	Bayesian Direct Method
DFTM	Direct Fourier Transform Method
DIWASP	DIrectional WAve SPectra toolbox
EMEP	Extended Maximum Entropy Principle
EMLM	Extended Maximum Likelihood Method
EP	Estimation Parameter
DHI	Danish Hydraulics Institute
ID	Instrument Data
IMLM	Iterated Maximum Likelihood Method
SM	Spectral Matrix

Table of Contents

List of Figures

List of Tables

1. Introduction

1.1 Breakwaters in general

To protect a shore area, harbour, anchorage or basin from waves several different measures can be taken. The most common solution is the use of one or more breakwaters. Offshore breakwaters for example reduce the wave intensity on the lee side of the structure reducing coastal erosion and acquiring land in the process. In the same manner anchorages or harbours can be protected by breakwaters as a calm area is created where wind and waves do not interfere. Without this protection ships would often not be able to berth.

Many different types of breakwaters exist:

- Mound breakwaters consisting of loose elements (stones, gravel, concrete blocks)
- Monolithic breakwaters in which the structure acts as one solid block (caisson)
- Composite breakwaters which combines a monolithic element with a berm of loose materials.
- Unconventional breakwaters such as pneumatic, hydraulic or floating breakwaters.

The type most commonly used is the conventional rubble mound breakwater. Design is then based on the requirement of static stability of the armour layer, which comes down to no displacement of the loose elements by wave action. In general the larger the elements are the higher the stability is. Therefore stability formulas have been defined in order to determine the size of the single loose elements.

Another commonly built type of rubble mound breakwater is the dynamically stable berm breakwater. As the name already mentions design is based on dynamic stability. This means that after completion stones are still allowed to move up and down the outer slope until static stability is reached. In other cases movement is allowed even after reaching a stable slope. Construction of these berm breakwaters has a major advantage compared to conventional rubble mounds. Namely the size of the stones used can be reduced which often also reduces the costs. This is especially beneficial when larger stones are not available in nearby quarries.

While these breakwaters are designed to withstand the governing boundary conditions after completion, in the design phase often little attention is given to hydraulic loads during the construction phase. During this phase core material and other underlayers can be exposed to storm conditions for long periods of time before the following protective layers are applied. Damage in the form of reshaping and loss of material is a constant concern for contractors, as Van Oord, and repairing this damage requires additional materials and leads to loss of valuable construction time.

Although extensive research was and is carried out concerning breakwaters, the focus has rather been on structures already finished and not on structures during construction. To avoid unnecessary damage and minimize the costs in the future, better understanding of the processes, occurring during construction phase, is necessary.

Besides the size of the loose stones and the hydraulic load several other governing parameters can be defined like the structure geometry. Other normative stone characteristics of influence include the stone density, shape and grading. Heavier stones contribute to the stability while rounded stones for example decrease interlocking and thus stability. The stone grading can then best be described as the distribution of stone masses/sizes. A wider grading leads to a reduction in porosity which, according to the currently accepted formulas, results in a lower stability.

This report describes a next step in this research. Especially the influence of grading will be further elaborated. The rest of this chapter gives a more detailed description of the research, together with a problem analysis and definition, which results in a research goal. In section 1.2.4 the approach of the research is described and the chapter concludes with a further outline of the report.

1.2 Description research

1.2.1 Problem Analysis

The design of a rubble mound breakwater is usually based on the static stability of the armour layer of the structure. As the total structure contains several layers of different stone diameters, the construction of the different layers cannot take place all at once. That is why every section of a breakwater is built layer for layer resulting in exposure of one or more intermediate layers to wave attack at any given time during construction.

These underlayers and core are not designed to resist severe or even moderate wave attack and, while the eventual armour layer will be statically stable, the underlayers might not be stable. In that case damage in the form of reshaping and loss of material takes place. However regarding successive construction stages, excessive reshaping is usually not allowed.

To compensate for the damage often extra material is placed afterwards. Another option is to minimize the time span of exposure. For this special care has to be taken choosing the construction method and the length of the separate breakwater sections. The longer the sections the longer the period in which the same stone class can be used. This makes the work itself more efficient by reducing the amount of substitutions between the different stone classes used, but it also results in a longer exposure time and thus damage of the underlayers. Apart from this, the weather conditions are not always easy to predict and delays due to machinery failure and unworkable conditions, such as storms or surges, could extend the periods of exposure and thereby aggravate the situation even further.

In reality contractors like Van Oord are often faced with considerable damage before the next construction stage can be executed. Especially the core, usually made of quarry run, is susceptible to wave attack as it contains the smallest fraction of stones together with a very wide grading. Most damage is therefore observed at exposed core material. As literature available on this subject does not provide the necessary guidelines, a hiatus exists in the current technical knowledge.

For research purposes two different parts of the breakwater structure will be defined: a straight part, called the trunk, and the roundhead. During construction every end of a section, which progresses in time, can be modelled as a roundhead. In the case of head-on wave attack, damage to the trunk can more or less be described as the tendency to reshape the profile in a more stable S-curve. This process is comparable to the reshaping of dynamically stable berm breakwaters. During oblique wave attack however a slightly different situation occurs. Besides the reshaping of the profile in an S-curve, also a transport of stones along the breakwater takes place resulting in even more loss of material. This longshore transport could then undermine the dynamical stability obtained by the reshaped profile. For the roundheads again a different situation occurs. Both during head-on and oblique wave attack three-dimensional processes occur resulting in more severe damage than at the trunk.

Although little is known about the damage occurring at the roundhead for head-on as well as oblique wave attack, extensive research is done throughout the years to model the other aspects of these processes. This has led to a variety of formulas for the deformation of the trunk and the longshore transport, which will be described in Chapter 2. Most of this research however was focused on the armour layer of reshaping berm breakwaters. Stone classes used for these purposes are relatively large and can be characterized as narrowly to very narrowly graded. So during these experiments no tests were done with very widely graded material, which is often typical for quarry run used for core material. Furthermore no attention was given to the influence of these gradings.

Nonetheless some two-dimensional studies into the influence of the stone grading in the deformation were already conducted resulting in three totally different relations between the grading and the berm/crest recession. From this research it is concluded, that the grading has a substantial influence on the reshaping ability of a slope. However these studies did not include three-dimensional environments and corresponding processes. Yet it is expected that influence of the grading on the damage to the roundhead and longshore transport is also considerable, which corresponds to observations in the field.

1.2.2 Problem Definition

The knowledge of the behaviour of quarry run in an exposed core under oblique wave attack is insufficient, resulting at the moment in unaccountable damage at breakwaters under construction which leads to an undesirable use of extra material.

1.2.3 MSc-Thesis Objective

To get better insights in the behaviour of an exposed breakwater core consisting of quarry run under oblique wave attack, the occurring processes need to be defined and investigated separately. Due to the large extent of the subject not all processes can be investigated. Therefore choices were made concerning the points of attention for further investigation.

The emphasis of this thesis will be on the measured influence of wide stone grading on the deformation of the trunk and the longshore transport. This behaviour will be investigated for both head-on and oblique waves during two different wave loads. The findings will be compared to the currently available formulas and the validity of these formulas for the tested range of parameters will be (re)checked. Damage occurring at the roundheads will also be investigated, but further processing falls outside the scope of this research.

Ultimately the goal of this MSc-thesis is to reach a better understanding of the two-dimensional deformation and longshore transport at exposed cores; regarding the influence of grading, wave obliquity and wave load; so that available formulas can be improved if necessary.

1.2.4 Approach

First of all the theoretical background on this topic was sought out. The concept of stability number was introduced, which will be used throughout this report. After that a clear distinction could be made between static and dynamic stability. For the static stability case some stability formulas were found for calculation of the armour layer. Dynamic stability could be explained on the basis of deformation of gravel beaches, rock slopes and berm breakwaters. For this purpose deformation parameters were defined that describe the profile after reshaping and a model was found connecting stone movement to stone mobility. Aside from the above-mentioned mainly two-dimensional processes also three-dimensional processes were investigated. Especially previous tests and formulas concerning the longshore transport were studied, but also current knowledge on the stability of roundheads and rear slopes. This theoretical background was then used to define the gaps in current knowledge leading to a demarcation of the further research.

Further research took place on the basis of physical model tests. These tests were carried out in the wave basin at the fluid mechanics laboratory of the Delft University of Technology. Objective was to investigate the influence of a wide stone grading on the reshaping and longshore transport of rubble mound cores. In order to conduct the tests a scale model of a breakwater core was built consisting of largely loose stones. The model together with the considerations for the input and investigated parameters will be explained later on, resulting in the elaboration of the complete test set-up together with possible sources of errors.

Data collected from the tests needed further processing into useful data, describing the required parameters, before it was used for analysis. Firstly the measured wave records were processed into useful wave and directional spectra out of which all important wave parameters, like significant wave height and wave period, were determined. Subsequently for each test all the cross-sectional measurements were integrated into one three-dimensional model, describing the total deformation, and an erosion/accretion model was created. Lastly also the longshore transport data were processed: measured stone displacements were transformed into an exponential relation for each test, which were then used to calculate the total longshore transport along an area of uniform transport.

After the processing phase all necessary deformation parameters were determined and then compared to the currently accepted formulas. Also the influence of the different varying parameters; wave load, grading and wave angle, were investigated further. Subsequently the same was done for the longshore transport. Firstly the influence of the different parameters on the stone displacement and longshore transport were examined. Then the total longshore transports could be compared to results of previous research and commonly accepted

formulas. Finally the stone transports of the narrow and wide grading were compared to the corresponding volume transports to find the effect of the grading on the volume transport.

1.3 Outline report

This thesis will proceed in Chapter 2 with a more detailed theoretical background on the topic. Subsequently Chapter 3 describes the test set-up of the physical model tests carried out for this thesis. The process itself of processing respectively the wave, profile and stone displacement measurements are described in Chapter 4. After that Chapter 5 deals with the actual analysis of respectively the two-dimensional deformation and longshore transport data. Finally the conclusions are formulated in Chapter 6. In this chapter also recommendations are given for further research.

2. Background of the research

As was already mentioned in paragraph 1.1, besides statically stable rubble mound breakwaters also dynamically stable versions exist. Then due to wave attack the outer profile deforms into a more stable profile. More or less the same deformation process takes place at rock slopes, like gravel beaches, under wave attack. During the last half of the previous century stability of loose materials under wave attack has been investigated extensively. This has resulted in various stability formulas of which most share an important common part. In this chapter the available theoretical knowledge is elaborated starting with the definition of the stability number in paragraph 2.1. The rest of the chapter deals with the design of a rubble mound breakwater and the current knowledge on the deformation processes. Firstly the conventional rubble mound breakwater (statically stable) is elaborated in paragraph 2.2 followed by berm breakwaters (mostly dynamically stable). The latter type will be split into a two-dimensional case in paragraph 2.3 and a three-dimensional case in paragraph 2.4 where the occurring three-dimensional processes will be elaborated as they cannot be neglected. Also a comparison is drawn with the behaviour of gravel beaches.

2.1 Stability number

To describe stability [VAN DER MEER 1988] gives a definition of the stability number, which was previously used by Hudson in 1959:

$$H_0 = N_s = \frac{H_s}{\Delta D_{n50}} \qquad (2\text{-}1)$$

In this formula:
H_s is the significant wave height defined as the mean of one third of the highest waves in $[m]$.

$\Delta = \frac{\rho_s}{\rho_w} - 1$ is the relative density, in which ρ_s is the dry density of the stones and ρ_w is the density of water.

$D_{n50} = \left(\frac{W_{50}}{\rho_s} \right)^{\frac{1}{3}}$ is the nominal diameter in $[m]$.

For statically stable conventional breakwaters the value of H_0 varies from 1 to 4, while dynamically stable berm breakwaters fall in between 3 and 6. In comparison rock slopes and gravel beaches have a H_0 of respectively 6-20 and 20-200.

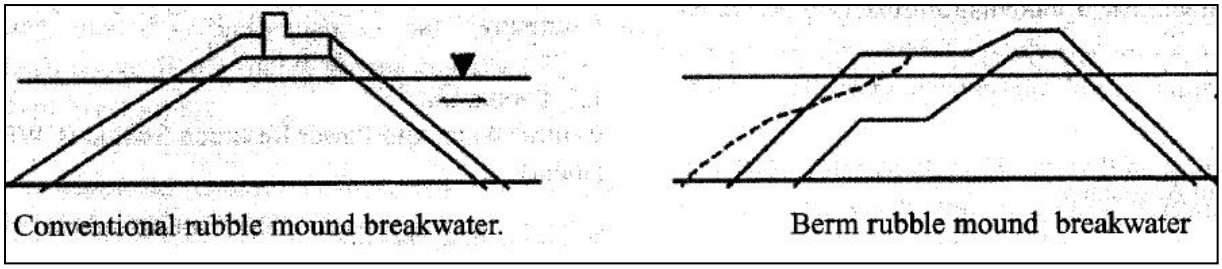

Figure 2.1: Comparison conventional rubble mound breakwaters with berm breakwaters

2.2 Stability of conventional rubble mound breakwaters

A conventional rubble mound breakwater is usually in the shape of a simple trapezoidal and consists of several layers of loose material (quarry stone or concrete blocks). It is designed in such a way that high pressures as

well as erosion of the core or bed material through the layers above are avoided (filter function). The greater part of the wave energy is absorbed by the armour layer of which the stability depends on the ratio between wave height on one hand and size and relative density on the other hand. Underneath the armour layer one or several underlayers, consisting of stones with a smaller diameter than the armour layer, and a core exist. The core can consist of sand or gravel, but usually quarry run is used, which represents the finer fractions of the quarry yield curve.

Design of a statically stable rubble mound breakwater should result in a unit mass for the armour layer. This mass is then based on an economically optimal solution, weighing the construction costs against maintenance costs. The building costs are often determined by the coarseness of the material, in that case the coarser the material the higher the costs. On the other hand the smaller the material the more damage and accompanying maintenance costs it brings along. As can be expected, damage, defined as the amount of displacement of loose materials, is an essential parameter in this process.

Figure 2.2 from [VAN DER MEER 1988] schematises the occurring wave forces with two forces:

- F_P : force parallel with the slope
- F_N : force normal to the slope

In this figure the slope angle is given by α and the natural angle of repose by φ while $W' = (\rho_s - \rho_w) D_{n50}^3$ is defined as the buoyant mass.

Both forces are related to the wave height by the following relation:

$$F = \rho g C D^2 H \qquad (2\text{-}2)$$

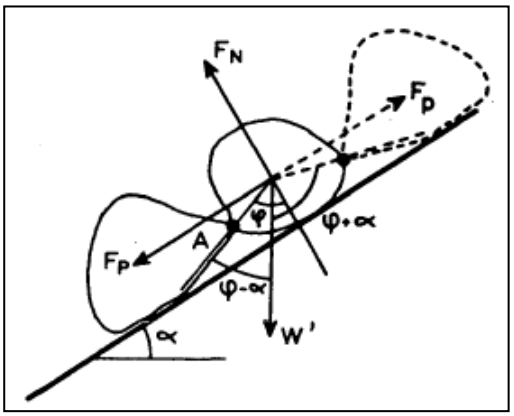

Figure 2.2: Overview forces [Van der Meer 1988]

In this relation C is a coefficient further defined as C_N for normal wave force and C_P for parallel wave force. The momentum equation for point A, assuming incipient instability, can then be given by:

$$F_N \sin\varphi \cdot D/2 + F_P \cos\varphi \cdot D/2 = gW' \sin(\varphi - \alpha) \cdot D/2 \qquad (2\text{-}3)$$

Together with the relations $D = KD_{n50}$ (K = coefficient) and $\mu = \tan\varphi$ this relation can be rewritten into:

$$\frac{H}{\Delta D_{n50}} = \frac{K(\mu\cos\alpha - \sin\alpha)}{\mu C_N + C_P} \qquad (2\text{-}4)$$

Eventually Hudson ([VAN DER MEER 1988]) assumed $\varphi = 1$ for rubble mound structures and combined all coefficients to one coefficient, K_D, as well as replacing the term $\cos\alpha - \sin\alpha$ by $(\cot\alpha)^{1/3}$. This resulted in the well-known Hudson formula:

$$\frac{H}{\Delta D_{n50}} = (K_D \cot\alpha)^{1/3} \qquad (2\text{-}5)$$

Later on [VAN DER MEER 1988] developed other formulas to calculate the required armour stone diameter, taking into account the wave period and a damage parameter amongst other parameters. This resulted in the Van der Meer stability formulas:

For quarry stone:

- For plunging waves: $$\frac{H_s}{\Delta D_{n50}} = 6.2 P^{0.18} \left(\frac{S}{\sqrt{N}}\right)^{0.2} \frac{1}{\sqrt{\xi_m}} \qquad (2\text{-}6)$$

- For surging waves: $$\frac{H_s}{\Delta D_{n50}} = 1.0 P^{-0.13} \left(\frac{S}{\sqrt{N}} \right)^{0.2} \sqrt{\cot \alpha} \cdot \xi_m{}^P \qquad (2\text{-}7)$$

where:
P = permeability coefficient
S = damage parameter
N = number of waves in a storm, record or test
$\xi = \frac{\tan \alpha}{\sqrt{s}}$ = Surf similarity parameter
$s = H/L$ = wave steepness
$L = 2\pi / gT^2$ = wave length $[m]$
ξ_m = Surf similarity parameter based on T_m

The transition between plunging and surging waves can be derived by intersecting the two stability curves which yields:

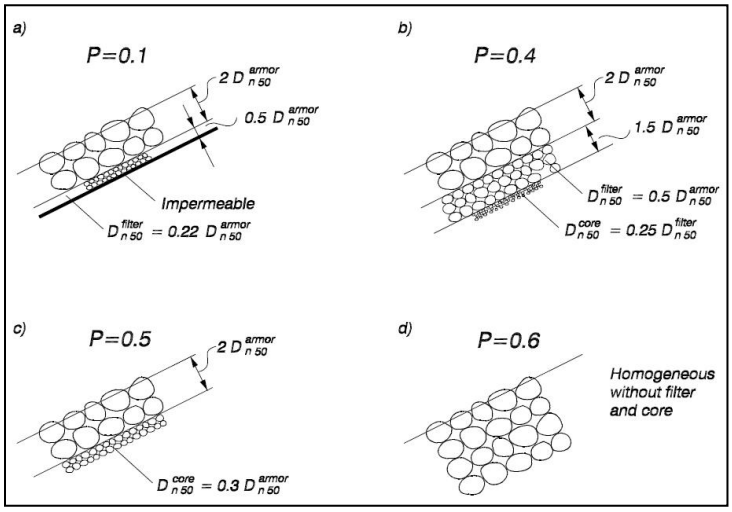

Figure 2.3: Assumptions permeability coefficient[VAN DER MEER 1988]

$$\xi_{mcrit} = \left[6.2 P^{0.31} \sqrt{\tan \alpha} \right]^{\frac{1}{P+0.5}} \qquad (2\text{-}8)$$

2.3 Stability of berm breakwaters: Two-dimensional case

The main difference between conventional rubble mound breakwaters and berm breakwaters is the fact that the second category is not always statically stable. According to [PIANC MarCom 2003] berm breakwaters can therefore be divided into 3 classes:

- *Static stable, no reshaping:* similar to the condition for conventional rubble mound breakwaters; few stones are allowed to move.
- *Static stable after reshaping:* profile is allowed to reshape into a stable profile after which individual stones are also stable.
- *Dynamic stable after reshaping:* individual stones may move up and down the slope even after reshaping into a more stable profile took place and equilibrium is reached.

In case of the last two classes extra material is placed on the sea side of the breakwater allowing deformation without jeopardising the structure itself. Caused by breaking and the following inertia a water mass is driven up the slope. Upon reaching the highest point the water flows back by gravity until elimination by the following wave. Due to this motion grains will be displaced resulting in a possible change of the profile. Material is removed from zones where it is unstable and is relocated into more stable positions. Severe wave attack then leads to reshaping of the outer slope into a more stable S-curve. Compared to the statically stable case, the size of the armour stones used can be reduced and the accuracy of placement is less important.

Several investigations into the deformation of the profile have been conducted which has led to a range of deformation parameters and models described in the following sections. To take into account oblique wave attack, [VAN HIJUM 1982] and [BURCHARTH 1988] used a reduction factor of $\sqrt{\cos \psi}$ to determine the deformation parameters. [VAN DER MEER 1988] continued the investigation for grading between $f_g = \frac{D_{85}}{D_{15}} = 1.25 - 2.25$ and an angle of wave attack of 0-50 degrees, and found a reduction factor of $\cos \psi$. In these reduction factors ψ stands for the angle of wave attack.

2.3.1 Gravel/shingle beaches and rock slopes

Although rock is more angular than gravel or shingle, reshaping of the outer slope of berm breakwaters is comparable to the reshaping of gravel beaches. Van Hijum and Pilarczyk developed a model in [VAN HIJUM 1982] for the dynamically stable profile of gravel beaches in the range $H_0 = 12-35$.

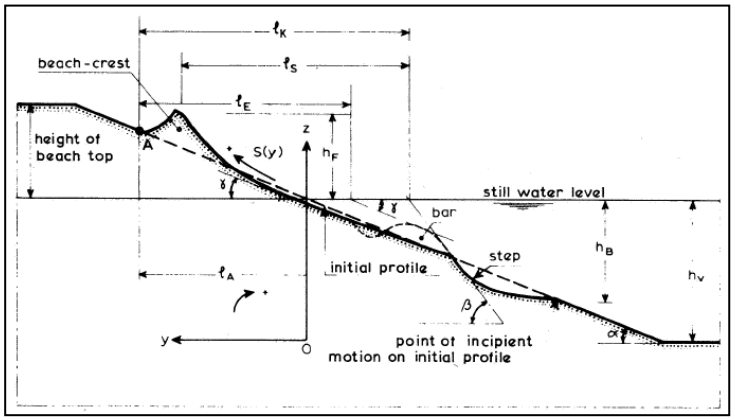

Figure 2.4: Explanation of equilibrium profile [Van Hijum 1982]

The influence of several external parameters, like grain diameter, shape and angle of wave attack, were examined in a physical model and several profile parameters were defined to characterize the equilibrium profile. Figure 2.4 shows an example of this equilibrium profile together with the parameters which will not be elaborated any further in this report.

By means of consecutive profile soundings the transverse transport $(S(y))$ was calculated leading to a continuity equation which also includes the longshore transport $(S(x))$:

$$\frac{\delta S(x)}{\delta x} + \frac{\delta S(y)}{\delta y} + \frac{\delta z}{\delta t} = 0 \qquad (2\text{-}9)$$

During the tests a phenomenon was observed which will be referred to from now on as sediment sorting. Loose material sorted along the transverse direction of the equilibrium profile. Under low waves the coarsest material was found on the beach crest while under higher waves it was in the vicinity of the step. In the longitudinal direction no sorting was found.

2.3.2 Dynamic stability rock slopes and berm breakwaters (Van der Meer)

In his doctoral thesis [VAN DER MEER 1988] extended the research done by Van Hijum and Pilarczyk for a wider scope of stability numbers $H_0 = 3-250$ including not only dynamically stable berm breakwaters, but very fine shingle beaches as well.

A schematized profile of a dynamically stable slope is shown in Figure 2.5. According to [VAN DER MEER 1988], the deformed equilibrium profile can be described with a number of profile parameters, comparable to Van Hijum and Pilarczyk. First three points are defined on the profile:

- Local origin at the intersection of the profile and the still water level.
- Crest point defined as the upper point of the beach crest.
- Step point which is the transition from the gentle sloping part to the steep part.

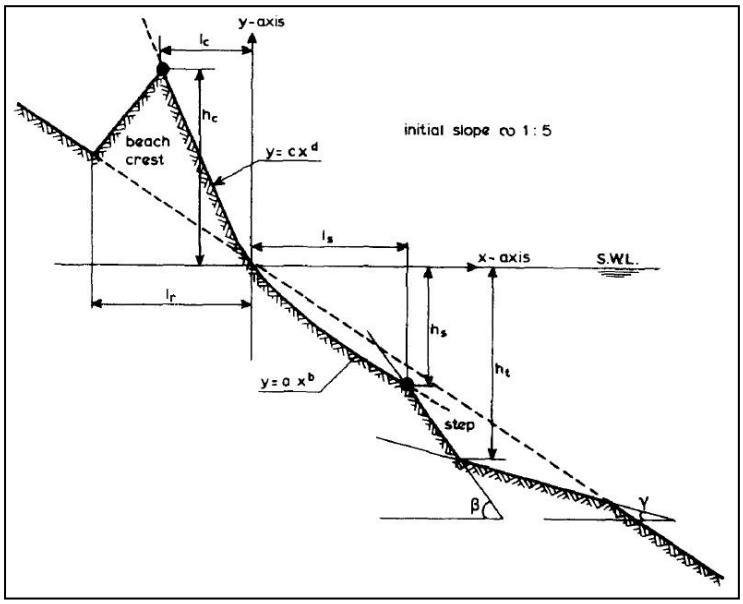

Figure 2.5: Schematized profile [VAN DER MEER 1988]

The beach crest can be described by crest height, $h_c\ [m]$, and crest length, $l_c\ [m]$ and the transition to the step is described by

the step height, $h_s\ [m]$, and step length, $l_s\ [m]$. The profiles in between these points can then be described by two different power functions, of which the curves start at the local origin and go through these two points. The length, $l_r\ [m]$, represents the run-up length and angles, β and γ, describe the step. The transition from β to γ can be described by the transition height, $h_t\ [m]$.

From the results of model tests it turned out that all profile parameters are related to H_0T_0, the dimensionless combined wave height-wave period parameter, or s_m, the fictitious wave steepness:

$$H_0T_0 = {H_s}/{\Delta D_{n50}} * \sqrt{{g}/{D_{n50}}}\, T_m \qquad (2\text{-}10)$$

$$s_m = {H_s}/{L_0} = {2\pi H_s}/{gT_m^2} \qquad (2\text{-}11)$$

s_m is called the fictitious wave steepness as H_s is taken at the toe of the structure while the wave length, L_0, is taken at deep water.

Apart from these related parameters also the storm duration defined as the number of waves, N, the water depth at the structure, h, and the angle of wave attack, ψ, were established as governing parameters. On the other hand no or only a minor influence on the development of the profile was found regarding the grading of the material. Only for very wide gradings an influence was found in the manner of a longer profile below still water level.

In [VAN DER MEER 1992] the relations regarding the profile parameters were expanded to make better predictions of the profile deformation of berm breakwaters. In these relations the influence of the initial profile is discounted by three equivalent initial slope angles $(\alpha_1, \alpha_2, \alpha_3)$, which are defined in Figure 2.6.

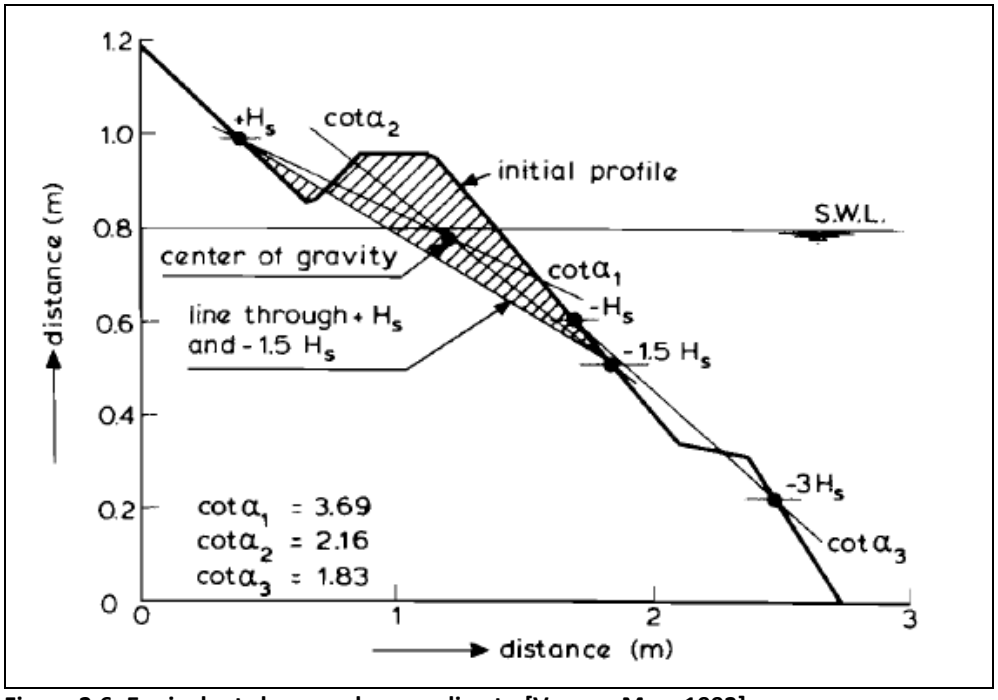

Figure 2.6: Equivalent slope angle according to [VAN DER MEER 1992]

Below the relations, derived by Van der Meer, are given for the whole investigated range:

Run-up length $l_r\ [m]$:

$$H_0T_0 = 2.9\left(l_r / D_{n50}N^{0.05}\right)^{1.3}$$
$$H_0T_0 = \left(20 - 1.5\cot\alpha_1\right) l_r / D_{n50}N^{0.05} - 40 \qquad (2\text{-}12)$$

The intersection of the two equations gives the transition from one to the other. The first equation holds for the highest H_0T_0 region.

Crest height h_c $[m]$:

$$h_c / H_s N^{0.15} = 0.089 s_m^{-0.5}; \qquad H_0T_0 > 900$$
$$H_0T_0 = 33\left(h_c / D_{n50}N^{0.15}\right)^{1.3} + 30\cot\alpha_1 - 30; \quad H_0T_0 < 900 \qquad (2\text{-}13)$$

Crest length l_c $[m]$:

$$H_0T_0 = 21\left(l_c / D_{n50}N^{0.12}\right)^{1.2}$$
$$H_0T_0 = \left(3\cot\alpha_1 + 25\right) l_c / D_{n50}N^{0.12} \qquad (2\text{-}14)$$

The first equation holds for the highest H_0T_0 region and the transition is formed by the intersection of the two equations.

Step height h_s $[m]$:

$$h_s / H_s N^{0.07} = 0.22 s_m^{-0.3}; \qquad H_0T_0 > 300\cot\alpha_2$$
$$H_0T_0 = 27\left(h_s / D_{n50}N^{0.07}\right)^{1.3} + 125\cot\alpha_2 - 475; \quad H_0T_0 < 300\cot\alpha_2 \qquad (2\text{-}15)$$

Step length l_s $[m]$:

$$H_0T_0 = 3.8\left(l_s / D_{n50}N^{0.07}\right)^{1.3}$$
$$H_0T_0 = 2.6\left(l_s / D_{n50}N^{0.07}\right) + 70\cot\alpha_2 - 210 \qquad (2\text{-}16)$$

The first equation holds for the highest H_0T_0 region and the transition is formed by the intersection of the two equations.

Transition height h_t $[m]$:

$$h_t / H_s N^{0.04} = 0.73 s_m^{-0.2}; \qquad H_0T_0 > 400\cot\alpha_3$$
$$H_0T_0 = 10\left(h_t / D_{n50}N^{0.04}\right)^{1.3} + 175\cot\alpha_3 - 725; \quad H_0T_0 < 400\cot\alpha_3 \qquad (2\text{-}17)$$

If $H_0T_0 < 875 - 125\cot\alpha_3$, no transition exists.

The profile around still water level can then be defined as follows:

- Below still water level: $y = a_1 x^{0.83}$ (2-18)
- Above still water level: $y = a_2\left(-x\right)^{1.15}$ (2-19)

In the above formulas a_1 and a_2 are coefficients which are determined by the values of h_c, l_c, h_s and l_s.

Furthermore the slopes describing the step can be calculated with $\tan\beta$ and $\tan\gamma$:

$$\tan\beta = 1.1\tan\alpha_3^{1-0.45\exp(-500/N)}$$
$$\tan\gamma = 0.5\tan\alpha_3 \qquad (2\text{-}20)$$

Finally oblique wave attack is taken into account by reducing all the length and height parameters, except for l_c, with a factor $\cos\psi$, as was mentioned earlier at the beginning of this section.

For the case of a relatively shallow foreshore, a reduction factor, r, can be defined which describes the influence of a limited water depth. This factor only influences h_s and l_s and is given by:

$$\begin{aligned} r &= 0.75\left(2.2 - h/H_s\right)^2; \text{ for } h/H_s < 2.2 \\ r &= 1; \qquad\qquad \text{for } h/H_s \geq 2.2 \end{aligned} \tag{2-21}$$

2.3.3 *Berm breakwaters in deep and shallow water*

Previous tests were conducted mainly in deep water conditions. To investigate the influence of both shallow water and deep water conditions further, physical model tests were carried out at Danish Hydraulic Institute (DHI) in 1992 and Estramed in 1993-1994. [LAMBERTI 1994] described these tests and concluded that the behaviour of reshaping berm breakwaters in deep and shallow water conditions is qualitatively similar, but differs quantitatively.

The profile dimensions of a berm breakwater in the breaker zone (shallow water) can be described by less parameters than Van der Meer defined, namely h_c, l_c, h_s and l_s. Furthermore the reduction factor for shallow water, r, turned out to be more pronounced than observed by Van der Meer. This difference cannot be attributed solely to the reduction of wave height due to breaking, but probably also depends on other possible parameters as wave period, foreshore slope and breaking depth. It seems to be caused by a change in the kinematic behaviour of waves when they hit the breakwater: from irrotational green-water breakers plunging on the rubble mound into action of white-water roller-shaped bores running up the mound.
As for the reduction factor itself, the reduction of l_s appeared to be even larger than the reduction of h_s with average limit values for r of respectively 0.3 and 0.5.

2.3.4 *Sorting and profile shape for berm breakwater trunks under oblique wave attack*

Within the framework of MAST2 additional tests with berm breakwater roundhead and adjacent trunk section were conducted at DHI and the Hydraulic & Coastal Engineering Laboratory of Aalborg University (AAU). In [ALIKHANI 1996] data from these tests were used to investigate the influence of wave obliquity on the profile.

For small obliquity at first unstable larger stones start swaying and rolling down the slope leading to a redistribution of the stone distribution itself. The W_{50}, defined as the stone weight for which 50% of the stones are smaller, of the stones in the lower steep part can then be even twice as much as the W_{50} found around mean water level. For wider stone gradings this stone sorting is even more pronounced, while for larger angles of wave incidence sorting is less evident. A modification should then be applied to the D_{n50} due to less sorting for larger wave incidence, ψ, and narrower stone grading.

During the long duration tests with oblique wave attack it became clear that the major part of the resorting and reshaping takes place in the first 1000 waves. However, while the lower part of the profile does not further evolve after a certain amount of waves, the upper part keeps on developing as a function of the duration. A lack of nourishment from upstream of the breakwater can be given as reason for this continued recession.

Accordingly the reduction of the upper part of the profile under oblique wave attack is more dependent on the duration, while this is not the case for head-on waves. Therefore the reduction factors determined by [VAN HIJUM 1982], $\sqrt{\cos\psi}$, and by [VAN DER MEER 1988], $\cos\psi$, both do not fit the reduction of the upper deformation parameters. As the berm recession under long duration storm conditions with oblique waves can even exceed the value for head-on waves, it was concluded that formulation of a new reduction factor for the upper part of the profile under a long duration storm is meaningless.

For several parameters some new equations were developed to calculate the reshaped profile under head-on and oblique wave attack:

$$h_s = \frac{H_0 T_{0p} D_{n50} N^{0.07} \sqrt{\cos\psi}}{40} \qquad (2\text{-}22)$$
$$h_t = H_s \cos\psi + h_s$$

Depending on the water depth, wave parameters, stone weight, incident wave angle, initial shape of the profile and angle of repose, finally two power functions were defined to characterise the lower and upper part of the reshaped profile:

- Lower part: $Y = -hm_1\left(\frac{X}{h}\right)^{1.7} + h - h_s$; $\quad m_1 = \frac{1.7e^{\left(-0.013H_0T_{0p}\right)}}{\cos\psi}$ (2-23)
- Upper part: $Y = hm_2\left(\frac{X}{h}\right)^{1.7} + h - h_s$; $\quad m_2 = \frac{1.7e^{\left(-0.01H_0T_{0p}\right)}}{\cos\psi}$ (2-24)

In these relations X and Y represent the length and height of the reshaped profile counted from the centre line of the breakwater, h is the water depth at the toe of the breakwater and m_1 and m_2 are coefficients.

2.3.5 *Stability rubble mound slopes (Merli)*

Merli adjusted the relations, found by Van der Meer, in [MERLI 2009] using curve-fitting to take into account the influence of stone grading. Seven parameters were defined directly related to the parameters of Van der Meer as is given in Figure 2.7. The local origin is defined as the intersection between the reshaped profile and the mean water level:

- $l_s[m]$: Horizontal offset between the step (below mean water level) and local origin.
- $h_s[m]$: Vertical offset between the step (below mean water level) and local origin.
- $l_c[m]$: Horizontal offset between crest (above mean water level) and local origin.
- $h_c[m]$: Vertical offset between crest (above mean water level) and local origin.
- θ_1 : Slope of line interpolating the last six points measured on the reshaped profile and connecting step to original profile.
- θ_2 : Slope of line interpolating measured profile below the local origin, until the slope of the profile does not become permanently steeper than 0.3.
- θ_3 : Slope of line connecting the observed crest with the local origin. θ_3 can be defined as the ratio between h_c and l_c. It is fairly independent of the height of the breakwater above mean water level and allows for an estimation of the recession of the crest regardless of the initial height.

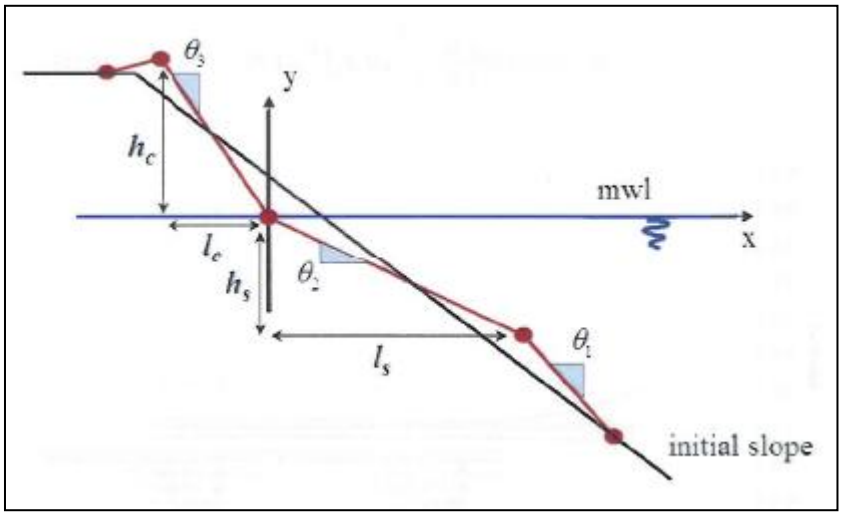

Figure 2.7: Deformation parameters according to Merli [MERLI 2009]

Three of these parameters were derived:

$$l_s \rightarrow H_0T_0 = 1.66\left(l_s / D_{n50}N^{0.07}\right)^{1.3}\left(\frac{D_{n85}}{D_{n15}}\right)^{-0.15} + 29.1\cot\alpha_2 - 9.38 \qquad (2\text{-}25)$$

$$l_c \rightarrow (H_0T_0 - 183)\cot\alpha_1 = 139(l_c / D_{n50}N^{0.12})\left(\frac{D_{n85}}{D_{n15}}\right)^{-0.29} - 667 \quad (2\text{-}26)$$

$$\theta_3 \rightarrow \theta_3^{-1} = 0.00023\left(\frac{D_{n85}}{D_{n15}}\right)^{1.58}(H_0T_0)^{0.84} + 1.50 \quad (2\text{-}27)$$

The remaining parameters can be derived according to [VAN DER MEER 1992].

2.3.6 Crest recession

To guarantee the protection of the underlying structure, another parameter called the recession length, Rec, was defined. For a safe structure, which means no exposure of the underlying layer, the berm should be wider than Rec. [HALL 1991] investigated the influence of the grading and rounded stones on the reshaping of the berm in model tests resulting in an inverted quadratic relation:

$$\frac{Rec}{D_{50}} = -10.4 + 0.51\left[\frac{H_s}{\Delta D_{50}}\right]^{2.5} + 7.52\left(\frac{D_{85}}{D_{15}}\right) - 1.07\left(\frac{D_{85}}{D_{15}}\right)^2 + 6.12P_R \quad (2\text{-}28)$$

In which:
D = sieve diameter $\approx 1.2D_n$ $[m]$
P_R = percentage per number of rounded stones in the armour

To express Rec in terms of nominal diameters, D_n, rather than sieve diameters, D, formula (2-28) can be converted into the following relation based on 3000 waves ([CIRIA 2007]):

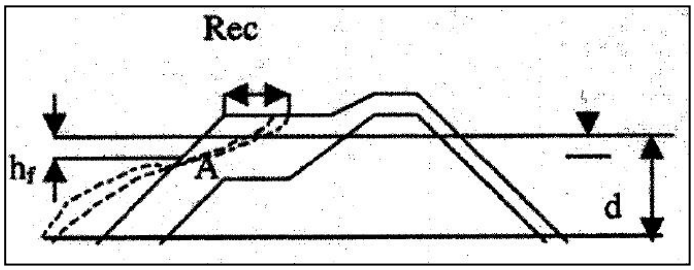

Figure 2.8: Sketch of crest recession [PIANC MarCom 2003]

$$\frac{Rec}{D_{n50}} = -12.4 + 0.39\left[\frac{H_s}{\Delta D_{n50}}\right]^{2.5} + 8.95\left(\frac{D_{n85}}{D_{n15}}\right) - 1.27\left(\frac{D_{n85}}{D_{n15}}\right)^2 + 7.3P_R \quad (2\text{-}29)$$

The following correction factor can then be used to define Rec relative to the number of waves, N:

$$\frac{Rec_N}{Rec_{3000}} = 1 + 0.111\cdot\ln\left(\frac{N}{3000}\right) \quad (2\text{-}30)$$

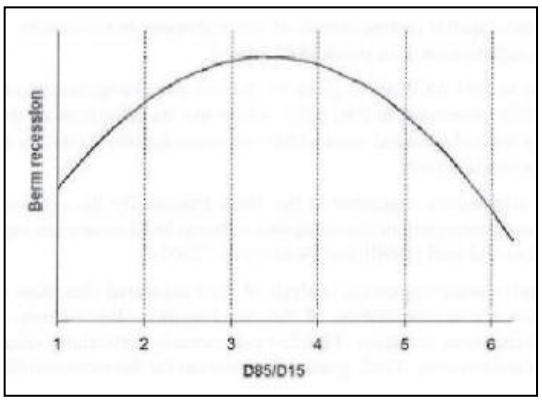

Figure 2.9: Berm recession as function of grading according to Hall and Kao [MERLI 2009]

Results from the tests show that for $f_g = \frac{D_{n85}}{D_{n15}} < 3$, narrowly graded stones are less prone to reshaping than wider graded stones. For the wider gradings the smaller stones will fill the voids between the larger stones, resulting in a lower permeability. This leads to a decrease in energy dissipation and consequently an increase in erosion volume and berm recession. For even wider gradings $(f_g > 3)$, the effect of very large stones starts to dominate the effect of the voids leading to a decrease in reshaping and Rec.

Later on Menze and Tørum and Krogh [PIANC MarCom 2003] found another quadratic relation and derived a formula to take into account the water depth, h, as well:

$$\frac{Rec}{D_{n50}} = 2.7\cdot10^{-6}\left(H_0T_0\right)^3 + 9.0\cdot10^{-6}\left(H_0T_0\right)^2 + 0.11\left(H_0T_0\right) - \left(-9.9\,f_g^2 + 23.9\,f_g - 10.5\right) - f\left(\frac{h}{D_{n50}}\right)$$

$$f\left(\frac{h}{D_{n50}}\right) = -0.16\left(\frac{h}{D_{n50}}\right) + 4.0; \quad \left(12.5\frac{h}{D_{n50}} < 25\right) \qquad (2\text{-}31)$$

$$f_g = \frac{D_{n85}}{D_{n15}}; \qquad \left(1.3 < f_g < 1.8\right)$$

Eventually [MERLI 2009] defined a new linear relation between stone grading and Recession length including validity for even wider gradings:

$$\frac{Rec}{D_{n50}} = 0.218H_0T_0 + 1.62\frac{D_{n85}}{D_{n15}} + 105\tan\alpha - 91.5 \qquad (2\text{-}32)$$

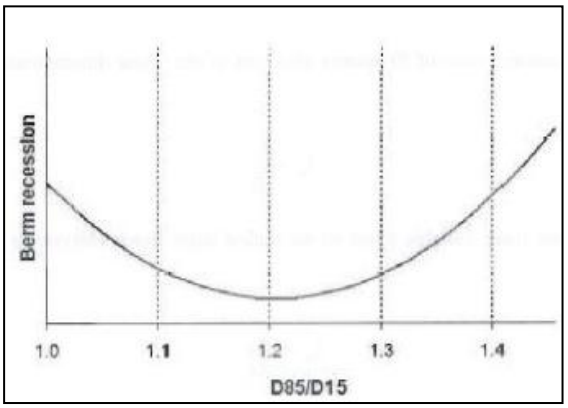

Figure 2.10: Berm recession as function of grading according to Tørum [MERLI 2009]

2.3.7 *Stone movement and stone mobility*

While reshaping of berm breakwaters lead to an equilibrium profile, as is described above, upward and downward movement of stones still takes place after reshaping. [LAMBERTI 1994] and [TOMASICCHIO 1994] analysed the threshold of stone movement along the reshaped profile in both deep and shallow water conditions and developed a model to describe this movement based on stone mobility. For this purpose two new parameters were defined by [TOMASICCHIO 1994] which can measure the movement on the profile: the damage index, N_{od}, and the surface damage level, S_s:

$$N_{od} = N_d D_{n50} / B_o$$
$$S_s = N_d D_{n50}^2 / A_o \qquad (2\text{-}33)$$

The latter describes the frequency of stone movements representing the probability of a generic stone moving at least once during 1000 waves from a layer of the reshaped profile one stone grain thick. N_d is the number of stones displaced from the active profile at least once during 1000 waves and B_o and A_o are respectively the width of the observed area and the area itself. An empirical relation between N_{od} and S_s is then given by:

$$N_{od} = \left(13.2 \pm 16\%\right) N_s^{**} S_s \qquad (2\text{-}34)$$

According to [LAMBERTI 1994] the wave height of irregular waves with a narrow spectrum is Rayleigh distributed for deep water conditions. In the breaker zone the water depth influences the breaking process and with it the wave height distribution. A characteristic wave height, $H_k = H_{1/50}$, was defined which is a good representative wave height for describing the phenomenon of stone movements in limited water depth. This H_k has a frequency of exceedance almost equal to the frequency of stone movements. Observed ratios between H_k and H_s in shallow and intermediate water conditions were $C_k = H_k / H_s = 1.33 \pm 0.12$, while $C_k = 1.55$ for deep water conditions.

[TOMASICCHIO 1994] defined a modified stability number to describe the wave attack intensity under the assumption that onshore wave energy flux is conserved:

$$N_s^{**} = \frac{H_k}{C_k \Delta D_{n50}} \left(\frac{s_{mo}}{s_{mk}}\right)^{-1/5} \left(\cos\psi\right)^{2/5} \simeq \frac{0.89 H_{kb}}{C_k \Delta D_{n50}} \qquad (2\text{-}35)$$

In this formula H_{kb} is defined as the characteristic breaking wave height, s_{mo} is the mean wave steepness in deep water, based on a mean wave period, and $s_{mk} = 0.03$ is assumed as reference wave steepness. For $s_{mo} = s_{mk}$ and head-on waves N_s^{**} equals H_0, the stability number. Threshold conditions correspond approximately to $N_s^{**} \simeq 2$ or $H_0 T_0 \simeq 33$. Furthermore average empirical correlations between mobility, N_s^{**}, and respectively damage index or displacement frequency (N_{od}), surface damage level (S_s) and dimensionless mean displacement length (D_s^{**}) were defined and refined by including more data on shallow water conditions:

$$\begin{aligned} N_{od} &= N_d\, D_{n50}/B_o = 1.8 N_s^{**}\left(N_s^{**} - 2.0\right)^{2.2}; \quad N_s^{**} > 2.0 \\ S_s &= 0.14\left(N_s^{**} - 2.0\right)^{2.2}; \qquad\qquad N_s^{**} > 2.0 \\ D_s^{**} &= l_d \tanh^2(kh)/D_{n50} = 1.4 N_s^{**} - 1.3 \end{aligned} \tag{2-36}$$

In the last relation l_d is the average length of displacements, k is the wave number defined as $k = \frac{2\pi}{L}$ and h is the water depth.

The results of the data analysis by [LAMBERTI 1997] are shown in Figure 2.11 in the form of criteria for movements in terms of N_{od} and S_s during 1000 waves.

Regime	Displacement N_{od}	Displacement S_s
No movement	< 0.10	$<4\ 10^{-3}$
Limited movement during reshaping, eventual static stability	0.10 - 2	$4\ 10^{-3} - 2\ 10^{-2}$
Relevant movement, dynamic stability	> 2	$> 2\ 10^{-2}$

Figure 2.11: Movement criterion [PIANC MarCom 2003]

Later on [LAMBERTI 1997] refined the empirical correlation between N_s^{**} and N_{od} In the range $1.5 < N_s^{**} < 3.5$:

$$\begin{aligned} N_{od} &= 2.05 N_s^{**}\left(N_s^{**} - 2.0\right)^{2.2}; \quad N_s^{**} > 2.0 \\ N_{od} &= \exp\left(4.8 N_s^{**} - 12\right); \qquad N_s^{**} \le 2.0 \end{aligned} \tag{2-37}$$

In [TOMASICCHIO 2007] this correlation was again calibrated now valid for $2 < N_s^{**} < 23$:

$$N_{od} = 20 N_s^{**}\left(N_s^{**} - 2.0\right)^2 \tag{2-38}$$

2.4 Stability of berm breakwaters: Three-dimensional case

The calculation formulas for dynamically stable berm breakwaters given in paragraph 2.3 are determined for a two-dimensional case of head-on waves. Changes in the profile occur only in the cross-sectional area. In the situation of oblique wave attack, reduction factors are applied to determine the profile and recession length. However other processes like longshore transport and the complex situation around the head are left out of consideration, while their influence on the stability can be substantial.

2.4.1 Longshore Transport

For statically stable breakwaters longshore transport is not of importance as it is already accounted for as damage. This is not the case for dynamically stable structures. When the waves come in at an angle, stones may be transported for some distance along the breakwater. This process starts when the stone diameter is

small enough compared to the wave height. Sections will then erode causing a deficit of armour stones and therefore damage to the profile. Equilibrium in the form of a stable S-shape is no longer possible. The same situation occurs at sandy or gravel beaches.
For sandy beaches $(H_0 > 50)$ the relationship is similar to the CERC-formula and can be given as is mentioned by [VAN HIJUM 1982]:

$$S_V = 0.12 \cdot 10^{-4} \pi H_s^2 c_{0p} \sin 2\psi \qquad (2\text{-}39)$$

[VAN HIJUM 1982] performed tests on the longshore transport at gravel beaches under regular waves (with angles of wave attack of 20° and 45°) and under random waves (with an angle of wave attack of 30°). The CERC-formula was then used as a basis to define two other relationships for gravel beaches, respectively one for regular waves and one for irregular waves in which $S_V(x)$ is specified as the longshore volume transport rate:

For $H_0 = \frac{H_s}{\Delta D_{n50}} = 12 - 27$:

$$\frac{S_V(x)}{g^2 D_{90} T^3} = 0.16 \cdot 10^{-6} \frac{H_0 \cos^{1/2}\psi}{D_{90}} \left[\frac{H_0 \cos^{1/2}\psi}{D_{90}} - 8.1 \right] \frac{\sin\psi}{\tanh(kh)}$$

$$\frac{S_V(x)}{g^2 D_{90}^2 T_s} = 7.12 \cdot 10^{-4} \frac{H_{sd} \cos^{1/2}\psi}{D_{90}} \left[\frac{H_{sd} \cos^{1/2}\psi}{D_{90}} - 8.3 \right] \frac{\sin\psi}{\tanh(k_s h)} \qquad (2\text{-}40)$$

For rock/gravel beaches $(10 < H_0 < 50)$ these formulas were revised by [VAN DER MEER 1988] :

$$\frac{S_V(x)}{g D_{n50}^2 T_p} = 0.0012 \frac{H_s \sqrt{\cos\psi}}{D_{n50}} \left(\frac{H_s \sqrt{\cos\psi}}{D_{n50}} - 11 \right) \sin\psi \qquad (2\text{-}41)$$

To get also more insight in the longshore transport of stones at reshaping berm breakwaters, several tests were done with lower stability numbers $(3 < H_0 < 10)$. [BURCHARTH 1987; BURCHARTH 1988] tested already developed profiles of berm breakwaters under irregular wave attack with an angle of 15°-30° and came up with some rough criteria for incipient motion, provided the grading of the stones is not too wide ($f_g < 3$):

- $\frac{H_s}{\Delta D_{n50}} \le 4.5$ (trunks exposed to steep waves)
- $\frac{H_s}{\Delta D_{n50}} \le 3.5$ (trunks exposed to oblique waves) (2-42)
- $\frac{H_s}{\Delta D_{n50}} \le 3$ (breakwater heads)

[VRIJLING 1991] used the results of Burcharth and Frigaard and data from Delft Hydraulics to formulate a relation for the transport of stones along the trunk under oblique waves. In this formula stone transport rate, $S_N(x)$, is defined as the number of stones transported per wave:

$$S_N(x) = 0.000048 (H_0 T_0 - 100)^2 \qquad H_0 T_0 = 100 - 400 \qquad (2\text{-}43)$$

Subsequently [VAN DER MEER 1992] tested already developed profiles of berm breakwaters under angles of 25° and 50° and concluded that the longshore transport for large angles of wave attack, like 50°, is much smaller than for 15° and 30°. They adjusted the probabilistic approach of Vrijling and came up with the following formula, valid for $H_0 < 10$ and 15°-35°:

$$S_N(x) = 0 \qquad H_0 T_0 < 105$$
$$S_N(x) = 0.00005 (H_0 T_0 - 105)^2 \qquad H_0 T_0 > 105 \qquad (2\text{-}44)$$

Later on [TOMASICCHIO 1994] proposed a model relating longshore transport to stone mobility on the already reshaped profile. In this model displacement of stones takes place during the up- and down-rush in the

direction of incident and reflected waves. The number of stones transported passing a given control section per wave, S_N, is then:

$$S_N \frac{\Delta t}{T_m} = \frac{l_d \cdot \sin\psi_{kb}}{D_{n50}} \frac{N_{od} \cdot \Delta t}{1000 \cdot T_m}$$

$$S_N = \frac{l_d}{D_{n50}} \frac{N_{od}}{1000} \sin\psi_{kb} \qquad (2\text{-}45)$$

During a small time interval, Δt, a particle will pass through a control section if and only if it is removed from the upstream area of extension equal to the displacement length, l_d. The number of stones removed from this area after 1000 waves, per one stone diameter wide strip, is then N_{od}. ψ_{kb} is the characteristic wave obliquity at breaking point and can be evaluated from the characteristics at measure point according to the following procedure (breaker index γ_b, is set to 1.42):

$$H_{kb} = \left(H_k^2 \cdot c_g \cos\psi \cdot \sqrt{\gamma_b / g} \right)^{2/5}$$

$$c_{kb} = \sqrt{g H_{kb} / \gamma_b}$$

$$\sin\psi_{kb} = \sin\psi \cdot c_{kb} / c$$

Where c is the wave celerity, c_g is the wave group celerity and c_{kb} is the characteristic celerity at breaking as a function of the characteristic breaking wave height, H_{kb}.

In the same tests at DHI, which were described in the previous section, [ALIKHANI 1996] investigated also the influence of wave obliquity on the initiation of longshore transport as well as on the longshore transport at the trunk itself both during and after reshaping. Additionally also the influence of storm duration and of short crested directional waves were studied from test results at AAU.

According to the research stones will not move in longitudinal direction for small angles of wave attack as long as the longshore component of the energy flux is not large enough to move them. This led to the following threshold values:

- Reshaping phase: $H_0 T_{0p} > \frac{50}{\sqrt{\sin 2\psi}}$ (2-46)
- After reshaping phase: $H_0 T_{0p} > \frac{75}{\sqrt{\sin 2\psi}}$ (2-47)

Subsequently equation (2-44) for transport after reshaping was modified by including the longshore component of the incident wave energy:

$$S_N = 0.8 \cdot 10^{-6} \sqrt{\cos\psi} \left(H_0 T_{0p} \sqrt{\sin 2\psi} - 75 \right)^2 \qquad (2\text{-}48)$$

According to [ALIKHANI 1996] this formula gives maximum transport for $\psi = 45^\circ$ with decreasing tendency for larger and smaller angles and zero transport for head-on waves and waves parallel to the structure. A small recheck concludes otherwise, namely maximum transport for head-on waves. Taking the threshold values strictly into account however the formula does describe the mentioned tendencies as the threshold value cannot be reached by $\psi = 0^\circ$.

Results from directional tests at AAU showed a reduction in the longshore transport rates due to directional short crested waves. One test with $H_0 = 4$ and $\psi = 60^\circ$ even induced a reduction of 4. Besides this it was found that the longshore transport rate also decreases with increasing number of waves, N. Experimental data fit resulted in an exponential relation:

$$S = \frac{ae^{-bN}}{1000} \tag{2-49}$$

For tests at AAU with $H_0 = 4$ and $\psi = 60^\circ$, $a = 350$.

In [TOMASICCHIO 2007] formula (2-45) was revised for an arbitrary number of waves, N:

$$S_N = \frac{l_d}{D_{n50}} \frac{N_{od}}{N} \sin\psi_{kb} \tag{2-50}$$

This transport can also be given in terms of a volume transport, S_V:

$$S_V = \frac{S_N D_{n50}^3}{(1-n)T_m} \quad \left[cm^3/s\right] \tag{2-51}$$

In this relation n is the porosity defined as the fraction of voids, V_v, over the total volume, V_T. Together with relation (2-38) for N_{od} formula (2-50) has led to satisfactorily results for S_N, even when compared with the longshore transport observed from tests with gravel beaches of Van Hijum and Pilarczyk, as becomes clear from the comparison between observed values and calculated values in Figure 2.12.

However the data for high obliquity observed from tests of Van der Meer and Veldman do not lead to a match. Apparently this model does not incorporate the effect of high obliquity in a correct way. Besides this also the data of longshore transport during reshaping (DHI 3D with armouring effect) result in a scatter showing a sensitivity of displacement and transport toward the armouring phenomenon.

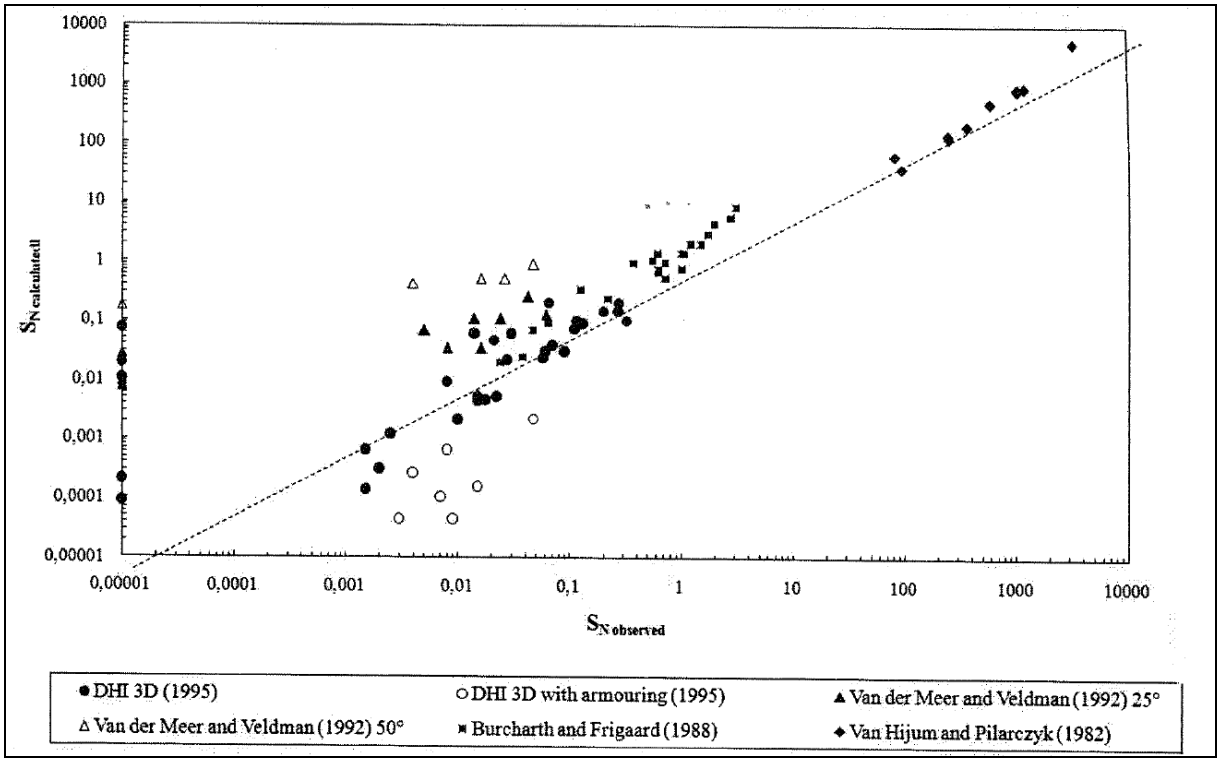

Figure 2.12: Observed and calculated longshore transport S_N, according to formula (2-50) [TOMASICCHIO 2007]

2.4.2 Head

Special attention has to be given to the design of the roundhead, as the head forms a vulnerable part of the breakwater. No real design criteria are determined and a physical model test is usually recommended. To

reinforce the head, normally larger size armour stones are used or the slope is reduced. As is already mentioned in the previous paragraph, [BURCHARTH 1987; BURCHARTH 1988] formulated a criterion for incipient motion for breakwater heads: $H_0 \leq 3$.

Tests at DHI, described by [JUHL 1997], showed erosion and sedimentation patterns around the roundhead. Also the recession at different radial cross sections were compared to the recession of the trunk. This led to a qualitative relationship of Rec at the roundhead per relative wave angle in relation to the observed value for Rec at the trunk.

2.4.3 *Crest and rear slope during overtopping*

According to model tests of [VAN DER MEER 1992], the crest level, R_c, determines the damage to the inner slope. Some design suggestions were given:

$$\begin{aligned} R_c / H_s s_{0p}^{1/3} &= 0.25 \text{ (start of damage)} \\ R_c / H_s s_{0p}^{1/3} &= 0.21 \text{ (moderate damage)} \\ R_c / H_s s_{0p}^{1/3} &= 0.17 \text{ (severe damage)} \end{aligned} \quad (2\text{-}52)$$

Andersen et al. [PIANC MarCom 2003] came up with the following criterion for rear side armour layer:

$$R_c > \tan\alpha \frac{H_{m0}}{\sqrt{s_{m02}}} - \Delta D_{n50} \frac{\mu\cos\beta - \sin\beta}{C_D + \mu C_L} \quad (2\text{-}53)$$

α and β are respectively the sea and rear side slope, C_D and C_L the drag and lift coefficient, s_{m02} represents the wave steepness based on T_{m02}, further explained in section 3.4.3, and μ the resistance against rolling and sliding.

2.5 Research Summary

In this paragraph a small overview is given of the background of the research described in the previous paragraphs. From here the gaps within the current knowledge can easily be determined, which will be used as basis for further research in the course of this thesis. As the focus of the remainder of this thesis lies on both the two-dimensional deformation and longshore transport, only these two topics are elaborated in this paragraph.

2.5.1 *Two-dimensional deformation*

The deformation parameters derived by Van der Meer can be used to describe the deformation of rubble mound slopes. However the grading in the tests described in [VAN DER MEER 1988; VAN DER MEER 1992] was varied only within the following range of $f_g = 1.25 - 2.25$ and no influence of grading was included in the derivation of formulas (2-12) to (2-20). Regarding the angle of wave attack, the tests were conducted for the range of 0-50 degrees. To discount wave obliquity in the formulas for deformation a reduction factor of $\cos\psi$ was added.

Merli expanded the data set by conducting tests in a wave flume to investigate the effect of grading. For this purpose only tests with head-on waves were executed within a range for grading of 2.7-17.7. In [MERLI 2009] the relations of Van der Meer were adapted to take into account this effect of grading leading to formulas (2-25) to (2-27).

Regarding the Recession length three different relations were derived for head-on waves, all describing the effect of stone grading in a totally different way. Hall and Kao tested in the range for grading of $1.35 < f_g < 5.4$

and found an inverted quadratic relation for Rec, described by formula (2-28), with a maximum at $f_g = 3$. For the range of $1.3 < f_g < 1.8$ a totally different quadratic relation, formula (2-31), was derived by Menze and Tørum and Krogh. The third and last relation is formula (2-32), which was derived by Merli who found a linear relation for Rec regarding the stone grading.

Summarizing it can be stated that although the effect of wide grading on the deformation parameters was already investigated, the combination of both wide grading and oblique waves is still unknown. Additionally the found relations for Rec concerning the effect of grading contradict each other. Therefore the tests described in the next chapter focus to a large extent on the effect of both the stone grading and oblique waves on the deformation.

2.5.2 *Longshore transport*

Also for the description of the longshore transport several formulas were already derived. While for relations (2-40) and (2-41), derived by respectively [VAN HIJUM 1982] and [VAN DER MEER 1988] for gravel beaches, the effect of wave obliquity was included, no effect of wave obliquity was discounted in formulas (2-43) and (2-44) for berm breakwaters. To include the effect of wave obliquity [ALIKHANI 1996] adapted these relations and reformulated them into formula (2-48). In here maximum transport was assumed for an angle of wave attack of 45° with decreasing tendency for both larger and smaller angles.

A totally different approach, by linking stone mobility to the longshore transport, is to calculate the longshore transport with the help of formula (2-50). This relation includes various different parameters and shows a decreasing tendency from 30° to 45° which is more in line with initial observations done by Van der Meer and Veldman.

Although the last relation mentioned here was also compared with data during reshaping phase, these relations were especially formulated for berm breakwaters after reshaping, when the equilibrium profile has already been reached. Moreover the effect of grading was not investigated at all and only very narrow to narrow graded stone material was used in the tests on which above-mentioned relations were based.

Accordingly the tests described in the next chapter concentrate to a great degree on the influence of (wide) grading on the longshore transport during reshaping. A second aim is to clear up the ambiguous tendencies regarding the angle of wave attack, especially for the range between 30° and 45°.

3. Experimental set-up

Phenomena like profile deformation and especially longshore transport are difficult to measure in real scale and cannot be easily described or interpreted analytically. Physical model tests are then a convenient way to reproduce these phenomena in a reduced geometrical scale.

In this chapter the test set-up for the upcoming tests will be described. Firstly an overview is given of the most important parameters after which decisions are explained concerning the parameters to vary. This is followed by explaining the pitfalls of scaling these parameters; the scale effects that can occur during the scaling process itself are discussed. Next the design of the breakwater model and its composition are elaborated in paragraph 3.3. Paragraph 3.4 deals with the wave generation in the course of which respectively the wave basin, the generators and actual hydraulic load are discussed. Subsequently the different measuring instruments used will be discussed in paragraph 3.5. Data then resulting from the measurements were obtained by computer which will be elaborated in paragraph 3.6. After that paragraph 3.7 will give a brief summary in the form of the testing schedule and the chapter will end with an inventory of possible sources of errors.

3.1 Overview

As was mentioned in the short introduction of this chapter, physical model tests are used to investigate phenomena which are impossible to measure in real life. Although the aim of the current tests was not to analyse the behaviour of a specific existing structure, its purpose was to give a general answer about the influence of a few specific parameters in the response of an arbitrary core exposed to wave attack. Therefore it was still of great importance that reality was reproduced in a correct way. Foremost this meant that scaling of the parameters had to be done without creating undesirable side-effects.

Therefore firstly the normative parameters needed to be defined. According to [MERLI 2009] Hughes suggested a classification of governing parameters which affect the behaviour of a coastal structure:

- Geometrical parameters: dimensions structure, crest height and width, outer slope (α), etc.
- Stone characteristics: stone density (ρ_s), stone dimensions (D_{n50}), grading $\left(f_g = \frac{D_{n85}}{D_{n15}} \right)$, porosity (n), stone shape, etc.
- Hydraulic load: wave height (H_s), wave period (T_p), angle of wave attack (ψ), mean water level (h), number of waves (N), etc.

As the main purpose of this research is to investigate the influence of grading on the deformation and longshore transport, f_g was the main parameter which was varied. Also because previous research was limited to only narrow grading, one half of the tests was conducted with more or less the same narrow grading to act as reference. The other half of the tests was carried out with a very wide grading in order to reproduce the grading of core material.

Seeing that the current investigation includes deformation as well as longshore transport, also the angle of wave attack needed to be varied. For deformation this means that the formulas defined for head-on waves will be compared by tests with head-on waves. Head-on waves however do not induce longshore transport and it was already concluded from previous research that a change in angle of wave incidence leads to a change in transport.

Furthermore also the hydraulic load was varied as it has a serious affect on the processes under investigation. The hydraulic load can to a large extent be described by the following three parameters: wave height (H_s), wave period (T_p) and wave steepness (s_p). In the current tests the choice was made to keep the s_p constant

while varying the other two. By doing this two different wave spectra were created: a high wave load and a low wave load.

As it is common practice in laboratory tests that the influence of one specific parameter is investigated while the others are kept constant, this was also the case for the other parameters concerned in the present tests. Although the nominal diameter, D_{n50}, is directly related to the stability of a rubble mound breakwater, it was decided to keep D_{n50} equal for each test. Also the density, stone shape, number of waves and last but not least the water depth were kept as constant as possible. In this way comparable tests were carried out so that the effect of the three varying parameters could be better observed.

The main observations were then done by means of two different measurements:

- Deformation was observed by profile measurements.
- Longshore transport was observed by measuring the stone displacements in longitudinal direction.

All in all it can be said that the test set-up used by [VANLISHOUT 2008] formed the basis for the new test set-up. Although the topic of this work did not correspond with the current tests, also a breakwater model was tested in the same wave basin under more or less similar wave conditions while using the same method of wave measurements. Furthermore [MERLI 2009] served as an example for the breakwater model itself and for the process of mixing the grading. Lastly the measuring methods of the longshore transport could be compared with the model and methods used during the tests carried out by [ALIKHANI 1996] at AAU.

3.2 Scale effects

In a scale model, the scale of a certain parameter x can be defined in the form of a prototype-to-model scale ratio λ_x. Incorrect reproduction of the water-structure interaction results in scale effects. Three important forces can therefore be defined: viscosity forces which are governed by Reynolds's law, gravitational forces described with Froude's law and surface tension forces (Weber's law). Effects resulting from ignoring these forces are called scale effects. In this thesis only the first two are elaborated below as they are considered normative:

- Froude's law: $Fr = \frac{U}{\sqrt{gl}}$ (3-1)
- Reynolds's number: $\mathrm{Re} = \frac{Ul}{\nu}$ (3-2)

In these formulas U and l represent respectively the velocity and length, while ν stands for the kinematic viscosity of water.

Only by fulfilling both Froude's and Reynolds's law, reliable results can be acquired. However that is not possible as the relations between the parameters in both laws contradict each other: $\lambda_U / \sqrt{\lambda_l} \neq \lambda_U \lambda_l$. So scale effects cannot be totally avoided while performing scale model tests.

Under the conditions of this particular scale model the viscous damping of the waves was considered to be negligible as the water depth (>2cm), wave heights (>5cm) and wave periods (>0.35s) were sufficiently high enough ([CIRIA 2007]). Therefore it is custom to scale this kind of hydraulic wave models according to Froude's law. In this case the time and velocity was scaled

Process	Relevant forces	Similitude law	Critical limits
Wave propagation	Gravity force Friction forces Surface tension	Fr_W, Re_W, We	$Re_W > Re_{W,crit} = 1x10^4$ T > 0,35 s; h > 2,0 cm
Wave breaking	Gravity force Friction forces Surface tension	Fr_W, Re_W, We	$Re_W > Re_{W,crit} = 1x10^4$ T > 0,35 s; h > 2,0 cm
Wave run-up	Gravity force Friction forces Surface tension	Fr_A, Fr_q Re_q, We	$Re_q > Re_{q,crit} = 10^3$ $We > We_{crit} = 10$
Wave overtopping	Gravity force Friction forces Surface tension	Fr_A , Fr_q, Re_q, We	$Re_q > Re_{q,crit} = 10^3$ $We > We_{crit} = 10$

With: $Fr_W = c/(g \cdot h)^{1/2}$; $Fr_A = v_A/(g \cdot h_A)^{1/2}$; $Fr_q = v_A/(2 \cdot g \cdot R_u)$; $Re_W = c \cdot h/\nu$; $Re_q = (R_u - R_c)^2/(\nu \cdot T)$; $We = v_A \cdot h_A \cdot \rho_W/\sigma_W$

Figure 3.1: Relevant forces and critical limits

according to: $\lambda_t = \lambda_U = \sqrt{\lambda_l}$

For the scaling of core material usually a slightly different approach is used. Core material used in these scale models is then out of proportionally large compared to the material used for the armour layer. Otherwise the scale effects by ignoring the viscosity forces in the pores of the core are not negligible anymore. In [BURCHARTH 1999] this alternative scaling process is described on the basis of Forchheimer equation, which will not further be elaborated:

$$I = \alpha U + b|U|U + c\frac{\partial U}{\partial t} \qquad (3\text{-}3)$$

Apart from these scale effects also model or laboratory effects could be expected due to an incorrect reproduction of the model structure and waves and currents or due to boundary conditions of the wave basin (wave generator, side walls, beach, etc.). The same holds true for measurement effects resulting from the use of different measuring techniques, which could influence the comparison between model and reality significantly.

3.3 Physical model

3.3.1 Consideration and dimensions

As one of the main goals of the experiments is to investigate the longshore transport, a sufficient long breakwater with loose stones was desired. To accomplish the tests without blocking the wave basin the length of the breakwater could not be too long. Also the longer the breakwater the more complicated and laborious the process of rebuilding and turning would be. For that reason a length of 6.7m was presumed. Different angles of wave attack were achieved by turning the breakwater itself in between tests as is shown in Figure 3.2. In this fashion a total of three different angles were tested ranging from 0° to 45°, in which 0° means perpendicular to the breakwater.

Figure 3.2: Turning process in between experiments

This length however together with the construction of stones would still make rotation difficult, if not impossible. Therefore the structure was divided in four separate pieces: two middle pieces with a length of 1.75 and two end pieces with a length of 1.6m length. All four pieces were made up of a multiplex floor board reinforced with a steel frame and equipped with four hoisting eyes, so the separate parts could be hoisted with

the laboratory crane. Figure 3.3 display the different sections together with the additional reinforcement and hoisting constructions.

Figure 3.3: Four sections together with reinforced ground plate

To minimize preparation time even further and make rebuilding easier, also the base of the breakwater was fixed leaving only a small strip of loose stones available for possible deformation. The area consisting of loose stones was then based on the current formulas for berm/crest recession. At both the roundheads this area was larger as more damage could be expected in these areas while less knowledge was available about the deformation.

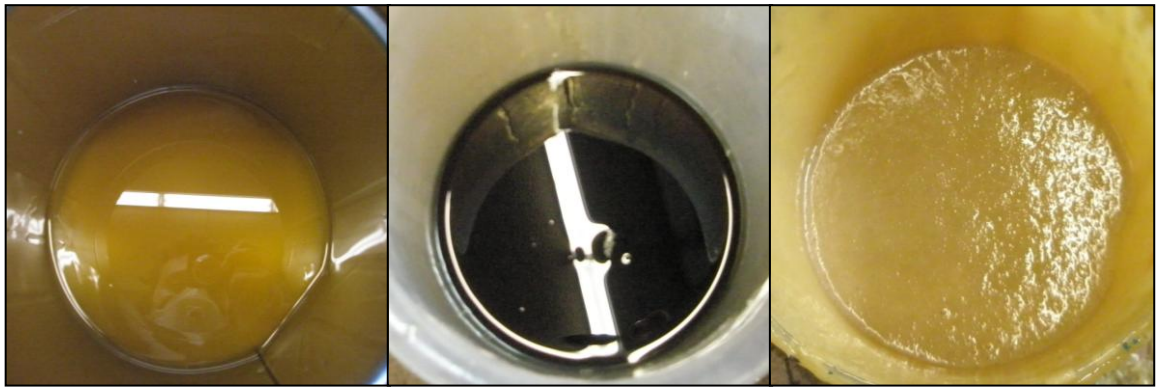

Figure 3.4: Mixing the elastocoast; from left to right: A component, B-component and mixture

Fixing the base on top of the floor boards was established by gluing the stones of one stone class $\left(f_g = 1.3 \right)$ together using polyurethane called Elastocoast. Elastocoast is composed of an A- and B-component (harder) which must be mixed in the right proportions (A (elasto): B (iso-harder) = 100:65) before usage (figure). After mixing with stones (ratio stone: polyurethane = 100:2.5) it creates a thin film around the stones while preserving the permeability of the breakwater at the same time. To mix the Elastocoast with the stones for the current tests a concrete mixer was used after which the mixture could be applied in the model and harden. Figure 3.4 Figure 3.5 show the total process of mixing. Stones processed in this way had to be clean and surface-dry on beforehand. Therefore before the stones used in the tests could be processed, dust and dirt were removed by rinsing the delivered big bags with water. Then several weeks of drying passed by before further processing took place.

Throughout the whole test sequence the same fixed part was used, even during the tests with the wide grading $\left(f_g = 6 \right)$. Only the part composed of loose stones formed the test area where two different gradings $f_g = 1.3$ and 6 were tested. These gradings were obtained by mixing different stone classes while retaining the same nominal diameter.

Figure 3.5: Process of mixing the stones with Elastocoast and application onto the model

Although the breakwater model was not meant to reproduce a specific existing structure, the geometric scale of the model could be considered as a scale of 1:20. Figure 3.6 to Figure 3.8 show the design of the breakwater model. The base of the model had a length of 6.7m and a width of 2.2m. With a slope of 2:3 and a height of 0.55m this led to a crest width of 0.55m. The radiuses of respectively the crest and the base of the roundhead were 0.275m and 1.1m. In the following drawings the test section is represented by the hatched part. Two strips of 0.10m filled with dyed stones were added to accommodate for visual measurements concerning the longshore transport.

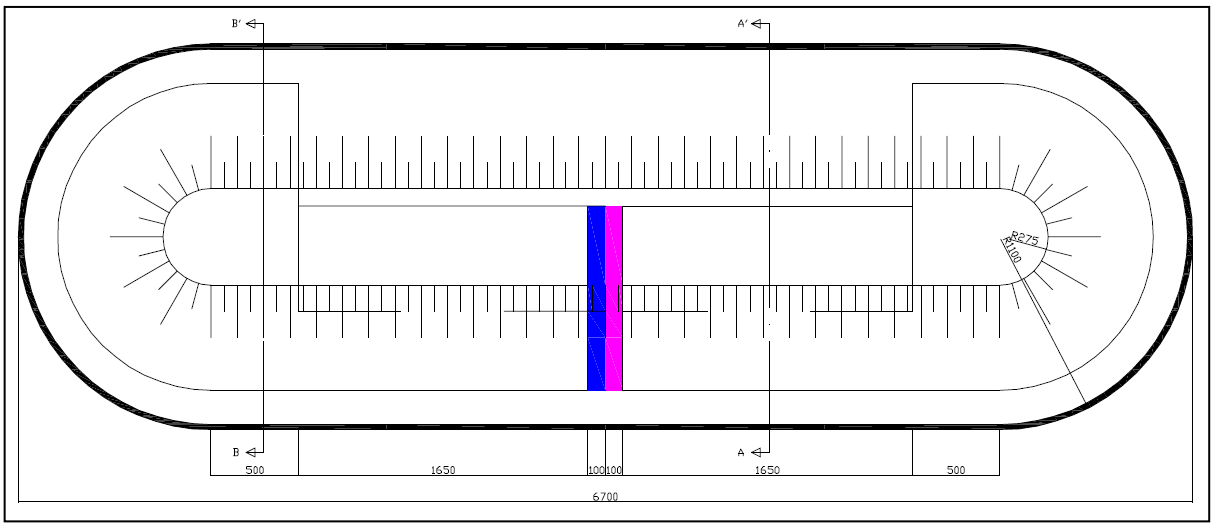

Figure 3.6: Top view of the breakwater model

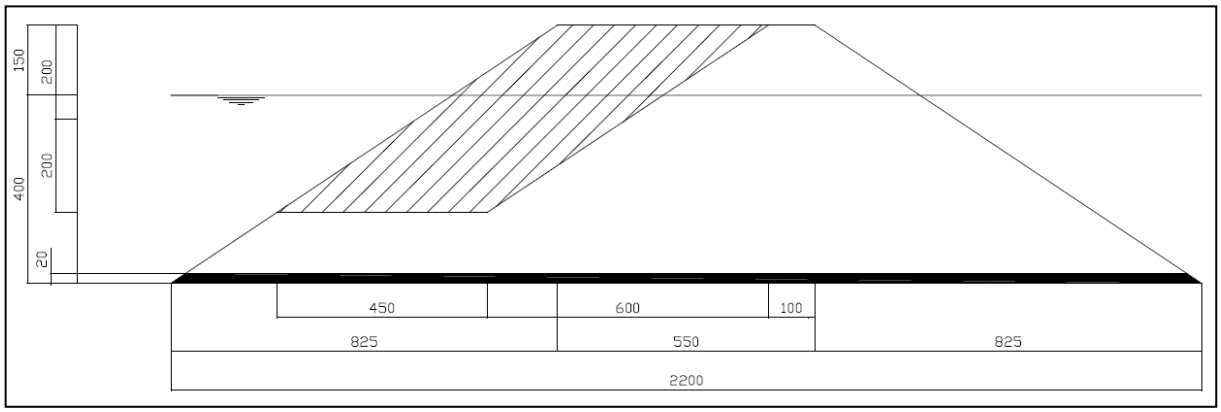

Figure 3.7: Cross-section A-A'

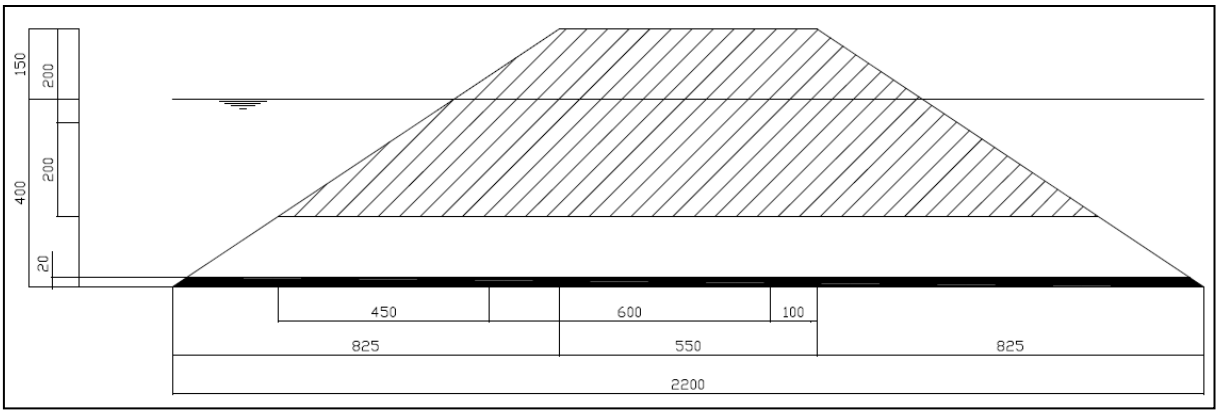

Figure 3.8: Cross-section B-B'

3.3.2 Stone characteristics

Both the fixed and the loose part of the breakwater model were composed of stones. As the research currently described handles exposed cores, no armour layer was present. For that reason the material used could be scaled down in the same manner as described for armour layers. No additional scaling was needed. The stones then used to build the model had a nominal diameter of $D_{n50} = 12.1\text{mm}$. However before the tests could be executed it was important to know also other characteristics of the stones used. Apart from stone size and weight, also grading and stone shape needed to be determined.

Stone classes

In total five different stone classes were used to compose the two different gradings. As none of the materials, optional for usage, could be found for the whole range needed, different materials had to be used for both the finest and coarsest fractions. So the finest fraction consisted of taunus quartz 4-8mm and the coarsest material (30-60mm) of a mixture of several stone materials including basalt. The three middle fractions consisted of yellow sun (8-11, 11-16 and 20-40mm), which is a kind of limestone. Figure 3.9 shows the five different fractions: above from left to right respectively the fractions 4-8mm, 8-11m and 11-16mm; below on the left side 20-40mm and on the right 30-60mm.

Figure 3.9: Samples of the five different fractions; 4-8mm, 8-11mm, 11-16mm, 20-40mm and 30-60mm

Before mixing of the gradings could commence, the grain-size distributions of the different classes needed to be determined by weighing. The density was then calculated after weighing a stone sample both dry (M) and in water (M_w) with the following relation:

$$\rho_s = \frac{M - M_w}{M}\rho_w \qquad (3\text{-}4)$$

For the yellow sun fraction this led to a mean value of $\rho_s = 2650\,kg/m^3$. And although the taunus quartz was slightly lighter $\left(\rho_s = 2640\,kg/m^3\right)$, the 30-60mm fraction was considerably heavier $\left(\rho_s = 2750\,kg/m^3\right)$.

Grading

By means of weighing for every stone fraction also the stone-size distribution was determined of which values for D_{n15}, D_{n50} and D_{n85} could be derived. In Figure 3.10 the different distributions are displayed.

These five fractions were then used to mix two different gradings while keeping the D_{n50} the same. For the narrow grading this meant only the 11-16mm stone class was used, which has a D_{n50} of 12.1mm and a value for f_g of 1.3. The wide grading was composed in such way that a realistic mixture was generated comparable to a breakwater core consisting of quarry run. Assuming a real time quarry run mixture of 3-640kg with a value for f_g of 6, corresponding values were found while scaling parameters down with a geometrical scale of 1:20. Table 3.1 shows the resulting values for the two different gradings while comparing the wide grading with the accompanying real time values.

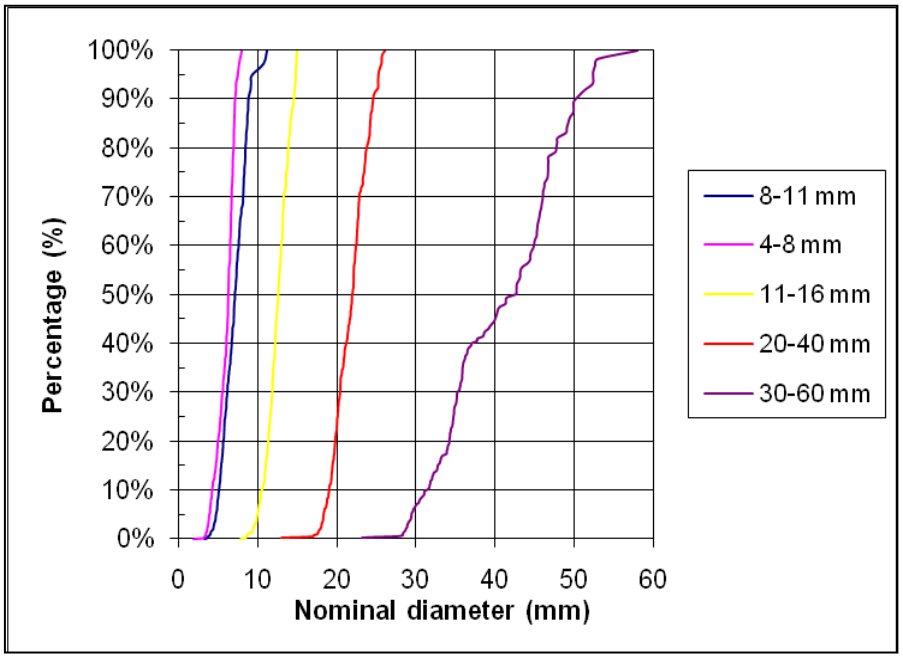

Figure 3.10: Stone grading for different stone fractions used

Table 3.1: Nominal diameters and weights of narrow and wide grading

Grading	D_{n85}/D_{n15} = 1.3	D_{n85}/D_{n15} = 6	D_{n85}/D_{n15} = 6 (scale factor 20)	W(kg) $\left(\rho_s D_n^3\right)$
D_{n15} (mm)	10.4	5.2	103.7	3.0 (W_{15})
D_{n50} (mm)	12.1	12.1	241.6	37.6 (W_{50})
D_{n85} (mm)	13.8	31.1	621.7	640.7 (W_{85})
D_{n85}/D_{n15}	1.33	6.00	6.00	

Subsequently the percentage of every stone fraction in the total mixture was determined so that the desirable grading was achieved. In Figure 3.11 the resulting stone-size distributions are visualised for both the narrowly and widely graded mixture.

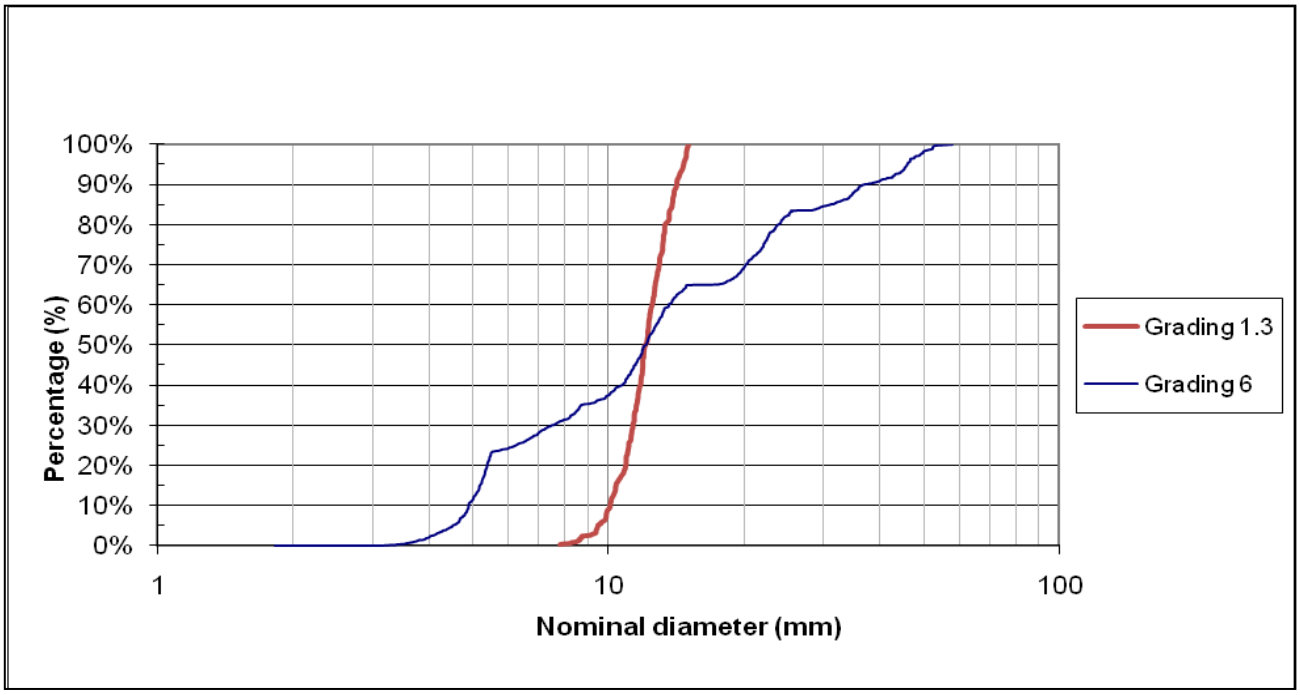

Figure 3.11: Distributions narrow and wide grading

To mix the wide grading every stone fraction was weighed into portions and mixed in a concrete mixer. Due to limitations in the amount of stones used and the impossibility of separating the mixture again after mixing, mixing in this manner took place only once during the experiments. Firstly the tests with the narrow grading were conducted. Then the mixing took place after which the other half of the test sequence was executed with the wide grading. Figure 3.12 gives an impression of the final results of the two different gradings.

Figure 3.12: Final results of the mixture on the breakwater model

Stone shape

Next to the above-mentioned parameters also the stone shape characteristics Lt ratio and BLc were determined. These are respectively the length-to-thickness ratio, defined by [CIRIA 2007] as maximum length divided by minimum distance between parallel lines through which the particle would just pass, and the blockiness, which can be defined as the volume of a stone divided by the volume of the smallest enclosing XYZ orthogonal box. In formula form the latter comes down to:

$$BLc = \left(\frac{M}{\rho} \cdot \frac{1}{XYZ} \right) \cdot 100 \quad \text{[CIRIA 2007]} \qquad (3\text{-}5)$$

A summary of the grain size distribution of the separate fractions together with the density and two shape parameters is given in Table 3.2. Additionally the percentages of each stone class in the final mixtures are given.

Table 3.2: Summary stone characteristics

Stone class	D_{n15} (mm)	D_{n50} (mm)	D_{n85} (mm)	Grading	Density (kg/m^3)	Lt ratio	BLc	Percentage in mixture grading 1.3	Percentage in mixture grading 6
4-8	4.7	6.2	7.0	1.48	2636.0	2.20	43.8		23.5
8-11	5.4	7.1	8.7	1.62	2649.0	2.89	41.4		11.5
11-16	10.4	12.1	13.8	1.33	2648.7	2.19	41.1	100	30.0
20-40	19.4	21.9	24.2	1.24	2666.8	2.10	40.6		18.5
30-60	32.8	42.6	49.2	1.50	2747.2	2.21	45.1		16.5

3.4 Wave generation

3.4.1 Wave basin

In this study the wave basin at the water lab of Delft University of Technology was used. The dimensions of this wave basin are 28.60 x 16.60m with a maximum depth of 0.60m. The last 1.60m is actually a gulley connected to the basin which is used to fill up the basin, so the effective width is 15m. During the tests a water depth of 0.40m was used.

The bed is fixed and made of concrete. It is horizontal until halfway a transition takes place into a sloping beach. This beach has a slope of 1:30 and higher upwards the beach a layer of coarse rubble was placed in order to dampen the waves and minimize the reflection back to the breakwater. For the same reason the side walls of the basin were covered with a sloping layer of coarse rubble.

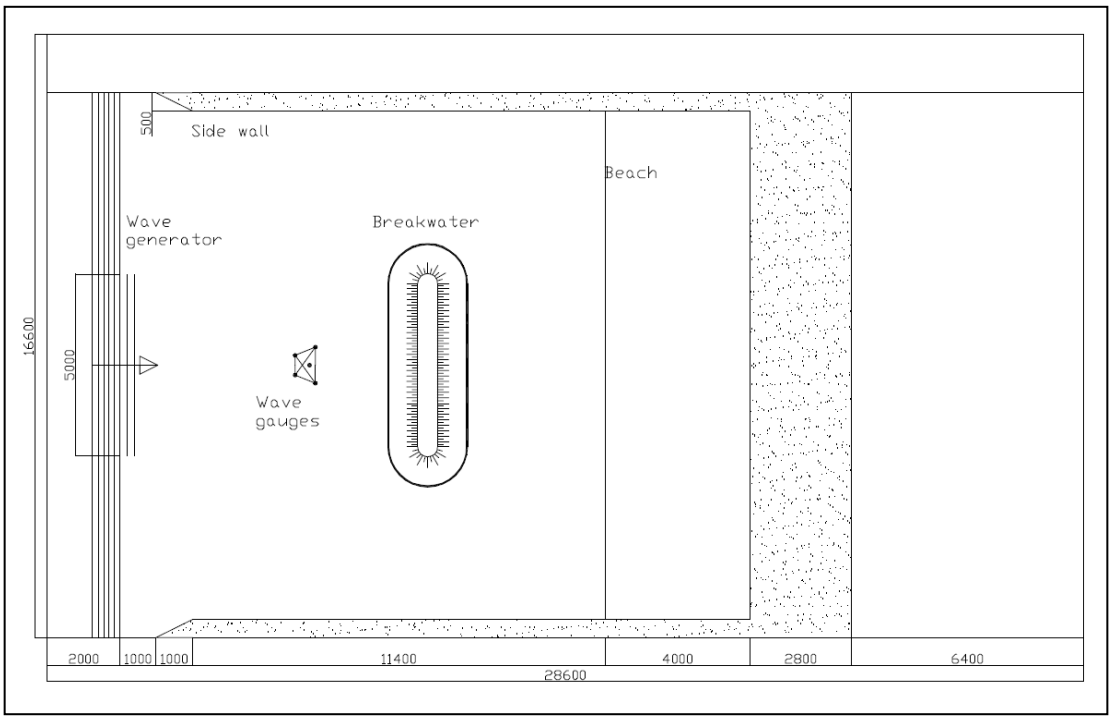

Figure 3.13: Top view test set-up

3.4.2 Wave generators

Three hydraulic piston-type wave generators with a length of 5m each were used to generate all kinds of waves, regular and irregular. The generators consisted each of one wave board which was driven from one meter above the bed and has a maximum stroke of 0.26m. They were placed alongside each other so they

spanned the entire width of the basin. At the same time they were synchronized to produce long crested waves, resulting in perpendicular wave generation.

Before the required wave record could be generated, a spectrum needed to be created. This spectrum was then described in a file containing all the main input values needed for wave generation. This file was then translated to a data file with the drive signals using the programme MultiLin and sent to the wave generators.

Figure 3.14: Wave generators

Waves generated in this fashion do not naturally lead to intended waves in the basin. As the wave generators were not equipped with a reflection compensator, waves reflected by the model to the wave boards were not dissipated, but re-reflected again towards the breakwater. This could result in higher wave energies, apart from the initially generated waves, and prematurely breaking of these higher waves. Formation of standing waves, thereby compromising the incident wave spectrum, was also a possibility. By testing a breakwater with a length significantly smaller than the width of the basin, enough space would be left open for wave energy to disperse. To minimize the chance of occurrence of standing waves even further, the signal sent to the generator was set at 90% capacity. Aside from this, previous experiences with wave generation have led to calibration of the driving signal in relation to actual occurring waves. This calibration already reckons to some extent with acting reflection.

3.4.3 Hydraulic load

For the wave load itself a JONSWAP (Joint North Sea Wave Programme) spectrum was used. This spectrum is widely used in research and represents a wave spectrum with limited fetch and storm duration. Because the fetch is limited no transition to a fully developed sea state takes place. Despite this limitation the spectrum could also be used for arbitrary wind conditions in deep water, since it has turned out to be rather universal.

A JONSWAP spectrum can be expressed as a variance density spectrum defined by [HOLTHUIJSEN 2007]:

$$E_{JONSWAP}(f) = \frac{\alpha_f g^2}{(2\pi)^4 f^5} \exp\left[-\frac{5}{4}\left(\frac{f}{f_p}\right)^{-4}\right] \gamma_f^{\exp\left[-\frac{1}{2}\left(\frac{f/f_p-1}{\sigma}\right)^2\right]}$$

$$f_p = 3.5\left[\frac{g^2 F_l}{U_{10}^3}\right]^{-0.33} ; \alpha = 0.076\left[\frac{gF_l}{U_{10}^2}\right]^{-0.22} ; 1 \le \gamma_f \le 7 \qquad (3\text{-}6)$$

where:

$E_{JONSWAP}(f)$	: variance density	$[m^2 s]$
f	: frequency	$[Hz]$
f_p	: peak frequency	$[Hz]$
g	: gravitational acceleration	$[m/s^2]$
α_f	: energy scale parameter	$[-]$
γ_f	: peak enhancement factor (=3.3)	$[-]$
σ	: peak width parameter	$[-]$
	$\sigma_a = 0.07$ if $f \le f_p$	
	$\sigma_b = 0.09$ if $f \ge f_p$	
F_l	: fetch length	$[km]$
U_{10}	: wind velocity at 10m elevation above sea surface	$[m/s]$

The n-th order moment of $E_{JONSWAP}(f)$ represents the area underneath spectrum m_n and can be calculated using the following formula:

$$m_n = \int_0^\infty f^n E(f) df \qquad \text{for } n = \ldots, -2, -1, 0, 1, 2, \ldots \tag{3-7}$$

m_0 is the 0th-order moment and is directly related to the wave energy and significant wave height, according to:

$$\begin{aligned} H_s &\approx H_{m_0} = 4\sqrt{m_0} \\ E &= \tfrac{1}{16}\rho g H_{m_0}^2 = \rho g m_0 \end{aligned} \tag{3-8}$$

From the spectrum it is also possible to determine mean wave period, T_m. [HOLTHUIJSEN 2007] mentioned the following relation:

$$T_m = T_{m02} = \sqrt{\frac{m_0}{m_2}} \tag{3-9}$$

As m_2 in relation (3-9) is rather sensitive to small errors or variations in the analysis, also another relation was defined which is less dependent on high-frequency noise:

$$T_m = T_{m01} = \frac{m_0}{m_1} \tag{3-10}$$

Because the experiments conducted here in the wave basin had a rather three-dimensional nature, a unidirectional spectrum as described above could be inadequate. A multi-directional wave spectrum is then needed to describe the occurring wave spectra in both the frequency and spatial domains. [VANLISHOUT 2008] refers to a definition of multi-directional wave $S(f,\theta)$ formulated by Hashimoto:

$$\begin{aligned} &S(f,\theta) = E_{JONSWAP}(f) \cdot G(\theta \mid f) \\ &\int_{-\pi}^{\pi} S(f,\theta)\, d\theta = E_{JONSWAP}(f) \\ &\int_{-\pi}^{\pi} G(\theta \mid f)\, d\theta = 1 \end{aligned} \tag{3-11}$$

In this formula θ stands for the wave propagation directions and $G(\theta \mid f)$ represents the directional spreading function, defined by Van Dongeren ([VANLISHOUT 2008]), which describes the distribution of wave energy on propagation direction:

$$\begin{aligned} &G(\theta \mid f) = \frac{1}{\sqrt{\pi}} \frac{\Gamma(s+1)}{\Gamma(s+0.5)} \cos^{2s}(\theta - \theta_0) \\ &-\pi \le \theta \le \pi \end{aligned} \tag{3-12}$$

In this equation Γ is defined as the standard Gamma function, θ_0 as the main wave propagation direction and s as a spreading parameter. A low value of s characterises a very wide directional spread belonging to short crested waves (for example $s = 5$). On the other hand long crested waves, propagating in one direction, have a very narrow directional spread and a high value of s. Since the wave generators used for the current tests can only generate waves in one direction, long crested waves with little energy spread were expected. Accordingly all wave energy would be concentrated in a very narrow range around $\theta_0 = 0^\circ$ $(s = 75)$. So in this case the wave spectrum of the drive signal could still be based on only the unidirectional spectrum described above.

For the current tests the following two wave loads were used, one with a lower energy spectrum and the second with a higher energy spectrum. In both wave spectra the fictitious peak wave steepness, s_{0p}, is kept constant:

Table 3.3: Generated wave parameters

Test wave load	$H_{m0}[m]$	$T_p[s]$	$s_{0p}[-]$
T1	0.08	1.30	0.030
T2	0.10	1.45	0.030

Apart from these parameters other input values, needed by the software programme MultiLin, for the generation of the wave spectra, included $h = 0.4$, $\gamma_f = 3.3$, $\sigma_a = 0.07$ and $\sigma_b = 0.09$. Furthermore durations of 50 and 30min were imported to generate wave records describing one full range of respectively the lower and higher spectra. After this duration the same wave records would start all over again. Due to limitations of MultiLin, it was however not possible to make this duration longer, while a wave record with a shorter duration would probably not be able to describe the full range.

The total durations of the tests were varied for both spectra. Tests with the lower spectrum lasted 65min and with the higher spectrum 72.5min. This corresponded to approximately 3500 waves.

3.5 Measuring devices

3.5.1 Wave gauges

Although the acquisition of wave data was not the main goal of the tests, it was very important to know under what conditions the tests took place. A wave spectrum generated by the computer and executed by the wave board does not naturally lead to exactly the same spectrum in the basin, especially when other factors like reflection and diffraction can play a part.

The water surface elevation in front of the breakwater can be measured with a resistive wave gauge. This sort of wave gauge consists of two thin poles next to each other and during operation a high frequency alternating voltage is passing through the wires. By recording the conductance between the two poles, the water level can be found as the conductance is linearly related to the surface elevation $(1V : 0.025m)$. By using several wave gauges placed in a spatial disposition, the occurring wave spectrum can be observed together with the directional spectrum. At least four wave gauges are needed for this purpose. For the tests described here, five wave gauges were used. The set-up of the wave gauges used is displayed in the figure below. It is the same set-up as is used in [VANLISHOUT 2008].

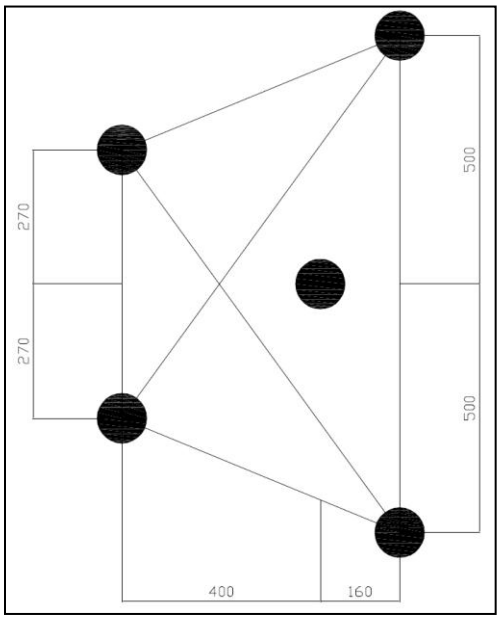

Figure 3.15: Positioning wave gauges

Raw data coming from the five different wave gauges from one test run were recorded in one asci-file, each column representing one wave gauge. Before testing the wave gauges needed to be calibrated. A second calibration took place halfway the test sequence to check the sensitivity of the gauges.

3.5.2 *Laser profiling*

One way of obtaining the occurring damage, and from that the longshore transport, is by measuring the profile of the breakwater model before and directly after the tests. The difference between the two profiles should deliver the areas of erosion and deposition.

To make these measurements possible a laser was built in a cart (Figure 3.16) running along a beam which was placed on a measuring frame (Figure 3.17). The cart was run manually using a handle attached to one end of the beam. At the other end of the beam a pulse counter delivered 500 pulses per rotation. Then this came down to one pulse per 1.005mm and one profile measurement per pulse. From there it was then possible to measure one cross-section of the profile. By moving the beam itself along the measuring frame several different cross-sections could be measured.

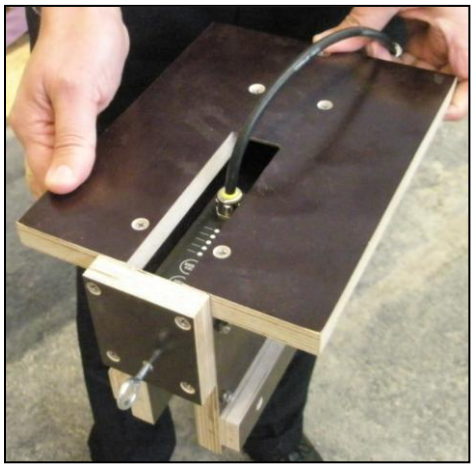

Figure 3.16: Cart containing laser device

Measuring the roundhead was done using a slightly different approach. In this case one end of the beam was hooked on a hinge. The beam itself was then rotated around this point and the cross-sectional profiles were measured radially, as is shown in Figure 3.18. Because of an unavoidable gap between the cart and hinge, the first 10cm from the centre of the roundhead were immeasurable.

Figure 3.17: Measuring frame during trunk measurement

Figure 3.18: Measuring frame during measurement of the roundhead

In the fashion described above one half of the breakwater model can be measured at a time. Before the other half could be measured, the measuring frame needed to be rotated and moved with a crane. Measurements were taken according to the following cross-sectional plan, displayed in Figure 3.19:

- At the roundhead every 15°.
- At the trunk every 0.5m.
- Around the colour beams every 0.1m.

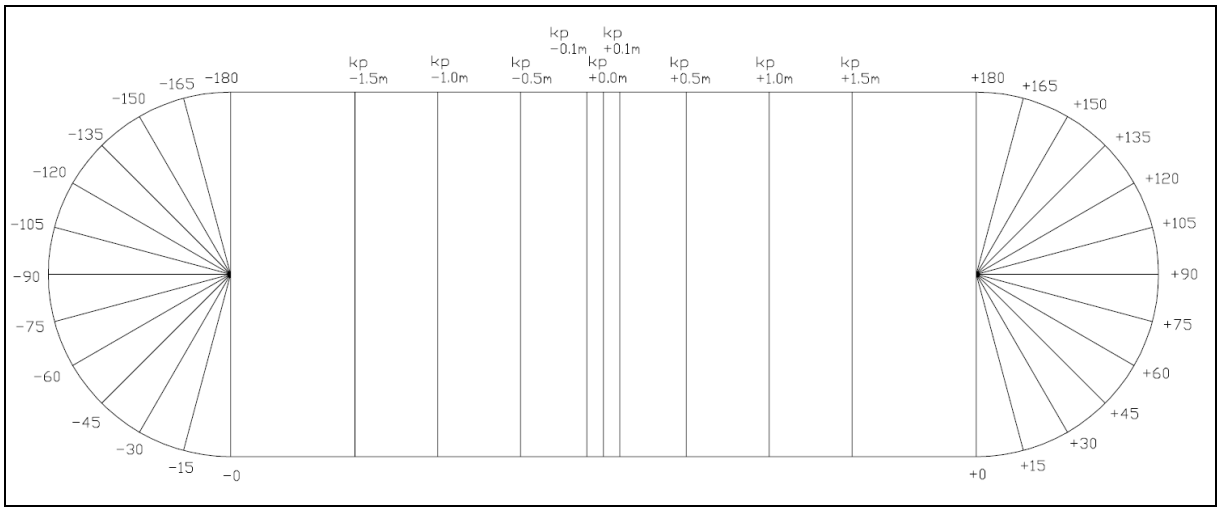

Figure 3.19: Cross-sectional measuring plan

Due to extensive damage sometimes additional measurements, providing extra information, were necessary at the roundhead.

3.5.3 Cameras

Another way to measure the reshaping process and longshore transport is by using a video camera. To make visual measuring possible, two 0.1m wide strips of loose stones in the middle of the testing section were painted. This painting took place in advance using a concrete mill, which provided sufficient cover while preventing the stones from being glued to each other.

During the tests the camera was placed on top of the laboratory crane. Because of the small sizes of the stones used, the camera had to be zoomed sufficiently so separate stones could be recognised from the footage. For this reason the actual filmed area was limited to the colour bands itself and a 1m wide area directly next to these colour bands. The observations were made during the reshaping process.

During some tests a second camera was used, which captured the deformation of the left or right roundhead in time.

3.5.4 Alternative determination of the stone displacement

Registering the longshore transport in the manner described in the section above turned out to be rather difficult. Firstly the longshore transport proved to be larger than expected. Secondly following the stones was complicated by the two-dimensional deformation which covered the transported stones as quickly as the stones itself were released.

The alternative measurement used was quite time consuming and came down to the digging up and counting of each displaced coloured stone afterwards. Accordingly the left half of the breakwater was divided in four different sections with a width of 0.5m. The stones originating from the two colour bands were then counted per colour per section and the stones found on the roundhead formed the rest (a fifth data point). For the stones originating from the pink colour band even a sixth section and corresponding data point was generated, namely the amount of pink stones inside the 0.1m wide blue colour band.

3.6 Data acquisition

Data generated from both the wave gauges as the laser profiling were sent to the computer. Here both data sets were processed with the same software package called DasyLab (Data Acquisition System LABoratory). For every wave record and every cross section one asci-file was created.

The asci-files created for the wave records consisted of seven columns: elapsed time, signal sent from the computer to the wave board and five columns containing the data of the five wave gauges. An example is given below in Figure 3.21.

DASYLab - V 9.00.00
WORKSHEET : Measure v3c
Recording Date : 9/9/2009, 9:38:03 AM
Block Length : 64
Delta : 0.01 sec.
Number of Channels : 6

Elapsed Time[s]	Write 0 [V]	Write 1 [V]	Write 2 [V]	Write 3 [V]	Write 4 [V]	Write 5 [V]
69.76	1.535	-0.067	-0.009	-0.031	-0.030	0.038
69.77	1.486	-0.066	-0.009	-0.031	-0.030	0.038
69.78	1.432	-0.067	-0.009	-0.032	-0.030	0.037
69.79	1.378	-0.066	-0.009	-0.031	-0.029	0.038
69.80	1.318	-0.066	-0.009	-0.031	-0.030	0.037
69.81	1.258	-0.066	-0.009	-0.031	-0.030	0.037
69.82	1.194	-0.067	-0.009	-0.031	-0.030	0.037
69.83	1.129	-0.066	-0.009	-0.031	-0.030	0.038
69.84	1.062	-0.067	-0.009	-0.031	-0.030	0.037
69.85	0.993	-0.067	-0.009	-0.031	-0.030	0.037
69.86	0.921	-0.066	-0.009	-0.031	-0.031	0.037
69.87	0.848	-0.067	-0.009	-0.031	-0.030	0.037
69.88	0.771	-0.066	-0.009	-0.031	-0.029	0.037
69.89	0.693	-0.067	-0.010	-0.031	-0.030	0.038
69.90	0.612	-0.066	-0.009	-0.031	-0.029	0.037
69.91	0.528	-0.065	-0.008	-0.031	-0.030	0.038
69.92	0.441	-0.066	-0.009	-0.031	-0.030	0.037
69.93	0.352	-0.067	-0.009	-0.031	-0.030	0.037
69.94	0.258	-0.066	-0.009	-0.031	-0.031	0.037
69.95	0.162	-0.066	-0.009	-0.031	-0.030	0.037
69.96	0.064	-0.067	-0.010	-0.031	-0.030	0.038
69.97	-0.038	-0.066	-0.009	-0.032	-0.029	0.037
69.98	-0.142	-0.066	-0.009	-0.031	-0.030	0.038

Figure 3.21: Asci file of wave measurement

Figure 3.20 shows an example of profile measurement. Per cross section an asci-file contained three columns: number of pulses, accompanying horizontal distance in millimetres and vertical distance measured from the laser.

DASYLab - V 9.00.00
WORKSHEET : PositieEXT TRIGGER v17
Recording Date : 9/7/2009, 3:45:43 PM
Block Length : 1
Delta : 1 sec.
Number of Channels : 2

Pulses[-]	Write 0 [mm]	Write 1 [mm]
0	0.0	241.9
1	1.0	242.1
2	2.0	242.3
3	3.0	242.5
4	4.0	242.9
5	5.0	243.3
6	6.0	241.4
7	7.0	239.1
8	8.0	238.1
9	9.0	237.5
10	10.1	237.0
11	11.1	236.8
12	12.1	236.8
13	13.1	238.2
14	14.1	239.0
15	15.1	239.6
16	16.1	239.9
17	17.1	240.3
18	18.1	250.0
19	19.1	250.7
20	20.1	251.0
21	21.1	251.1
22	22.1	247.5
23	23.1	950.0
24	24.1	238.6
25	25.1	237.7
26	26.1	237.4
27	27.1	237.3
28	28.1	237.3
29	29.2	237.7
30	30.2	237.5
31	31.2	248.7
32	32.2	247.4
33	33.2	245.8
34	34.2	244.2
35	35.2	242.9
36	36.2	242.4
37	37.2	242.3
38	38.2	242.6
39	39.2	243.2

Figure 3.20: Profile measurement

3.7 Schedule Experiment

In Table 3.4 an overview is given of the range of the grading, wave load and angle of wave attack used in the currently described tests. These variables are all independent and had to be tested consequently, resulting in a minimum of 12 tests. The tests with 0° acted as reference tests to measure the recession of the test section.

Before the tests could commence, first of all the order of the test runs had to be determined. This sequence depended mostly on the time it took to change the different variables. For example the wave spectrum produced by the wave generator could easily be altered by changing the settings in the computer with a direct link to the generator. The damage occurring during a test with more severe wave conditions was more extensive, so this would also lead to more rebuilding than after the tests with lower waves. Accordingly it was preferred to precede the tests with the lower waves.

Table 3.4: Parameters varied

Variable	Range	Test runs
Wave load (Hs)	0.08-0.10	2
Grading (Fg)	1.3-6	2
Angle (degrees)	0-30-45	3
		12 tests

Changing the angle of wave attack took more time. For this the laboratory crane had to be used, which lifted and rotated the four different sections around a fixed point. The rotation of the model itself could be realised in an hour, but then the model still needed to be rebuild again.

By far the most drastic alteration was changing the grading of the loose outer layer of the breakwater model. Mixing the five different stone fractions to get enough material took about a week. For this reason the total test sequence was divided into two series, one with narrow grading and one with the wide grading. As the stones of the narrow grading were also used for the widely graded mixture, the first half of the tests was carried out with the narrow grading. Subsequently the wide grading was mixed and the second half of the tests was executed.

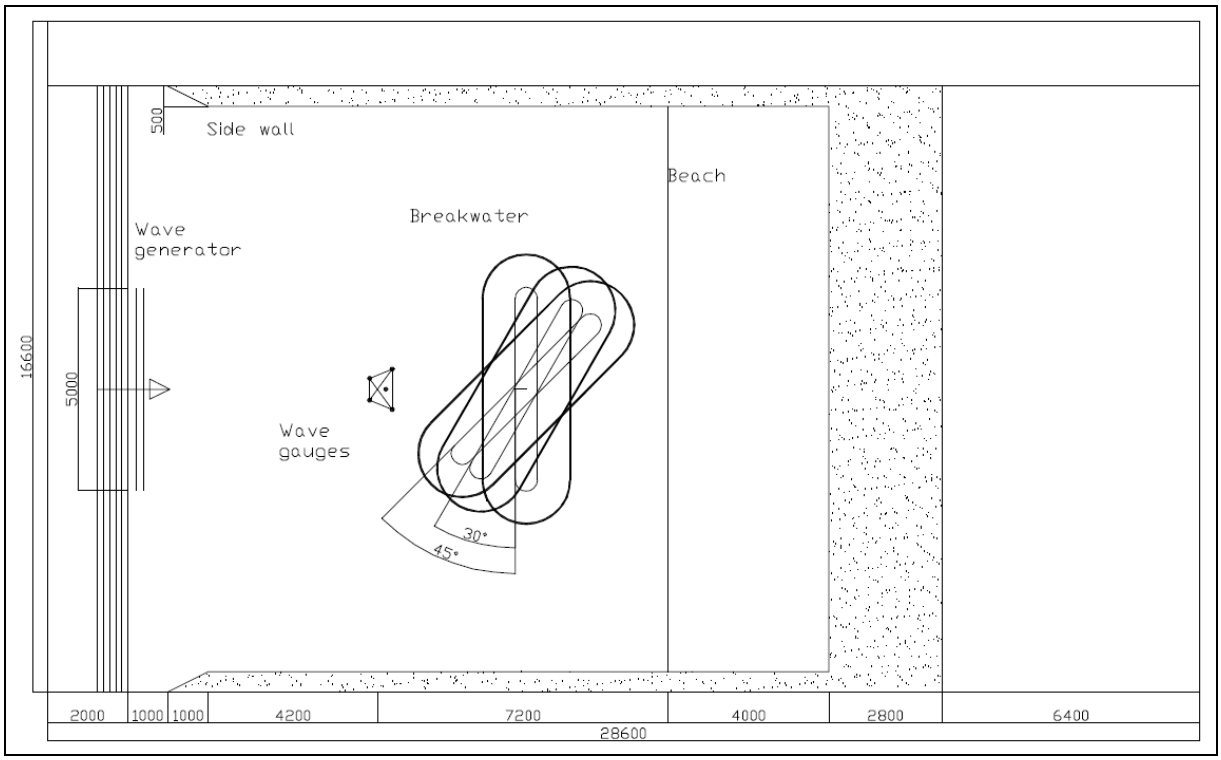

Figure 3.22: Rotation of breakwater model inside the wave basin

All in all a test hierarchy was chosen as is displayed in Table 3.5. To keep the different tests apart every test was given a name composed of the values of the varied parameters. In this name the 'N' stands for the narrow grading of 1.3, while 'W' represents the wide grading of 6. The significant wave height is indicated in centimetres.

Table 3.5: Test schedule as executed

Fg (1.3)						Fg (6)					
0°		30°		45°		45°		0°		30°	
0.08m	0.10m	0.08m	0.10m	0.08m	0.10m	0.08m	0.10m	0.08m	0.10m	0.08m	0.10m
N-0-8	N-0-10	N-30-8	N-30-10	N-45-8	N-45-10	W-45-8	W-45-10	W-0-8	W-0-10	W-30-8	W-30-10

To save time, the second half of the test sequence kicked off with the same angle of wave attack, 45°, as the last test of the first half of the test sequence (less use of the laboratory crane).

Apart from changing these variables, a significant amount of time was required in between the tests to take measurements and rebuild the model again. Before anything could be measured the wave basin had to be empty. As long as there was still water inside the basin, the measuring frame could not be placed accurately and laser profiling would deliver errors due to disturbing reflections. Emptying this basin involved at least two hours while filling it up again took about half an hour. Next the laser profiling could be executed using the measuring frame. While the measurement of the initial profile usually could be finished in half a day, measuring the deformed profile often involved a whole day. This difference could be attributed to the measuring of additional cross-sections for a better survey of the total deformation. After the deformed profile was measured, it was time to measure the longshore transport. Dependent on the test conditions these measurements involved one day up to a whole week. The more severe the transport was, the longer the measurement took.

Following the measuring phase the breakwater model had to be repaired/rebuilt again before each test run. Also this phase took more or less time depending on the conditions and thus deformation of the previous test. Especially repairing the colour bands, for which a mould was used, was a laborious activity. Obviously the total

process of rebuilding was more extensive after rotation of the model, even more so after changing the grading. Usually it took half a day to a whole day to rebuild the profile.

Because the main part of the profile was built without a mould, it could not be guaranteed that exactly the same initial profile was created each time. This was the main reason why all initial profiles were also measured in advance. All in all theoretically two tests could be conducted per week. In reality this turned out to be impossible and a mean of one test per week was reached.

3.8 Sources of error

During the test sequence many sources could be of influence to the results thereby decreasing the reliability of the data. It was important to account for these sources and validate them prior to the further analysis.

3.8.1 Reproducibility of the experiments

Two different wave spectra were used. In order to have reproducible tests, it was important that the wave spectra, which should be the same during each test, did not vary significantly from each other. Due to time constraints each test was run only once. If an occurring wave spectrum then deviated significantly from the other wave spectra at other tests, the results could not be compared with the other results and a rerun would be required. It was therefore important to check if the wave spectra of separate tests stayed more or less the same. This was the case for the currently described tests.

3.8.2 Rebuilding the model

Reproducibility could also be found in the rebuilding of the model. In order to compare the results of the different tests, every test needed to be conducted under the same conditions. In that case rebuilding the model between each test brought along two different possible sources of errors:

- Profile

In the rebuilding process no mould was used, except for applying the colour beams. Therefore the initial profile could not be guaranteed to be the same for each test. Especially at the wider grading variations occurred which counted for the crest width, crest height and the slope. Accordingly the initial profile was measured each time prior to the tests.

- Grading

Although the gradings and characteristics of the five different original stone classes were measured accurately, local variations occurred in the eventual structure. Due to time constraints and a limited amount of materials, mixing the wide grading only took place before the second halve of the test series. Segregation of the mixture however occurred as soon as the mixture left the concrete mixer into the wheelbarrow; even more so when the mixture was applied onto the breakwater thereafter. The larger stones rolled down to the toe while the finer materials stayed on top. In this way it was impossible to produce a perfectly mixed mixture and attempts to improve the mixture were not successful. Fortunately the grown situation was comparable to the real situation in which a breakwater core is normally constructed.

Figure 3.23: Segregation due to (re)building

Complete separation of the mixture and remixing it again in the right proportions however proved to be impossible. So in

between the test runs no further mixing was applied other than the careful reconstruction of the initial profile by shovel. This way of mixing did not lead to noticeable deviations from the first method and was far less time consuming.

Moreover from visual observations it was noticeable that finer particles sank away in the underlying glued part, making at the same time the porosity of this underlying glued part smaller and the grading of the loose part narrower. As it concerned only the finest parts of the materials, no significant change in the grading was expected. The same process was also visible for the narrow grading.

3.8.3 Experimental layout

Waves angles calculated in the analysis were relative to the x-axis: from wave generator to the beach. The same x-axis was used for the positioning of the set of five wave gauges. To simulate oblique waves, the breakwater model itself was then rotated. In the end the actual incident wave angle was equal to the incident wave angle from the analysis added by the layout angle of the breakwater.

To make sure waves were fully developed when they encountered the breakwater model, the distance between the wave board and wave gauges needed to be sufficiently long. A minimum of two wave lengths is often used in model tests so this minimum was also applied in this case. In spite of this length of 6.2m not fully developed waves could still occur.

Another drawback was the proximity of the beach. Because of the required wave developing length for wave measurements, the rotation space needed by the model and the placement of the model itself; the beach started at not more than 30cm from the left roundhead in the 45° layout. Although some sort of influence of this beach could be present, it was expected that this influence could be neglected.

However the rotating and placing of the breakwater model together with the placing of the wave gauges were not negligible and could probably lead to the largest errors in this case. As the wave gauges were removed after each test to allow for profile measurement, replacement could lead to deviations in distance from the model and wave board as well as an undesired rotation relative to the x-axis. Besides this also rotations and therefore deviations of the wave gauges between each other could occur. Replacement of the wave gauges needed therefore to be done with the utmost care so that possible error could be minimized.

3.8.4 Wave gauge error

As was mentioned earlier, a total of five resistive wave gauges were used, which were calibrated on two different occasions during the test sequence. From these calibrations it was found that the differences in the calibration factors were negligible ($\pm 2 \cdot 10^{-4} m/V$) . Together with the standard error of the wave gauges ($\pm 0.001V$) it can be concluded that the wave records were sufficiently accurate.

For the processing phase of the wave data the averages of the two calibrations were used.

3.8.5 Accuracy profile measuring

Before the tests were conducted, the laser used for profile measurements was calibrated. The laser itself had a range of 200-950mm in which the standard error is negligible ($\pm 5 \cdot 10^{-5} m$) . Values outside the range as well as reflections from both stone surfaces as water films on the ground led to errors, which could be filtered out easily. Also running the cart along the beam using the handle was very accurate. With 500 measurements every revolution this came down to one measurement every 1.005mm. This proved to be more than enough for the purposes of these tests.

Less accurate was the moving of the beam itself along the measuring frame for measurement of other cross sections. This movement was done manually and measured with a tape measure. A wedge was then used to level the beam. In time the beam itself warped slightly through use and the beam could not be levelled for the whole length. For this reason only the starting point of the beam was levelled.

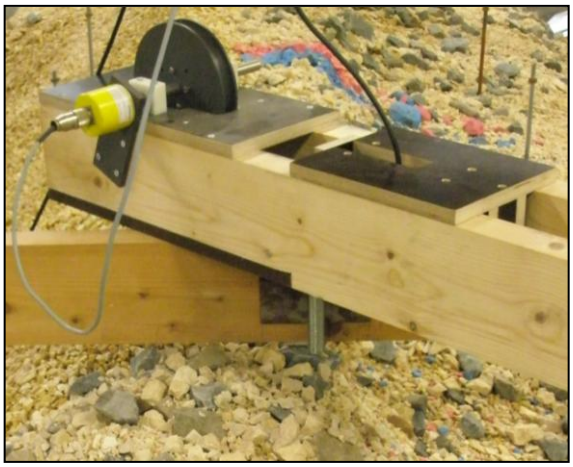

Figure 3.24: Gap first 10cm from turning point

At the roundhead other sources of errors occurred. The first 10cm of the cross section could not be measured as both the edge of the cart and the hinge prevented that. Furthermore deviations of the measured angles occurred as the angles were measured manually with a tape measure. Due to shifting of the measuring frame, the first 10cm and extensive deformation of the roundhead were measured. Because of this the angles became distorted.

Even so the main source of errors originated from placing the measuring frame itself. Placing this frame both prior as after every test could lead to slight deviations; especially as the frame had to be shifted again from the original location due to extensive deformation of the roundhead.

3.8.6 Stability colour bands

On several occasions during the tests it seemed as if the stability of the colour bands was higher than the stability of the surrounding test area. At first this was noted as a visual illusion, as the colour bands stood out naturally because of their distinctive colours compared with the rest of the breakwater. However profile measurements afterwards confirmed the higher stability. The cause for this unexpected and unfavourable event should then not be seen in the dyeing of the stones but rather in the manner of placing. Special attention was given to the placing and finishing of the colour bands as slopes partially caved in while the mould was pulled away. This process probably resulted in a higher packing density in and around the colour bands.

Figure 3.25: Top view of colour bands after test

3.8.7 Limitation model

During one test (‘W-45-10’) the damage to the model was so extensive that the glued part became exposed. The concerned area was in this case at the rear of the right roundhead and the area of influence contained the right roundhead. It was expected that the influence on the deformation and longshore transport of the trunk was limited, while the influence on the left roundhead was probably nil.

At another occasion (‘W-0-10’) the erosion area was also very large. After the test only a small film of stones was left and although the glued part did not become exposed, the shortage of stones could have influenced further development of the deformation.

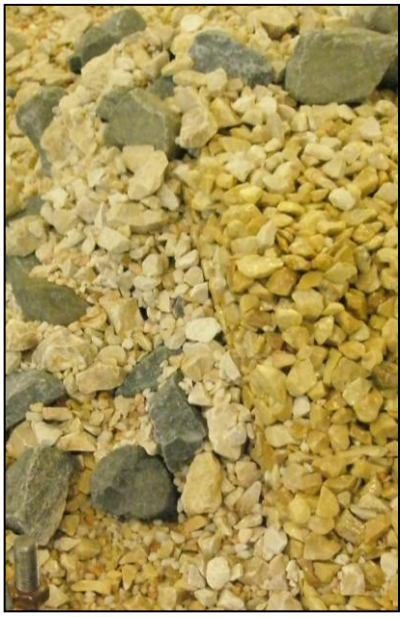

Figure 3.26: Exposure rear side

Figure 3.27: Thin layer around the crest (W-0-10)

3.8.8 Sampling length

As the incident wave spectrum should resemble the target wave spectrum, each test needed to carry on long enough so waves of all frequencies of the desired spectrum were generated. The same held true for the spectral analysis of the data itself as a sufficient amount of data was required to get satisfactorily results.

According to a general guideline, mentioned by [VANLISHOUT 2008], a minimum of 1000 waves should be generated to obtain a full spectral range. This comes down to a minimum sampling length of 25min for tests undergoing a wave spectrum with a period of 1.45s. Seeing the tests described here lasted approximately 3500 waves each, this criterion was amply satisfied.

For the spectral analysis done in this case the first ten minutes of the wave records were discarded as the wave spectrum was still building up. Also the last parts of the wave records were discarded as they included data acquired after finishing the tests. All in all a record of 50 minutes of the total wave record was adopted for each test which corresponded to respectively 2440 $(T_p = 1.45s; T_m = 1.23s)$ and 2700 $(T_p = 1.30s; T_m = 1.11s)$ waves. This was assumed to be more than sufficient, as it was more than twice the minimum sampling length needed.

3.8.9 Water depth

By use of a measuring ruler the water depth was measured manually directly prior to each test. The accuracy of these measurements was $\pm 1 \cdot 10^{-3} m$. However because the water basin had to be emptied and subsequently be refilled again between the tests, the water depth varied $\pm 5 \cdot 10^{-3} m$ between the tests.

This measured water depth was further used by the DIWASP software, used to process the wave data and described in the next paragraph, to calculate the consecutive wave numbers. [VANLISHOUT 2008] already checked the sensitivity of the software to an error in the water depth measurement and found out that this sensitivity was negligible.

4. Data Processing

Before the acquired data from the tests can be used for further analysis, the available data need to be converted into usable parameters and models. In this chapter a description is given of the processing methods used and the resulting models are presented. Paragraph 4.1 starts with the processing of the wave data into wave and directional spectra. Subsequently the profile measurements are converted into three-dimensional profile models and erosion models in paragraph 4.2. A conceptual model, describing the stone displacements during the reshaping phase as well as after reshaping, is then given in paragraph 4.3. In this paragraph both the transverse and longitudinal direction are elaborated qualitatively. Regarding the longitudinal direction also quantitatively data was obtained. Finally paragraph 4.4 deals with the processing of this data leading to exponential relations which are then used to determine the longshore transport.

4.1 Processing wave data

The first and foremost important datasets are the different wave records. A spectral wave analysis of the wave records was done by using the DIrectional WAve SPectra toolbox version 1.3 (DIWASP). DIWASP is an open source software package developed by [JOHNSON 2007] at the Centre for Water Research at the University of Western Australia, Perth. Currently it is distributed and maintained by MetOcean Solutions Ltd, New Zealand. The package consists of a collection of Matlab function and script files which can calculate the directional spectrum from a given data set. DIWASP assumes that the waves analysed are short crested wind waves with a high directional spread. Due to the characteristics of the available wave generators, the real incident wave conditions were long crested together with a very narrow directional spread, as the waves were travelling foremost in one direction (0 degrees). Therefore the package is actually not intended for these circumstances. Still [VANLISHOUT 2008] used the same software package for more or less the same circumstances with satisfying results.

Before the analysis can commence, several input parameters, elaborated in the following section, were required. Then the cross power spectra of the discrete time signals were calculated which were translated into a three dimensional variance density spectrum. From this spectrum the wave direction together with the significant wave height and peak period were calculated.

4.1.1 Input parameters

According to [JOHNSON 2007] three different data structures can be distinguished:

- *Instrument data (ID)* containing all specifications required concerning the measuring devices. The data matrix was directly taken from the processed asci wave data files and the layout of the wave gauges was defined in a xyz-coordinate system. In this coordinate system the x-axis is in the direction of the wave propagation and the z-axis is the vertical axis originating from the bed of the basin. Other input parameters include the sampling frequency (100Hz) of the wave gauges, the water depth and the types of data coming from the measuring devices. Different types of input data, like surface elevation, pressure or current velocity components can be used to compute the spectrum. However in this research only the surface elevations measured by the five wave gauges were used.

- *Spectral matrix (SM)* containing the variance density matrix of the wave spectrum per unit frequency and per unit of direction. Before the analysis took place, the frequency as well as the direction needed to be specified by two evenly spaced vectors. These vectors formed the bin structure for the matrix and the values were the centre of the bin. Several additional options can also be specified, like the units of the two vectors. In this case the frequencies were defined in Hertz, while the directions were specified in radians measured anticlockwise from the positive x-axis.

- *Estimation parameter (EP)* describing the method of estimation used. In total five different estimation methods can be used each with different levels of performance in terms of accuracy, speed and suitability for different data types:

  - Direct Fourier transform method ('DFTM')
    DFTM is a very fast and stable method which produces a good initial overview of the spectral shape. The directional resolution however is poor and physically impossible negative energy distributions can occur. Also the tolerance of errors in the data is poor.

  - Extended maximum likelihood method ('EMLM')
    EMLM is a fast method performing well with narrow unidirectional spectra. Just like the previous method, the EMLM has a poor tolerance of errors in the data, which can lead to negative energy.

  - Iterated maximum likelihood method ('IMLM')
    IMLM is a refinement of the EMLM improving it iteratively. The method tends to perform poorly in the same situations as the EMLM as it is very dependent on the quality of the original solution. Furthermore the accuracy and computation time depend on the number of iterations.

  - Extended maximum entropy principle ('EMEP')
    EMEP is an all-round method accounting for errors in the data and can best be used for three quantity measurements. This method can be as fast as the IMLM while giving far more superior results. However low spectral energies at both high and low frequencies can trigger problems increasing the computation time drastically in the process.

  - Bayesian direct method ('BDM')
    Even though BDM gives overall the best estimate, it is at the same time the most computationally intensive method. Like the EMEP the computation time to reach convergence is drastically increased at low energies due to over-relaxation. Besides this BDM can also have problems with three quantity measurements. That is why the method is more suited for four or more quantity measurements.

  [VANLISHOUT 2008] compared the different EP methods and validated the software package quantitatively using a synthetic signal. It turned out that the IMLM is the most accurate of all. Both the EMLM as the IMLM seemed to cope well with the long crested waves and very narrow directional spectra. Additionally these two methods calculated and displayed occurring reflections unlike the other methods. Compared to each other the IMLM is a little bit more accurate as it modifies the estimated spectrum iteratively until it is sufficiently close to the true directional spectrum. For this reason the IMLM was used for the wave analysis.

  Besides the estimation method some other parameters needed to be defined including the number of frequency bins, the directional bins and the number of iterations. Although the number of iterations does not appear to have a visible effect on the frequency spectrum, the directional spreading function has a tendency to overshoot itself at a high number of iterations. However the effect of the number of frequency bins is much larger. The higher the number of bins the higher the resolution, but this goes at the expense of the quality of the results within the bins. Also the directional resolution is dependent on the number of bins although the effect on the directional spread is not significant. Yet at high directional resolution the directional plot has a tendency to have a double peak in the main wave direction. Apart from these input parameters there is an option to apply smoothing to the final spectra.

  According to [VANLISHOUT 2008] 5 iterations together with 512 frequency bins and 120 directional bins give the best results.

4.1.2 *Actual wave spectra*

After importing the in the previous section mentioned input parameters, the accompanying Matlab script files were run resulting in a wave spectrum and a directional spectrum for each test. These spectra then described the conditions that occurred during the tests, from which the following wave parameters could be determined: significant incident wave height H_{m0}, peak wave period T_p, mean wave period T_{m01} and the accompanying wave steepness s_m.

Table 4.1 gives an overview of the most important parameters that occurred during the tests. The accompanying unidirectional variance density spectrum of each test is displayed in appendix A1 together with the theoretical wave spectra of the drive signals. Figure 4.1 and Figure 4.2 give examples of respectively one variance density spectrum and the corresponding directional spreading which occurred during test N_0_10.

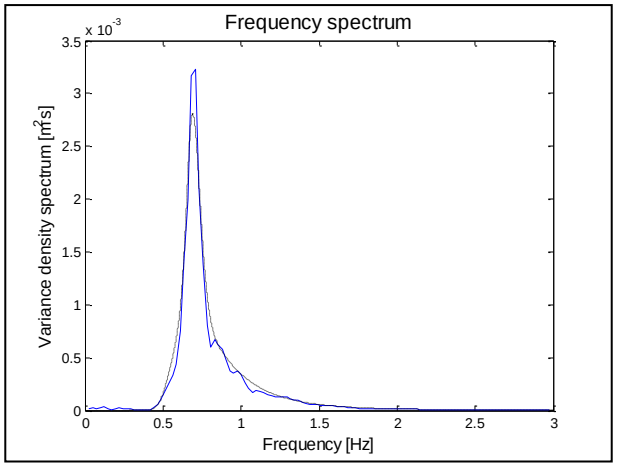

Figure 4.1: Variance density spectrum N-0-10

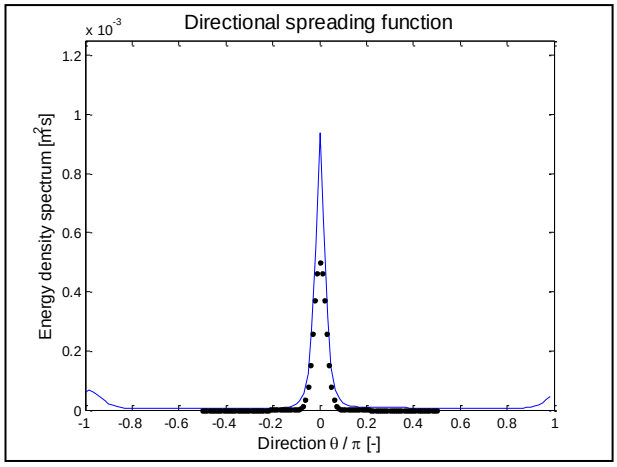

Figure 4.2: Directional spectrum N-0-10

In general the occurring wave spectra follow the spectra of the drive signals rather well. Apart from some minor peak shape differences, especially the height, the compared wave spectra are more or less the same. Only in two pair of test cases, firstly higher wave load and head-on waves (N_0_10/W_0_10) and secondly lower wave load and oblique waves of 30 degrees (N_30_8/W_30_8), the match is complete as also the peaks coincide. An obvious reason for the two matches together with the slight deviations of the others cannot be given although it can be stated that the start and duration of the wave sample have a major influence on the eventual wave spectrum. Computations with wave samples of the same wave test record, same duration but different starting moment, has led to significant differences in peak periods. No major differences were found while comparing wave spectra of tests with the same wave conditions, so no influence was found regarding the stone grading for this matter.

To complete the picture also the directional spreading is given for each test in appendix A1. As expected the directional spreading of the wave energies was very narrow around $\theta_0 = 0^\circ$, but some differences were found concerning the height of this peak. Again no obvious reasons causing these differences were found, apart from an observed influence of the estimation method. While using IMLM the peaks tended to be higher than when the EMLM was used.

Of the graphs displaying the directional spreading, only the graphs of tests with head-on waves show some influence of

Table 4.1: Wave parameters as measured

Test	$H_s(m)$	$T_p(s)$	$s_p(-) = H_s / L = \frac{2\pi H_s}{gT_p^2}$
N_0_8	0.077	1.321	0.028
N_0_10	0.097	1.463	0.029
N_30_8	0.079	1.280	0.031
N_30_10	0.092	1.365	0.032
N_45_8	0.074	1.321	0.027
N_45_10	0.094	1.412	0.030
W_0_8	0.076	1.321	0.028
W_0_10	0.097	1.463	0.029
W_30_8	0.078	1.321	0.029
W_30_10	0.093	1.365	0.032
W_45_8	0.076	1.321	0.028
W_45_10	0.095	1.412	0.031

reflection. At -180 and 180 degrees these graphs show a minor peak in the energy spectrum. This does not come as a surprise, since most reflection was expected during head-on wave attack in the first place.

4.2 Processing of the different cross sections

4.2.1 *Procedure*

As is mentioned earlier in paragraph 3.6, every measurement of the laser profiling was recorded in more or less the same manner as the wave records. Per cross section one asci-file with data was created. The first follow-up operation was then to convert the data of the different cross-sections into one file, so it could be processed into one three-dimensional model.

Because of major deformations at the crest of the roundheads and the immeasurability of the first 10cm around the centre of the measuring frame, it was often not possible to measure the profile of the roundhead in one take without shifting the measuring frame. The amount of displacement needed varied each test and per roundhead and led to a distortion of the angles measured. In order to use the data of the cross sections, the data points needed to be converted into a standard xyz-coordinate system.

By using the software package Matlab, the data were eventually converted and processed into one matrix for each test containing the x and y coordinates together with the measured height z. The result can be seen in Figure 4.3 and Figure 4.4.

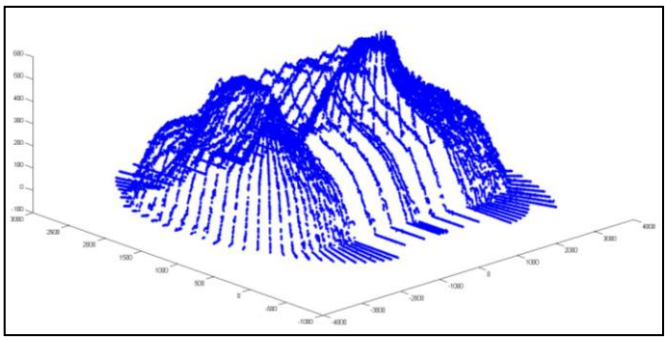

Figure 4.3: All profile measurements in one graph

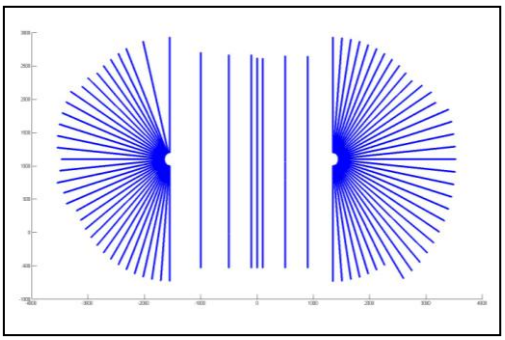

Figure 4.4: Top view profile measurements

As the profile in between the measurements was not known, interpolation of the data was needed to create the final three-dimensional model. To make an interpolation between the different cross sections possible firstly a regular grid was required. Again Matlab was used to create this grid and after careful consideration a grid size of 1cm was used, which was roughly the same as the nominal diameter, D_{n50}, of the stones used. A larger grid would lead to less detail and could therefore lead to a loss of information, while a smaller grid could lead to meaningless details and a drastically increase of computation time. Finally by means of linear interpolation three dimensional models were created of each initial and deformed profile.

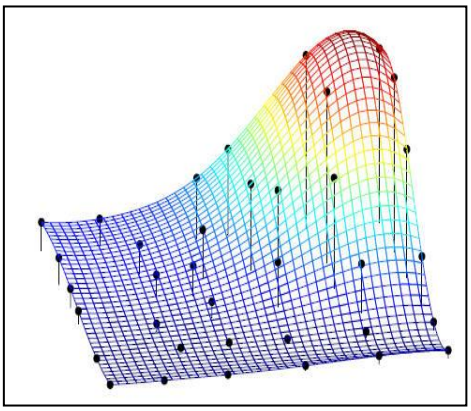

Figure 4.5: Example of interpolation

4.2.2 *Outcome*

Figure 4.6 shows the deformed profile of test N-0-10. In appendix B2 for every test the three dimensional models are given. Both the initial and the deformed profiles are displayed per tests followed by a model of the fixed profile without the loose material. The models show a clear deformation of the outer slope and especially

the deformations at the roundheads are nicely visualized. So it is clearly visible, for instance, that the roundheads evolved in the direction of the waves.

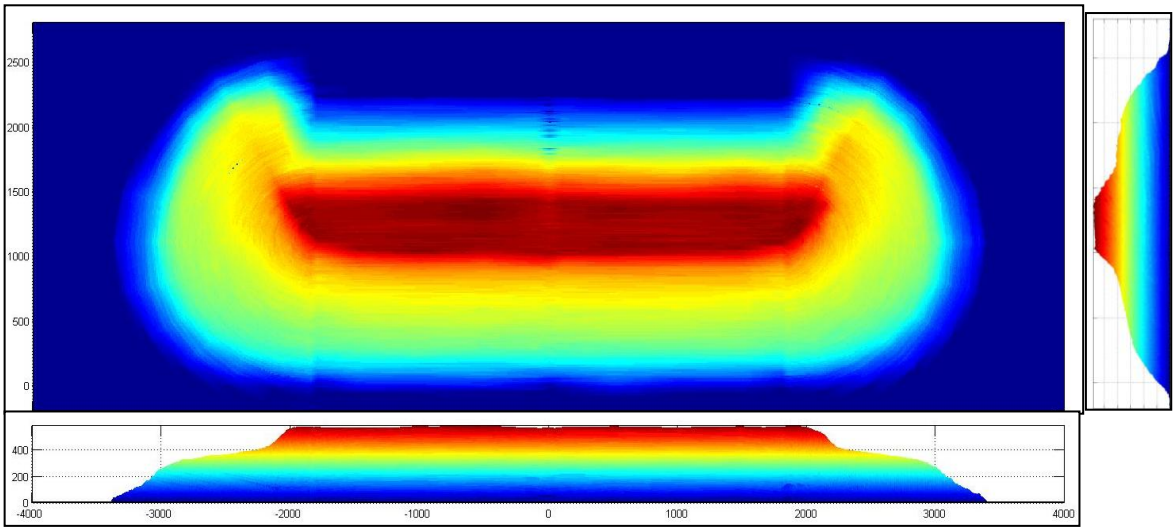

Figure 4.6: Three-dimensional model after test N-0-10

From these three dimensional models it is possible to go back to the two-dimensional deformation for further processing. As every model is set up in a grid with xyz coordinates, it was fairly simple to determine and plot every cross-section desired, so all deformation parameters could be determined separately.

4.2.3 Erosion model

Once the profiles of both the initial profile and deformed profiles were reproduced it was only a small step away from a three-dimensional erosion model. By subtracting the initial profile from the deformed profile an erosion model was created in which areas of erosion and accretion become clear in an instant. Integrating these differences over the concerned areas led to the desired erosion volumes from which the erosion of the roundhead could be determined and together with the longshore transport volume originating from the trunk. Figure 4.7 shows an example of the three-dimensional erosion model for test N-0-10. In appendix B3 all erosion models are displayed for each test.

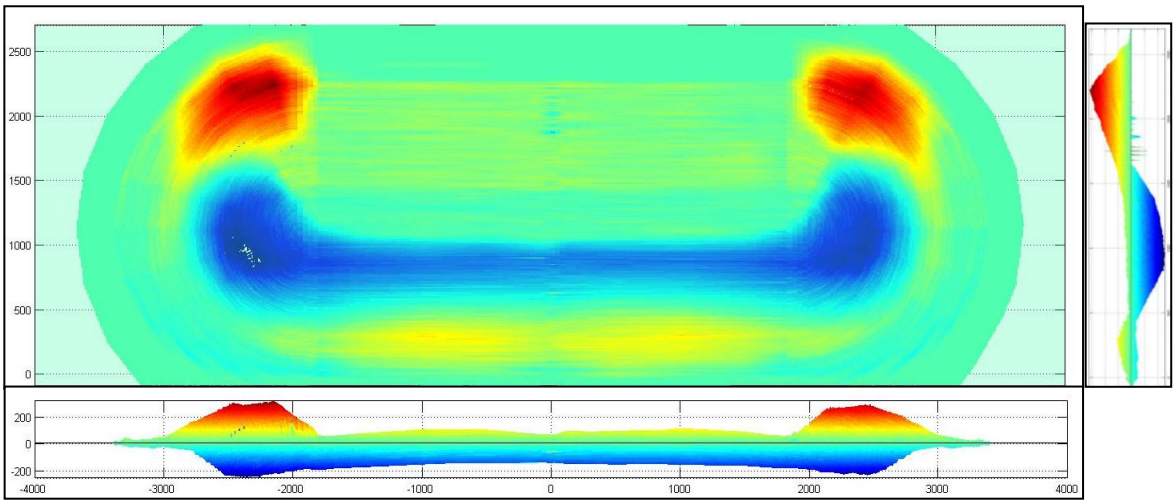

Figure 4.7: Erosion model after test N-0-10

4.3 Conceptual model stone transport

During the tests both video recordings and photos were taken. Although it was still difficult to define the exact point in time at which the equilibrium profile was reached, these visual observations did give a better insight in the processes occurring during reshaping as well as after reshaping. Accordingly for both phases a conceptual model was formulated which describe the stone movements causing deformation as well as longshore transport. In the second half of this paragraph this model is expanded including the segregation process observed during tests with the wide grading.

4.3.1 Description transport both during reshaping and after reshaping

The tests described in this thesis were executed for the main part during the reshaping phase. As the initial profile of 1:1.5 proved to be unstable, the outer slope adapted into a more stable slope under the influence of the generated waves. This large scale deformation was foremost dominated by stones rolling down the slope due to the instability created by wave attack and gravity. Especially the larger stones were susceptible to this phenomenon dragging finer material along in the process. The resulting landslides then deposited the material lower on the slope outside the area under influence of wave attack. Through this a more stable s-curve was created with a gentle slope around the still water line.

For head-on waves this transverse transport was accompanied by some minor spreading in longitudinal direction as not all stones rolled down in a straight line. For oblique waves this spreading was far better visible as besides the transverse transport also a longshore transport was generated. However during the reshaping phase this longitudinal transport was suppressed as the transported stones were quickly overwhelmed by a dominant transverse component. Although a large amount of stones were displaced in the longitudinal direction only minor displacement lengths were obtained.

In time the dominance of the transverse transport of stones diminished until a sort of equilibrium profile was reached for the greater part of the slope. After reaching this equilibrium the crest still continued to crumble off, though slowly due to only the higher waves of the wave spectrum, until ultimately the tests were shut down. During this remainder of the tests also the movement of finer material around the still water line carried on. Stones transported in this way moved in the direction of the incoming and reflected waves without significantly affecting the deformed profile. For the case of oblique waves this even led to an increase in stone displacement length in the longitudinal direction as the transport was no longer suppressed by a dominant transverse component. While the amount of stones transported was actually lower the stones were transported further until finally upon reaching the rear side of the breakwater further movement was prevented.

As profile and displacement measurements were only conducted once after the tests were run, no quantitative data was obtained of the stone displacements in time during the reshaping phase as well as after reshaping. It is therefore not possible to determine separate relations for both phases describing the stone displacements in time. Accordingly it is also impossible to define the exact point in time in which an equilibrium profile was reached and the reshaping phase turned into the phase after reshaping.

4.3.2 Segregation due to stone displacements of different stone fractions

During the tests with the wide grading a clear segregation of the mixture occurred for transverse direction as well as the longitudinal direction. In the initial phase the coarsest fractions proved to be the most unstable thereby dominating the transport as result of gravity in mainly transverse direction. In this transport, which can better be described by large stones tumbling down the slope to a more stable position at the foot of the breakwater, other stone fractions were also dragged along. Later on after initial deformation, in which already an s-curve was visible, the coarsest fractions that came loose through deformation were deposited in a stable position on the gentle slope around still water level. Subsequently while no further movement of the coarsest fractions was observed, the finer fractions still kept moving up and down the slope in the direction of the run-up and run-down of the waves, even after a more or less equilibrium profile was achieved.

Due to the wave obliquity also a longitudinal component was present besides the transverse transport. Also here the magnitude of the longitudinal component depended on the fraction size. As the coarsest fractions were mainly dominated by the transverse component, the longitudinal component was far less, leading to only minor transport distances before a stable position was reached.

For smaller fractions a different situation occurred. In this case stones were transported in the direction of wave run-up and run-down resulting in a large transverse displacement as well as a longer transport distance in longitudinal direction. Even after reaching a more or less stable slope, movement of the finer fractions continued until eventually the rear side of the roundhead was reached and further transport was prevented. The finer the material the larger the scale on which this process occurred. Figure 4.8 shows the concept of stone movement for the different fractions as was observed and described above.

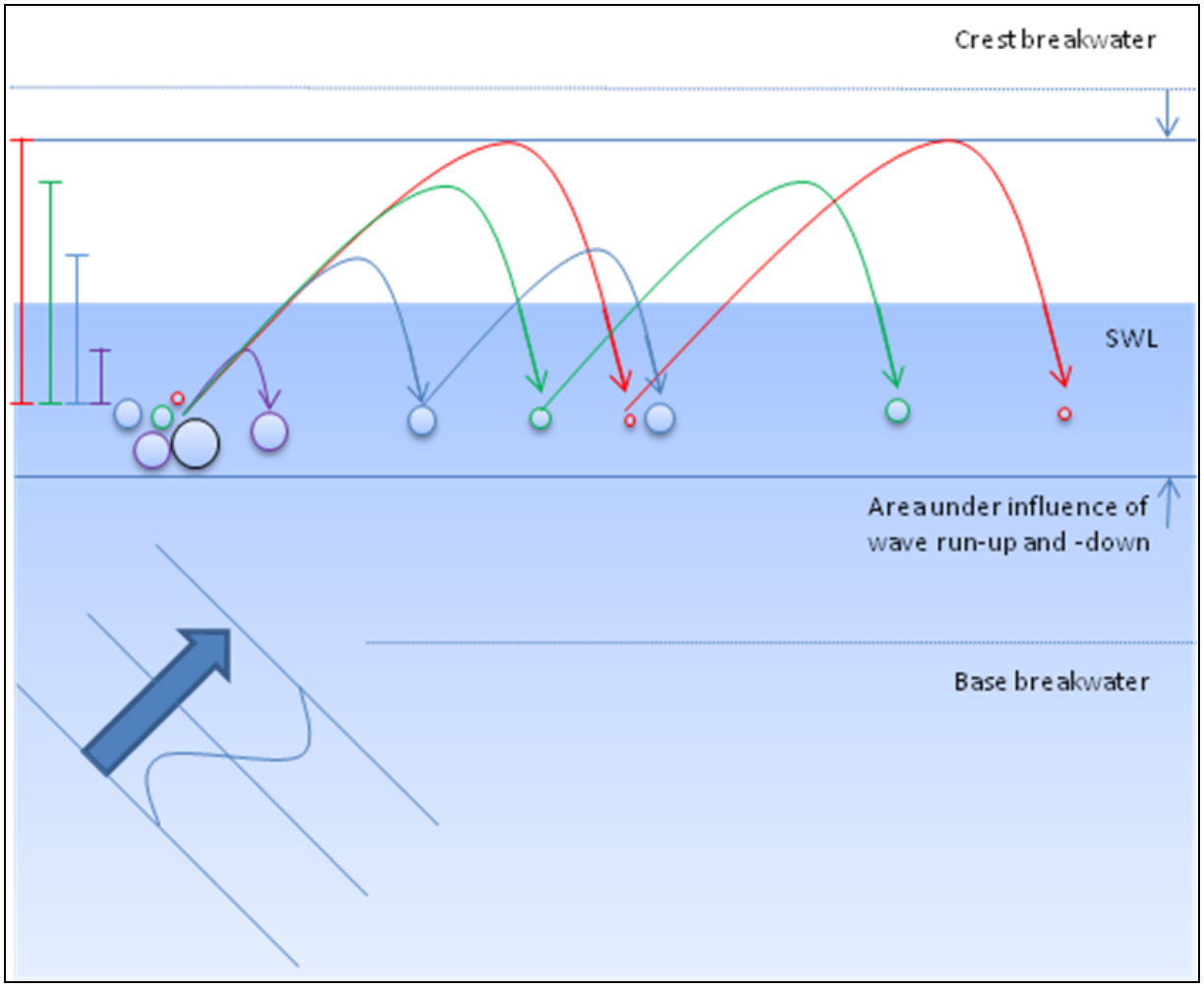

Figure 4.8: Segregation due stone displacement in longitudinal direction

4.4 Processing the longshore transport

4.4.1 Displacement spreading

After each test the displaced stones originating from both the blue and red colour beams were counted. The manner, in which this was done, was already briefly discussed in section 3.5.4. By counting the amount of stones and measuring the corresponding distance from the centre, the spreading of stones along the length of the breakwater was found.
Consequently the left half of the breakwater was divided into six sections:

- One strip of 0.1m wide (blue colour beam) which served as an extra data point for the transport of pink stones.
- Four sections of 0.5m wide on the trunk.
- Last part of the trunk together with the left roundhead, which served as a data point for the rest factor.

Except for the first section in which only one data point was generated, for each section two data points were generated, one for blue and one for pink stones, which were located in the middle of the concerned sections. These data points formed the basis for further research into the relation between the amounts of stones found, originating from a 10 cm wide strip in the centre of the breakwater, and the distance from this centre of the breakwater. For every test with oblique waves the transport data was computed and in respectively appendix C1 and C2 all these measurements and graphs are displayed. In Figure 4.9 the displacement data is plotted for the two separate colour beams of test N-30-10. By merging the data points of the two different coloured stones one relation was found as is shown in Figure 4.10.

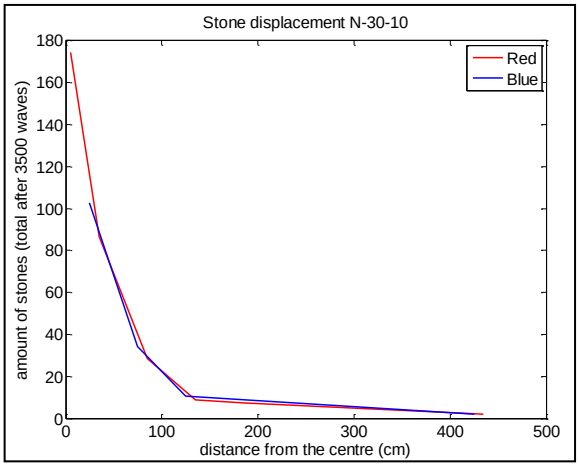

Figure 4.9: Displacement measured per colour beam

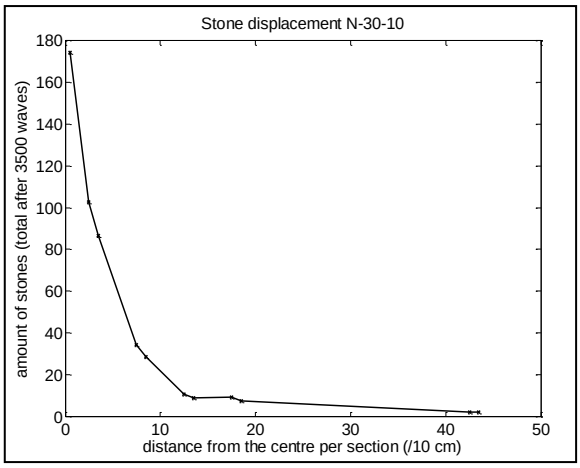

Figure 4.10: Combined displacement measurement

As the graphs only describe the spreading of stones originating from one 10cm wide strip in the centre of the breakwater, transport of stones originating from other areas were thus not included. Nevertheless, under the assumption of uniform transport at the trunk, data from this strip was extrapolated to other 10cm wide sections along the breakwater from which the total longshore transport could be determined. Before the data sets and graphs could be used for the determination of the total longshore transport, the data sets needed to be expanded. By means of extrapolation additional data points were generated in the first 5cm from the centre and beyond the roundhead. The final curves found have an exponential relation and through curve-fitting a good fit was produced, even for tests W-45-8 and W-45-10 for which difficulties in measuring the transported stones close to the colour beams itself had led to deviations in comparison with other tests. An example of this interpolation and fitting process for test W-45-10 is given by Figure 4.11 and Figure 4.12. Graphs displaying the stone displacements per fraction for each test are printed in appendix C3.

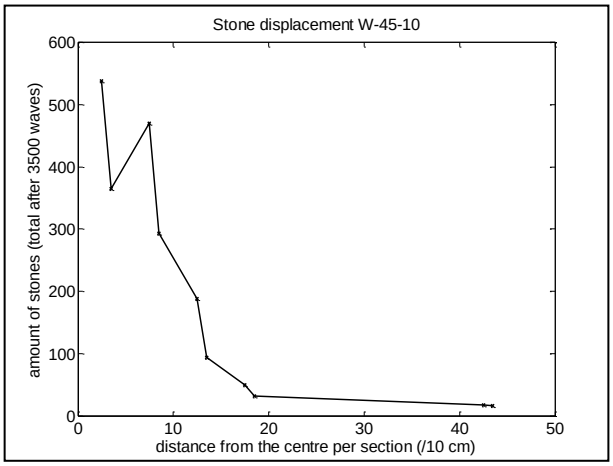

Figure 4.11: Displacement measurement W-45-10

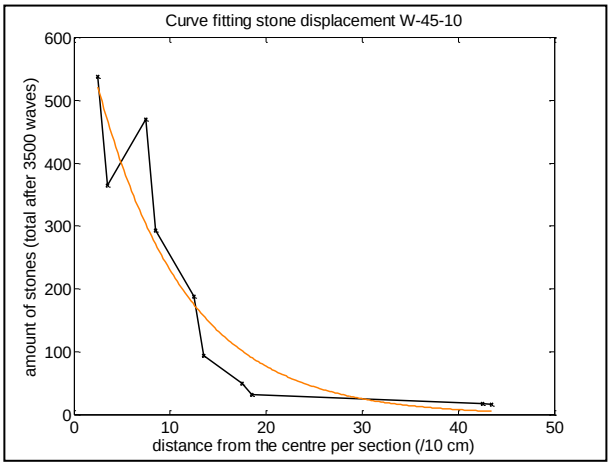

Figure 4.12: Exponential relation through curve-fitting

4.4.2 *Area of uniform transport*

The exponential relations found in the previous section can be used to calculate the total longshore transport. By extrapolating the relations for one strip of 10cm to the rest of the breakwater trunk this transport can be determined through integration.

In case of uniform transport then the following is true: the amount of stones entering the area through longshore transport is the same as the amount of stones leaving:

$$\Delta S = S_{in} - S_{out} = 0 \qquad (4\text{-}1)$$

Extrapolation of the transport data under the assumption of uniform transport is then relatively easy, as exactly the same exponential relations can be used for each strip of 10cm along the area of uniform transport. Accordingly it was important that an area of uniform transport was established for the current tests. For this purpose the breakwater trunk was firstly divided up in sections with a width of 10cm. Subsequently for every section the cross section of the deformed profile were compared to each other. When variations in deformation of the successive cross sections were sufficiently small, so they could be neglected, then these cross sections were assumed to be under influence of uniform transport.

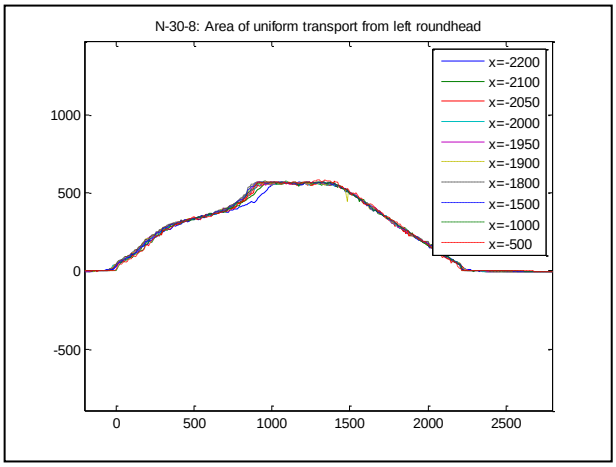

Figure 4.13: Different cross-sections N-30-8

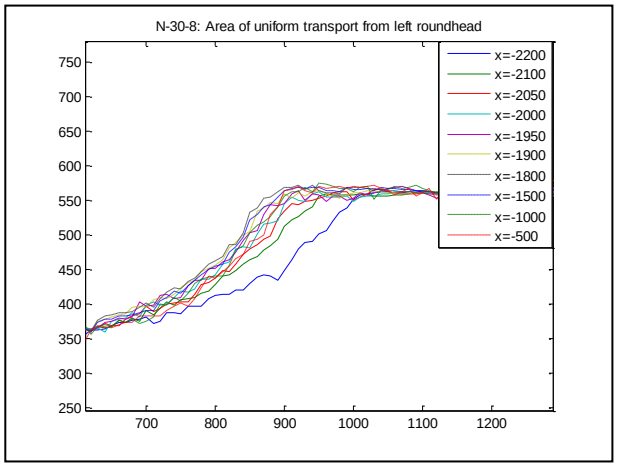

Figure 4.14: Determination of area of uniform transport

By means of plotting the cross sections of the deformed profile for every 0.10m (Figure 4.13 and Figure 4.14), it was possible to determine which cross sections were under influence of uniform transport. Then by adding up the lengths between these cross sections, areas of uniform transport were obtained. For each test this area was determined leading to the following Table 4.2.

Table 4.2: Areas of uniform transport per test

Area	N_30_8	N_30_10	N_45_8	N_45_10	W_30_8	W_30_10	W_45_8	W_45_10
Length (cm)	400	340	400	330	400	330	370	360

4.4.3 *Determination of the total longshore transport*

From the relations found for the spreading of stones along the length of the trunk together with the area of uniform transport it is finally possible to determine the total longshore stone transport. The method of determination used is visualized in Figure 4.15. This transport is then defined as the total amount of stones that has passed the downstream border of the area of uniform transport after 3500 waves. It can then be obtained by integrating the relations for every 10cm wide section upstream of this border and adding them up. Stones transported from the area upstream of the area of uniform transport were discarded. As the influence over the long distance proved to be rather small, the anticipated error by doing this was also small.

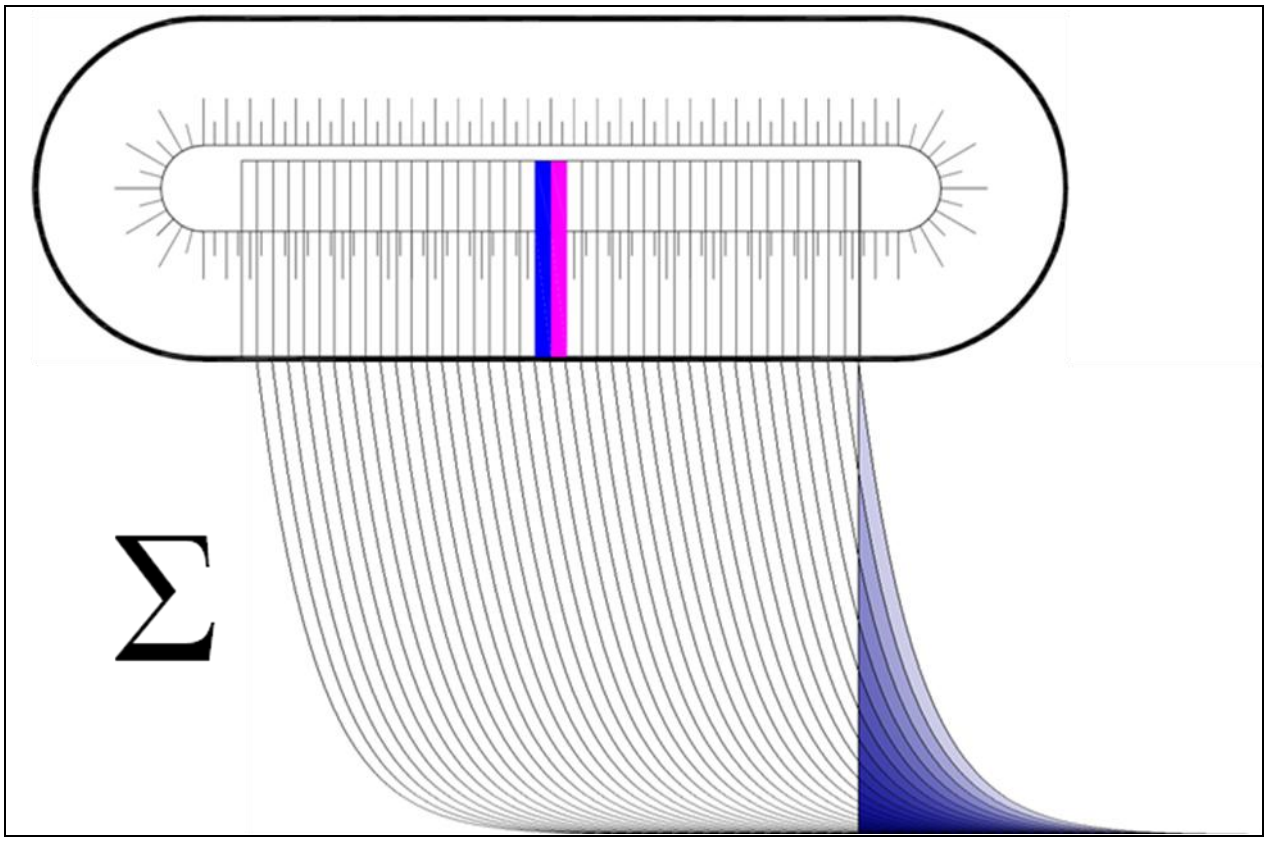

Figure 4.15: Determination of longshore transport from stone displacement graphs

Following the above-mentioned method the longshore transports were determined for every test with oblique waves. The results are displayed in Table 4.3 together with the corresponding transport rate, defined as the total longshore transport divided by the number of waves $(N = 3500)$.

Table 4.3: Longshore transport per test

	N_30_8	N_30_10	N_45_8	N_45_10	W_30_8	W_30_10	W_45_8	W_45_10
Total transport (3500 waves)	1525	4147	702	3629	1845	24096	6912	19583
Transport (/wave)	0.445	1.235	0.196	1.061	0. 520	7.161	1.933	5. 705

4.4.4 Alternative method: Accretion volume roundhead

Another method to calculate the longshore transport is by determination of the accretion volume at the left roundhead. This extra volume originates from the trunk and can be used to determine the longshore volume transport rate.

Computation takes then place using the erosion models determined in section 4.2.3. By integrating these erosion models over the left roundhead and the adjacent part of the trunk, which is not included in the area of uniform transport, the volume originating from the trunk is directly calculated. With formula (2-51) it should then be possible to compute more or less the same longshore transport and transport rate as was defined in the previous section.

However in reality this method turned out to be rather difficult as the integration process itself did not lead to satisfactory results. Apparently other processes occurred at the roundhead and trunk with each their own influence on the eventual volume. From those influences it seems that the largest contribution is delivered by compaction of the deformed material.

As was mentioned in section 1.2.3, deformation of the roundheads falls outside the scope of this thesis. This together with the difficulties described above have led to the decision of not elaborating this method any

further. Accordingly for the further analysis of the longshore transport the method described in section 4.4.3 was applied.

5. Analysis of Test Results

In order to come to a better understanding of the occurring processes, the mutual relations with the governing parameters have to be studied in more detail. Therefore the data processed in the previous chapter need to be analyzed further. This chapter deals with the analysis of the processed test results and is subdivided into two parts. The first part contains the analysis of the two-dimensional deformation and is discussed in paragraph 5.1. Paragraph 5.2 then discusses the analysis of the longshore transport.

5.1 Two-Dimensional deformation

This paragraph treats the occurring two-dimensional deformation of the profiles during the tests. Only the deformations of the trunk profiles are elaborated, as the deformation of the roundheads is beyond the scope of this report.

Firstly the deformation parameters defined by Van der Meer and Merli are determined from the deformed profiles. Then these parameters are compared with the empirical relations found by both Van der Meer (stone grading excluded) and Merli (stone grading included). The former was obtained by running the software programme 'Breakwat', which uses the relations found by Van der Meer in its computation for berm breakwaters. The latter was acquired by calculation by hand. Although Merli derived his formulas from data of tests with only head-on waves, these formulas were also used for the comparison with current test results under oblique waves. Oblique waves were then taken into account using the same reduction factor, $\cos\psi$, as used in the Van der Meer formulas.

Subsequently in section 5.1.2 also the recession of the crest will be elaborated. For this a comparison is made of the test data with the relations formulated by Hall & Kao and Merli as well as Tørum. Like in the comparisons of the deformation parameters between the relations of Van der Meer and Merli, oblique waves are discounted with the reduction factor, $\cos\psi$. All in all it is possible to draw some preliminary conclusions regarding the applicability of the available empirical relations for the current test data.

5.1.1 Deformation parameters (Van der Meer and Merli)

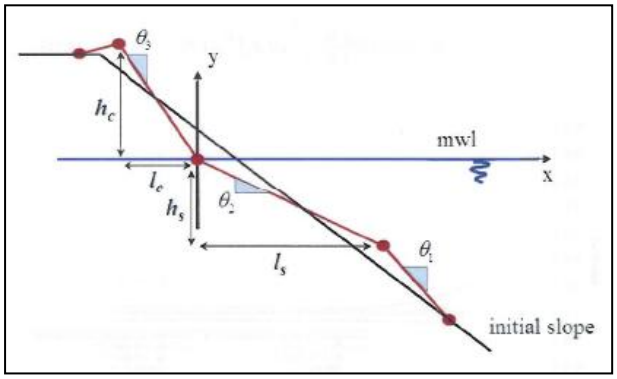

Figure 5.1: Deformation parameters according to Merli [MERLI 2009]

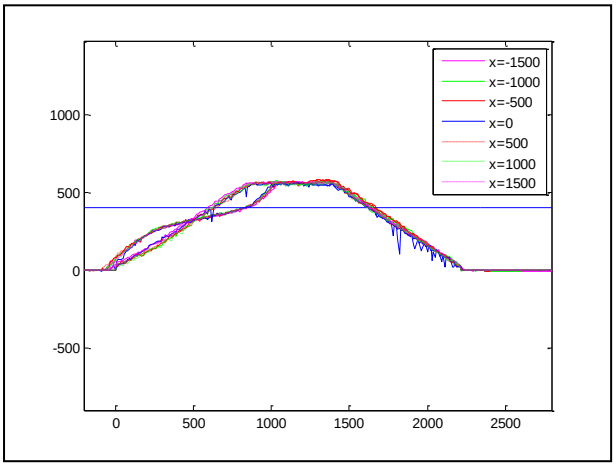

Figure 5.2: Determination of deformation parameters

Crest length 'lc'

In section 2.3.2 and 2.3.5 the crest length was already described by relations formulated by respectively Van der Meer and Merli:

$$H_0T_0 = (3\cot\alpha_1 + 25)\, l_c / D_{n50} N^{0.12} \qquad (2\text{-}14)$$

$$(H_0T_0 - 183)\cot\alpha_1 = 139(l_c / D_{n50} N^{0.12}) \left(\frac{D_{n85}}{D_{n15}}\right)^{-0.29} - 667 \qquad (2\text{-}26)$$

In the Figure 5.3 and Figure 5.4 below the measured values of l_c from the tests are compared with the corresponding theoretically computed values. The first graph compares the measured data with the Merli formula, while the second one compares it with the Van der Meer formulas.

As was already concluded by Van der Meer, the value of l_c appears to be independent of the angle of wave attack. Furthermore Van der Meer stated that the influence of grading on this parameter is negligible and no relation was included in the formulas. From the second graph however it is clearly visible that the use of the Van der Meer formulas leads to an underestimation of l_c. This underestimation seems to increase for both a lower wave load, H_0T_0, and wider grading. While it seems to be more influenced by the low wave load than by the wide grading used in the current tests, it is especially the combination of both parameters that leads to a substantial underestimation of the test results. Apparently l_c is really affected by the grading resulting in longer crest length for wider gradings. However as Van der Meer tested for values of the grading up to 2.5, it can be stated that the grading of 6 used in the present tests clearly falls outside the range of validity of the formulas.

Subsequently the relation with H_0T_0 becomes less accurate when the wave load becomes less severe. The decrease in crest length is not as pronounced as the formulas presume.

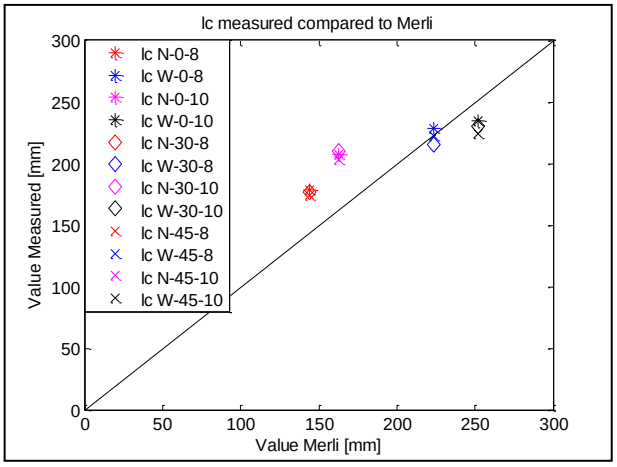

Figure 5.3: Comparison 'lc' with Merli

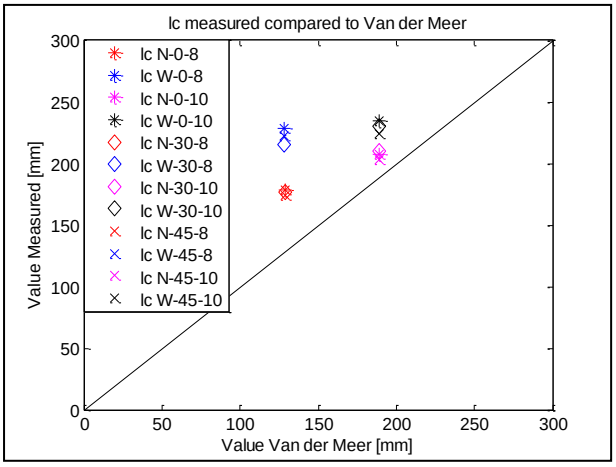

Figure 5.4: Comparison 'lc' with Van der Meer

Unlike the Van der Meer formulas the method defined by Merli takes into account the grading. As can be seen from the first graph, this leads to an overall better fit with the measured data. However of the measured data points only those of tests with wide grading and low wave load match the computed data perfectly, while the data of tests with wide grading and high wave load are slightly overestimated. For data points of tests with the narrow grading the formula leads to a clear underestimation, even more so for tests with high wave load although the differences are minor.

From these findings it can be concluded that, although the influence of the wider gradings are described well, the reduction of l_c due to lower values for the grading is less pronounced than the formula presumes. As the grading of 1.3, used in the present tests, is lower than the lowest value of 2.71 tested by Merli it can be stated that the currently used grading falls outside the range of the formula. Moreover the formula needs adjustment

before it can be used for low values of grading outside the range. In the case of the narrow grading and high wave load the crest length is actually described better by the relation of Van der Meer.

On the other hand the influence of H_0T_0 appears to be described better by Merli. The slight overestimation of the test results for tests with wide grading and high wave load is followed by an underestimation for tests with narrow grading and high wave load which is even larger compared to results of tests with narrow grading and low wave load.

Step length 'ls'

Also for the step length two different relations of Van der Meer and Merli were found and described in section 2.3.2 and 2.3.5:

$$H_0T_0 = 2.6\left(l_s / D_{n50}N^{0.07}\right) + 70\cot\alpha_2 - 210 \qquad (2\text{-}16)$$

$$H_0T_0 = 1.66\left(l_s / D_{n50}N^{0.07}\right)^{1.3}\left(\frac{D_{n85}}{D_{n15}}\right)^{-0.15} + 29.1\cot\alpha_2 - 9.38 \qquad (2\text{-}25)$$

In Figure 5.5 and Figure 5.6 comparisons are given between the measured step lengths, l_s, and values computed with the formulas of respectively Merli and Van der Meer. While both relations fit rather nicely with the measured data, the formula defined by Merli results in less scatter of the data around the straight line representing equality between computed values and measured data.

In the graphs the influence of grading is clearly visible leading to a longer l_s for the wide grading. Although Van der Meer already observed a longer profile under still water level for wider gradings, eventually no influence of grading was included in the formulas. This is clearly visible in the second graph in which data of tests with narrow grading are constantly overestimated, while data with the wide grading and oblique waves tend to be underestimated. In the relation of Merli the influence of grading is included which results in a better fit compared to the comparison with the Van der Meer relation. Still, apart from data concerning head-on waves for which the opposite is true, the computed values tend to lag behind the observed values as the grading increases.

Besides the grading also the wave obliquity is of influence, especially at narrow grading where this influence is described rather well by both relations. At measured data from tests with wide grading however this influence seems to be almost non-existent leading to clear differences in comparison with the calculated values for both relations. As Merli only tested his structure under head-on waves, the effect of obliquity was discounted with the same reduction factor as is used in de Van der Meer formulas. Therefore the same deviations concerning obliquity are found for both relations. Apparently the reduction factor of $\cos\psi$ is also dependent on the grading for large values of this grading.

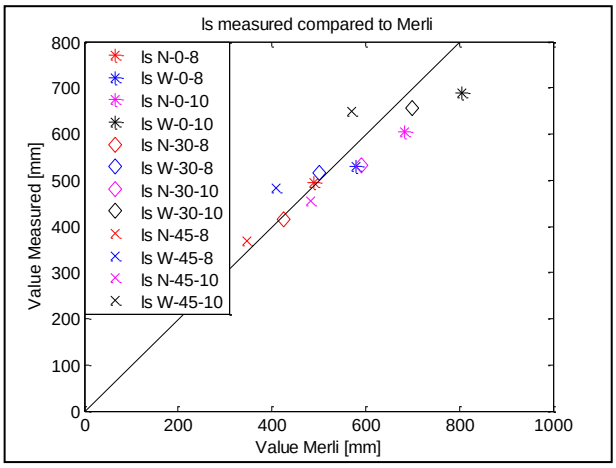

Figure 5.5: Comparison 'ls' with Merli

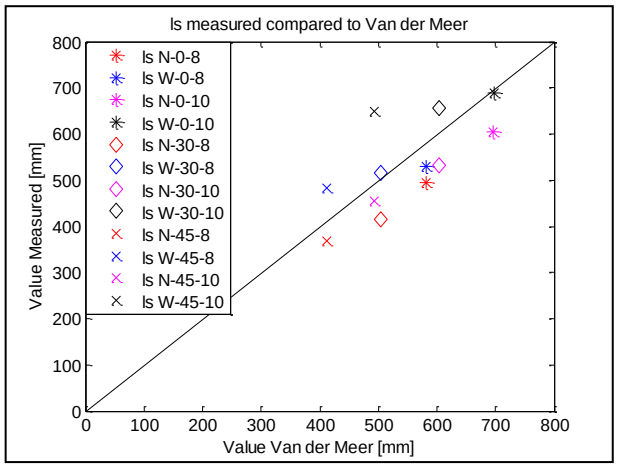

Figure 5.6: Comparison 'ls' with Van der Meer

For the influence of the wave load, discounted by H_0T_0, a different situation arises. In this case the relation seems to be better fitted by the Van der Meer formula. Still the computed values tend to increase more slowly than the observed values indicate, when H_0T_0 increases. This trend is better visible for the data of tests with wide grading. In comparison with the relation of Merli the opposite holds true: as H_0T_0 increases, the calculated values tend to increase faster than their observed counterparts. Furthermore the computations with the high wave load, except for the value for wide grading and an obliquity of 45°, seem to overestimate the observed values.

Crest height 'hc' and step height 'hs'

For h_c and h_s only the relations formulated by Van der Meer can be used for comparison with the test data as no relations were found by Merli regarding the stone grading:

$$H_0T_0 = 33\left(h_c / D_{n50}N^{0.15}\right)^{1.3} + 30\cot\alpha_1 - 30 \qquad (2\text{-}13)$$

$$H_0T_0 = 27\left(h_s / D_{n50}N^{0.07}\right)^{1.3} + 125\cot\alpha_2 - 475 \qquad (2\text{-}15)$$

Figure 5.7 and Figure 5.8 display the graphs concerning both parameters in which the current test data are compared with the values calculated according to the Van der Meer formulas.

In case of the crest height, h_c, the comparison does not produce a satisfying fit. According to the test data the crest height did not vary between the different tests. Apparently the crest height was not influenced by the differences in grading, wave obliquity and wave load, while the computed values clearly show a dependence on both wave load and angle of wave attack. During the tests however the initial crest height was higher than the computed values. Presumably due to instability, partly due to the relatively steep outer slope, the part of the slope above the predicted values crumbled off during wave attack after initial deformation. This process then continued until the initial crest height was achieved subsequently leading to an underestimation of all predicted values.

In the opposite case when the initial crest height is less than h_c, stones will presumably be tossed up the slope, erecting a higher crest in the process, until more or less the predicted values will be achieved. However from the data of current tests no clear relation can be found regarding any of the three parameters.

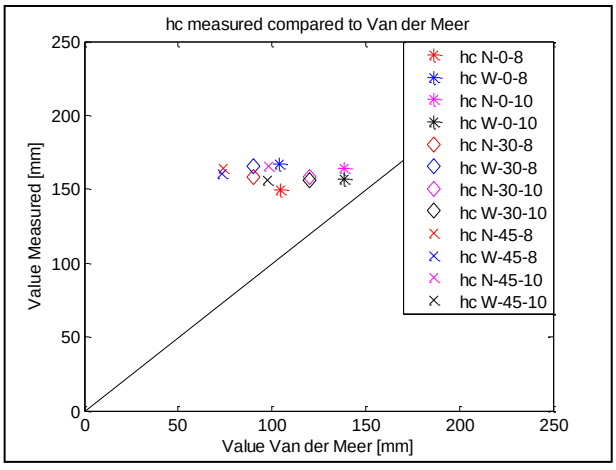

Figure 5.7: Comparison 'hc' with Van der Meer

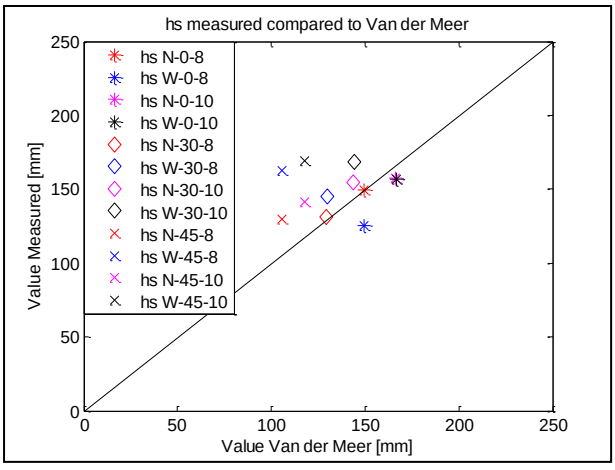

Figure 5.8: Comparison 'hs' with Van der Meer

The comparison between the measured data and computed values, regarding h_s, shows a better fit. Nevertheless the relation of Van der Meer shows a clear distinction in the values for the different angles of

wave attack, while this is not visible in the measured data. The effect of wave obliquity was, if present in the current tests, at first sight practically non-existent and certainly not as large as $\cos\psi$ indicates.

However the measured data, apart from the data from tests with high wave load and head-on waves, do show a distinction in stone grading. This amount of discrepancy then seems to be dependent on the angle of wave attack. Except for data from head-on waves and low wave load, the larger the angle of wave attack the larger the difference between wide and narrow grading appears to be. While the measured values for h_s tend to grow smaller for narrow grading and increasing angle of wave attack, the opposite trend can be observed for the wide grading.

Although the spread of the data points seems to be less for high wave load than for the low wave load, the data points for high wave load appear to be shifted revealing a tendency to underestimate the measured values. The influence of the wave load, denoted as H_0T_0, is more pronounced than the formula of Van der Meer supposes.

Slope below crest 'Θ3'

To describe the deformed slope even further, Merli came up with another parameter: Θ_3. This parameter, which was already defined in section 2.3.5, allows for an estimate of the crest recession regardless of the structure height, as it is considered to be fairly independent of the height above still water level. He found a relation for Θ_3 from tests with head-on waves, which was already mentioned in section 2.3.5:

$$\theta_3^{-1} = 0.00023\left(\frac{D_{n85}}{D_{n15}}\right)^{1.58}(H_0T_0)^{0.84} + 1.50 \qquad (2\text{-}27)$$

In Figure 5.9 the measured data points are compared with these values including data from tests with oblique waves. For the computed values no further reduction factor was used to include obliquity.

Generally the graph shows a tendency of the formula to underestimate the real values. A shift of the data points to the right would therefore be in order. However, while the computed values were calculated using formula(2-27), the measured values for the current tests were derived from the values for h_c. As indicated above, analysis of h_c turned out to be rather difficult; values were constantly underestimated and turned out to be highly dependent on the initial crest height. All in all the same conclusion can be drawn for values of Θ_3.

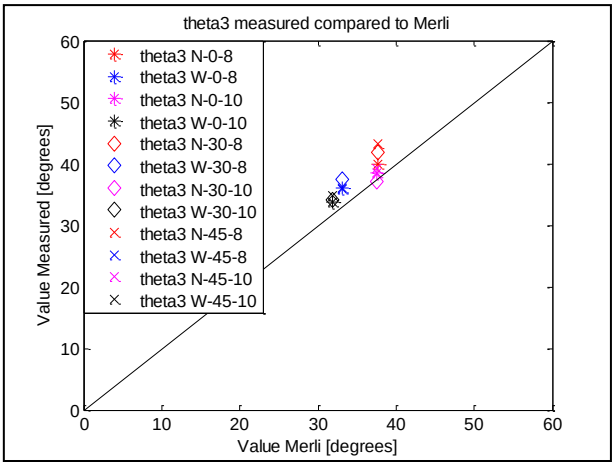

Figure 5.9: Comparison 'Θ3' with Merli

For the rest a large spreading is visible in the test data regarding the angle of wave attack. Although this spreading appears to be larger for the narrow grading, it is not possible to derive an unambiguous relation describing the effect of wave obliquity. The relation of the wave load and grading with Θ_3 however is better visible: both a higher wave load and a wider grading lead to a lower value of Θ_3, which is in conformity with larger expected values for the recession length under these conditions. Still, except for the data of low wave load and an obliquity of 45°, the measured data do not decrease with the same ratio as can be expected from the formula: the decrease due to a wider grading tends to be less pronounced than the relation of Merli indicates.

Also the effect of solely the wave load differs from the formula. A lower wave load, defined by a lower value for H_0T_0, results in a greater angle, Θ_3, than the computed values show. This tendency is more pronounced for the narrow grading, but is still visible for the wide grading.

5.1.2 Crest recession

Apart from the parameters defined by Van der Meer and Merli, another parameter which was first defined by Hall and Kao, the berm/crest recession Rec, can be used to characterize the deformed profile. Tørum and Merli expanded this research and both of them found a totally different relation for the recession length. These three relations were already described in section 2.3.6. In this section these formulas are compared to the measured data from the current tests, but first the relations of respectively Hall and Kao, Tørum and Merli are repeated:

$$\frac{Rec}{D_{n50}} = -12.4 + 0.39\left[\frac{H_s}{\Delta D_{n50}}\right]^{2.5} + 8.95\left(\frac{D_{n85}}{D_{n15}}\right) - 1.27\left(\frac{D_{n85}}{D_{n15}}\right)^2 + 7.3P_R \quad (2\text{-}29)$$

$$\frac{Rec}{D_{n50}} = 2.7\cdot10^{-6}\left(H_0T_0\right)^3 + 9.0\cdot10^{-6}\left(H_0T_0\right)^2 + 0.11\left(H_0T_0\right) - \left(-9.9\,f_g^2 + 23.9\,f_g - 10.5\right) - f\left(\frac{h}{D_{n50}}\right) \quad (2\text{-}31)$$

$$\frac{Rec}{D_{n50}} = 0.218H_0T_0 + 1.62\frac{D_{85}}{D_{15}} + 105\tan\alpha - 91.5 \quad (2\text{-}32)$$

In Figure 5.10 the measured recession length is compared to values computed while using the formula of Merli. From the measured values a clear distinction is visible between the gradings and wave loads tested. Both a more severe wave load and wider grading lead to a larger Rec, but the influence of the wide grading appears to be even larger than the affect of the higher wave load used. Also the effect of obliquity is obvious, a larger angle of wave attack results in a smaller Rec.

Furthermore the graph clearly shows an overestimation of all computed values. In the previous section it became clear that the both the values of h_c and Θ_3 were constantly underestimated. As the recession length is directly related to h_c, and with it also Θ_3, then the resulting overestimation comes as no surprise. This overestimation tends to become larger for the more severe wave load except in the case of narrow grading and obliquity of 45°.

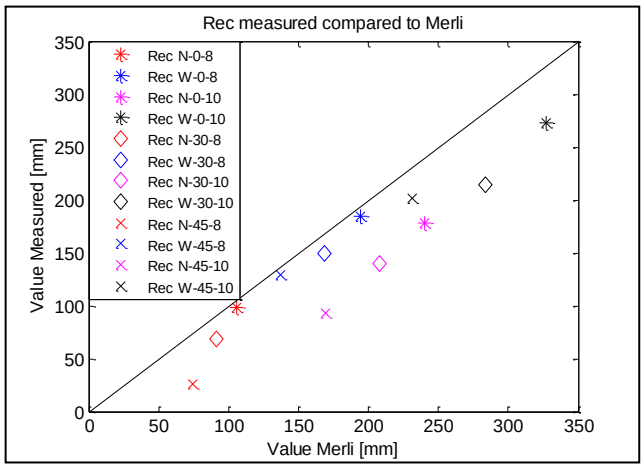

Figure 5.10: Comparison 'Rec' with Merli

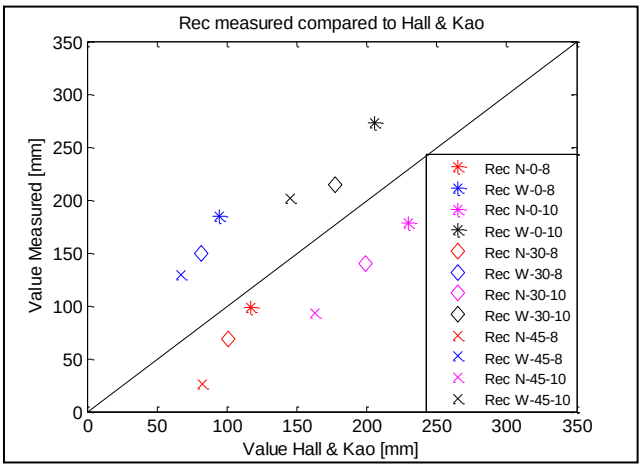

Figure 5.11: Comparison 'Rec' with Hall and Kao

As far as the influence of the grading is concerned, the values of the wide grading are generally speaking less overestimated than their narrow graded counterparts. Also a trend is visible in the data concerning narrow grading in which the overestimation becomes larger for a larger angle of wave attack. In the same comparison regarding wide grading the same relation is found for an obliquity of 0° and 30°, but the influence of 45° deviates considerably resulting in an overestimation in the same order of magnitude as for head-on waves.

In case of comparison with the formula of Hall and Kao, displayed in Figure 5.11, a different conclusion can be drawn. While the narrow graded values are overestimated, the widely graded values are just underestimated. This latter conclusion is not surprising as an inverted quadratic relation was found by Hall and Kao, in which the

stability increases and thus the recession decreases for wider gradings $\left(f_g > 3 \right)$. However from the data of the current tests a totally different relation can be found, the wider the grading the larger the crest recession, which is again more in accordance with the linear relation of Merli.

The overestimation of the computed values with narrow grading seems to be constantly larger in the case of low wave load when compared to Merli. In the case of high wave load this overestimation appears to be in the same order of magnitude as Merli.

Finally the current test data are compared with the relation formulated by Tørum, displayed in Figure 5.12. In this formula the grading is quadratically related to Rec leading to an even higher increase of Rec for wider grading than is the case for the relation of Merli. As the wide grading of 6 used in the tests falls clearly outside the limited range of validity $\left(1.3 < f_g < 1.8 \right)$, unrealistic results for the crest recession could be expected which were also found: some even as high as 3m. Due to these unrealistic results the comparison with the wide grading can be left out of consideration. The narrow grading of 1.3 however falls directly within the range of validity and some good predictions were expected. Nonetheless also these values are overestimated and the overestimation turns out to be even larger than was the case for the previous two relations. Apparently the description of Rec given by relation (2-31) is not correct and values of f_g outside the range, as well as values within the range of validation lead to a clear overestimation.

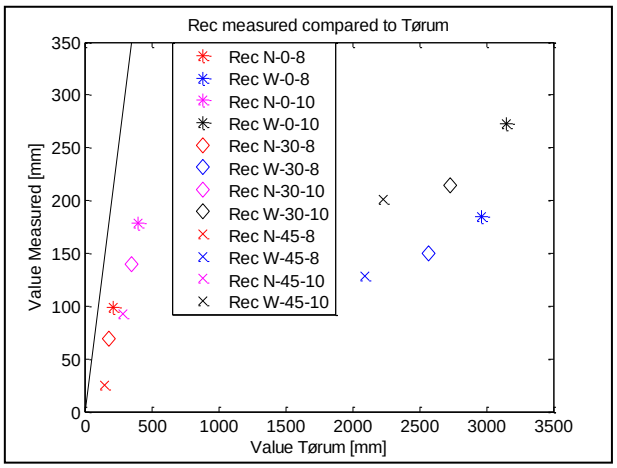

Figure 5.12: Comparison 'Rec' with Tørum

5.2 Longshore transport

This paragraph deals with the stone displacement and longshore transport. The graphs from the previous chapter regarding the stone displacement are used to determine the influence of the wave load, angle of wave attack and grading. Subsequently the total longshore transport is elaborated further and compared to the commonly accepted formulas.

5.2.1 Stone displacement

For each test graphs are displayed in appendix C2 representing the stone displacement for the separate colour beams. Aside from test W-45-10 little difference could be found between the displacements of stones originating from blue or pink colour beams. Apparently the distance between and the width of the two colour beams were too small to make a major difference visible. The exception of W-45-10 could be attributed to difficulties in measuring the first two sections as a result of premature cave-ins. This led to a greater inaccuracy concerning this data and no first data point could be extracted. For the same reasons, this was also the case for test W-45-8. However, in section 4.4.1 a satisfying exponential relation was found for each test, even for these two test results. In the remainder of this section the relations found are used for a qualitative analysis of the stone displacement.

Influence wave load

In Figure 5.13 to Figure 5.16 the stone displacements of the two different wave loads are compared to each other while keeping the angle of wave attack and grading the same. The graphs represent the amount of stones relative to the distance from the centre of the breakwater. Distinction between higher and lower wave load is made by respectively the red and black line.

Clearly visible from the graphs is the distinction between the data points of both wave loads. A higher wave load obviously leads to an increase in the stone displacement in the first two metres, while most of the displacement of the low wave load takes place in the first metre from the centre. The accompanying difference appears to increase even further for the wider grading. Especially around the colour beams itself a clear distinction is visible for the wide grading, whereas the difference in this area for the narrow grading is practically non-existent. Over longer distance the differences are levelled as also the stone displacements diminish.

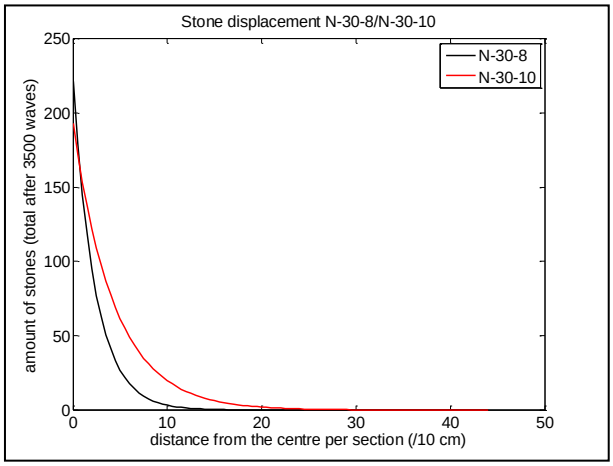

Figure 5.13: Stone displacement N-30-8/N-30-10

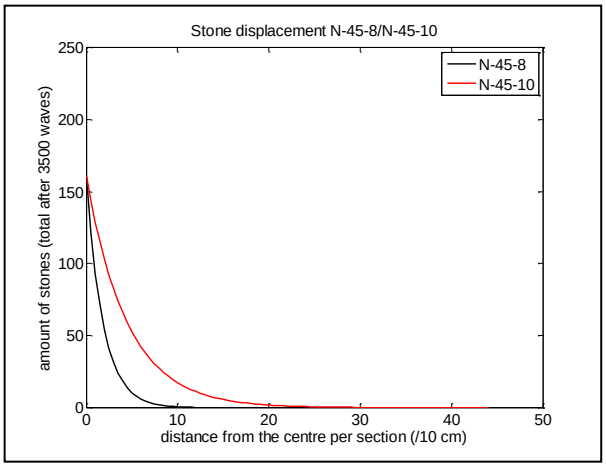

Figure 5.14: Stone displacement N-45-8/N-30-10

As mentioned before the first data points in the data set of test W-45-8 and W-45-10 could not be acquired. Interpolations of the first 10 centimetres are therefore based on less data points and thus less accurate, than for the other tests. For the curve of W-45-10 this inaccuracy is even extended to the first metre as also the acquirement of data points from the second section turned out to be difficult.

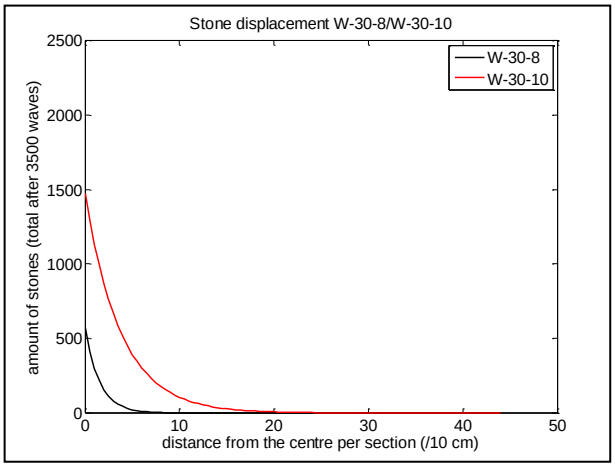

Figure 5.15: Stone displacement W-30-8/W-30-10

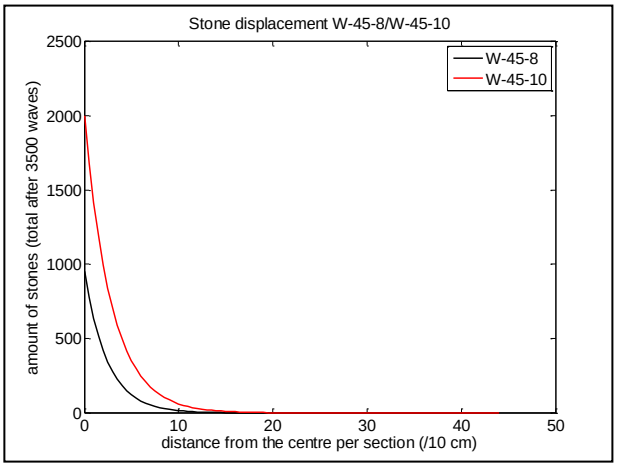

Figure 5.16: Stone displacement W-45-8/W-45-10

Influence of angle of wave attack

In this section the graphs are plotted which show the influence of the angle of wave attack while keeping the wave load and grading the same. In these figures, Figure 5.17 to Figure 5.20, the black lines represent data of tests occurring under an angle of wave attack of 30 degrees while the data extracted from tests with an angle of wave attack of 45 degrees are represented by red lines.

In general no clear distinction can be found in the longshore transport between angles of wave attack of 30 or 45 degrees. Nonetheless some differences are visible, but they are less distinctive than when the wave load

was varied in the previous section. Apparently the data from tests with narrow grading show a slight tendency of increased transport under 30 degrees wave attack.

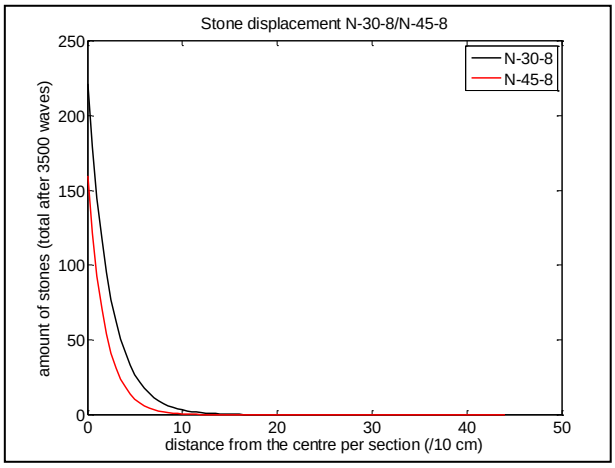

Figure 5.17: Stone displacement N-30-8/N-45-8

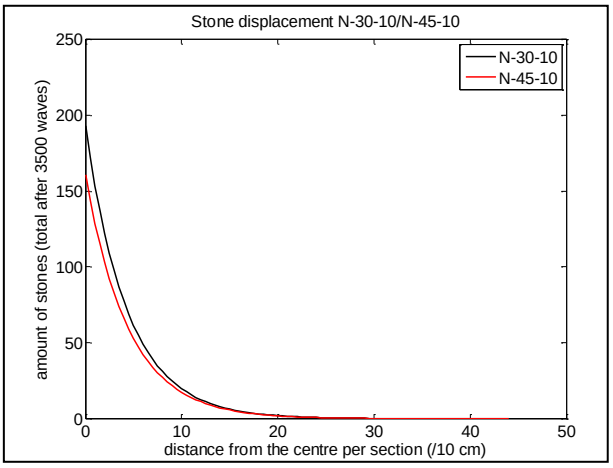

Figure 5.18: Stone displacement N-30-10/N-45-10

Remarkably enough, the comparison between test W-30-8 and test W-45-8 leads to a totally different conclusion with an opposite tendency. This opposite tendency however does not match entirely with the outcome of the other comparison between tests with wide grading (W-30-10 and W-45-10). From the last comparison no clear conclusion can be drawn aside from an increased displacement for 45° wave attack around the centre itself and an increased displacement for 30° further along the breakwater.

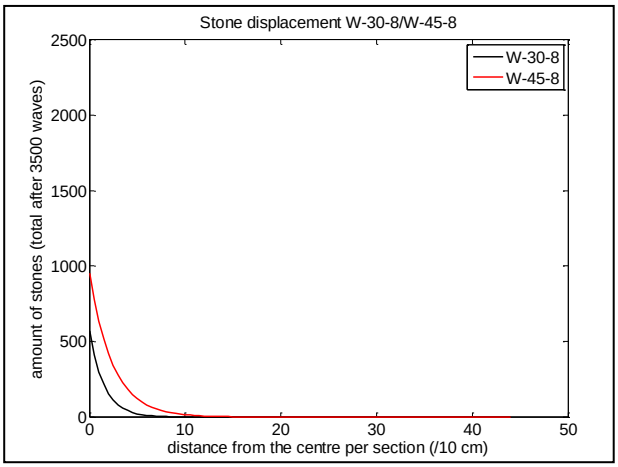

Figure 5.19: Stone displacement W-30-8/W-45-8

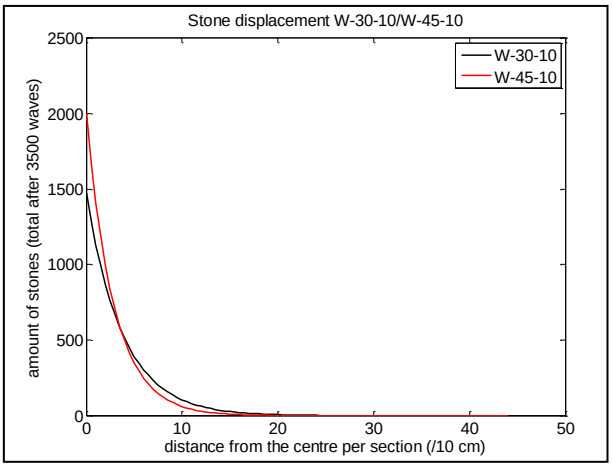

Figure 5.20: Stone displacement W-30-10/W-45-10

The minimal differences in displacement found between 30° and 45° are rather surprising as they deviate from previously observed trends. And although the available formulas concerning longshore transport, formulas (2-48) and (2-50), describe different relations between wave obliquity and longshore transport, they still make a clear distinction between the two angles.

Influence of grading

After elaborating both the influence of the wave load and angle of wave attack in the first part of the section now only the influence of the grading on the longshore transport remains. In the Figure 5.21 to Figure 5.24 the graphs are plotted to provide this insight while keeping the angle of wave attack and wave load constant. Data of tests with narrow and wide grading are indicated by respectively black and red lines.

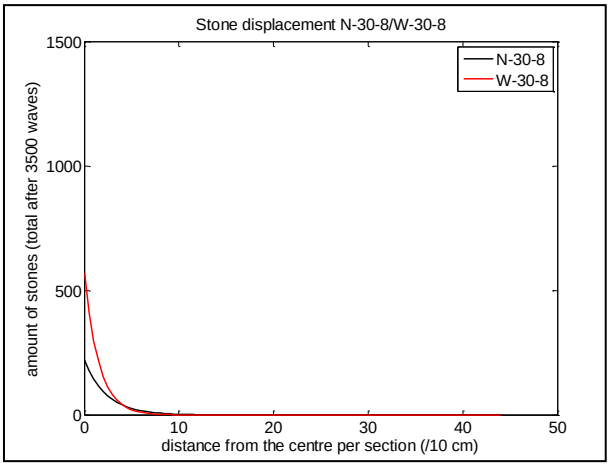

Figure 5.21: Stone displacement N-30-8/W-30-8

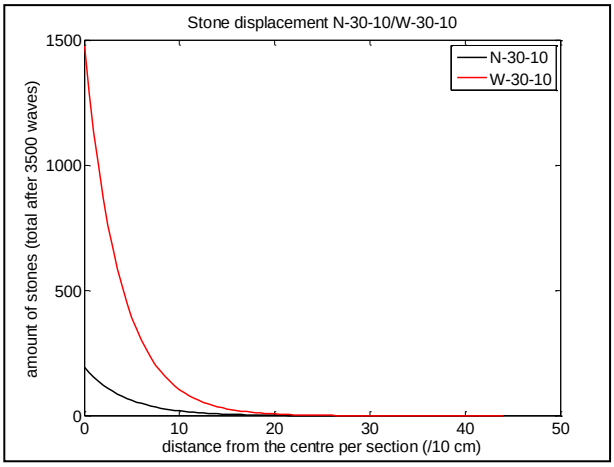

Figure 5.22: Stone displacement N-30-10/W-30-10

With no exception a clear distinction can be made between the transports of tests with wide and narrow grading. As expected the wide grading leads to an increase in the stone displacement. This distinction becomes even more evident during the tests with the higher wave load. The first graph, which compares the tests N-30-8 and W-30-8, stands out as the difference observed is far less than the other tests indicate. Also an increase in angle of incidence appears to induce an increase in displacement, but only for the lower wave load.

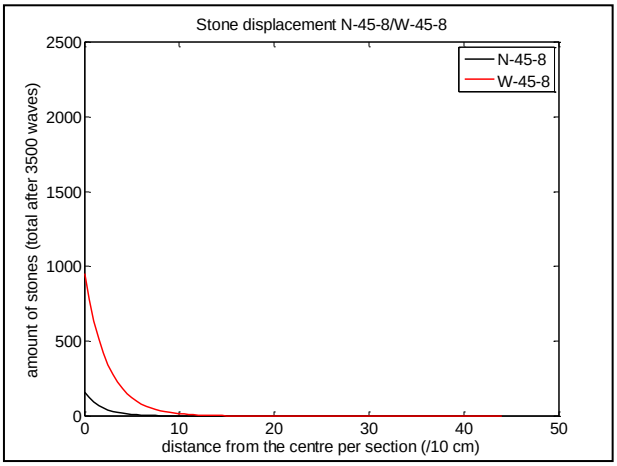

Figure 5.23: Stone displacement N-45-8/W-45-8

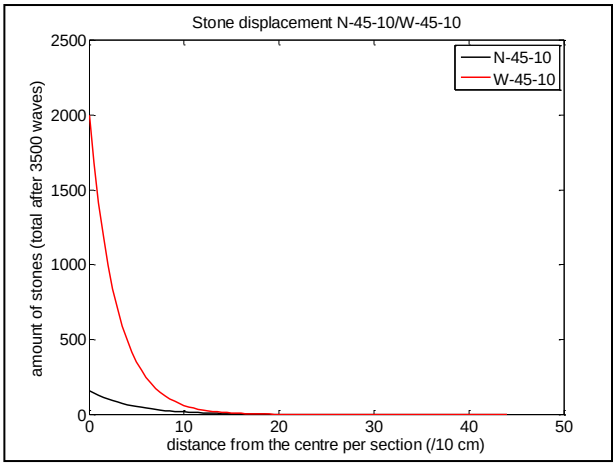

Figure 5.24: Stone displacement N-45-10/W-45-10

5.2.2 Total longshore transport using extrapolation

In section 4.4.1 the displacement data were already extrapolated for the length of breakwater in which uniform transport was assumed. This resulted in a total longshore transport along the trunk for each test. In the following graphs, displayed in Figure 5.25, these transports are plotted together to portray the influences of consecutively grading, angle of wave attack and wave load.

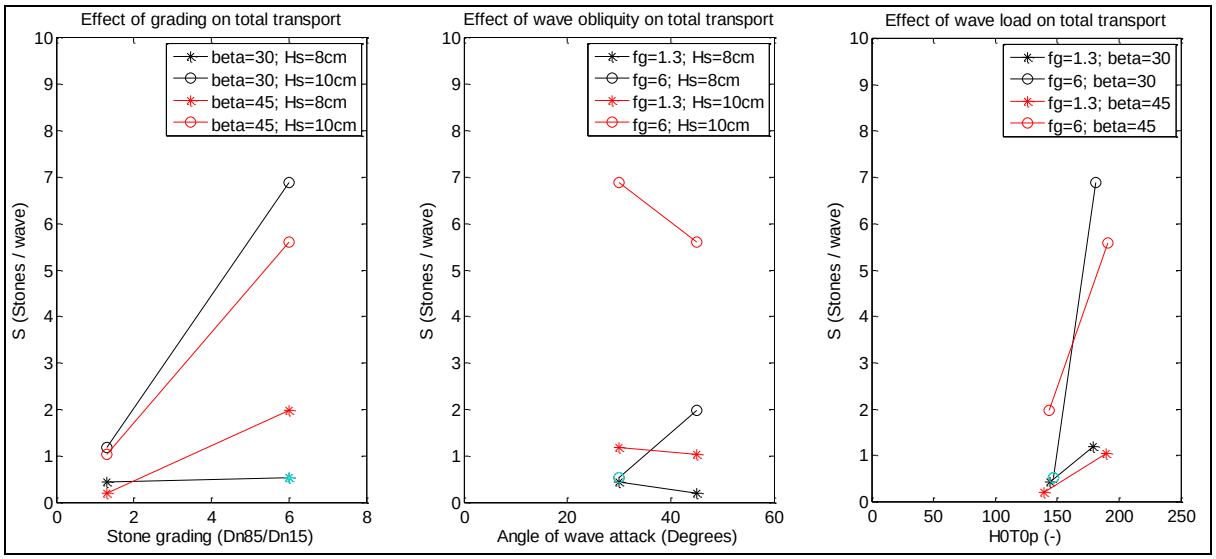

Figure 5.25: Influence of grading, wave obliquity and wave load on longshore transport

From these graphs one data point really stands out, namely the data point representing the longshore transport of test W-30-8 which does not agree with the other data points. In the previous section displacement data of this test also resulted in deviations regarding the comparisons with other tests. In fact in all three graphs; describing respectively the influence of wave load, wave obliquity and stone grading of test W-30-8; a relation was presented which was in one way or another deviant from the data of other tests. Apparently the displacement measurements of test W-30-8 did not lead to a representative result.

Multiple causes for this deviancy could be given, such as measurement errors or differences in wave loads and the rebuilding of the colour beams. As the wave spectrum during this test did not vary significantly from other tests with the lower wave spectrum, the wave load can be excluded. Also no strange abnormalities were observed in the initial profile and deformation. Moreover the displacement measurements were conducted in the same manner as the other tests, even without the problems that occurred during the measurement at test W-45-8 and W-45-10. Consequently the error probably originated from the rebuilding of the colour beams. The most obvious cause would then be a difference in grading. Should less material be available of the finer fractions, less stones would be displaced leading to a decrease in the total longshore transport. This can be checked later on when the contributions of the different stone fractions to the total longshore transport are elaborated in section 5.2.4.

Aside from the data point of test W-30-8 consistent tendencies can be found regarding each varying parameter. For this reason the same graphs are displayed again in Figure 5.26, now without the value for test W-30-8. Clearly visible is the increasing trend for increasing grading and wave parameter, H_0T_0. In both cases this leads to a much larger spreading. Furthermore the increase in longshore transport, due to an increase in grading, seems to be stronger for the more severe wave load. The same is true for a wave obliquity of 30° which leads to a larger increase in transport, for a wider grading, than an angle of 45°.

In the second graph a decreasing trend between 30° and 45° is evident, which is in accordance with [VAN DER MEER 1992] and [TOMASICCHIO 2007], but not with the transport formula of [ALIKHANI 1996]. However the rate of decrease for the tests with narrow grading is far less than for wide grading and severe wave load. In the displacement graphs of the previous section the same minor differences were found for the narrow grading. As was already mentioned there, this observation deviates from the currently available formulas of Tomasicchio and Alikhani, which each give a totally different relation, but agree on a clear distinction between these angles of incidence. At first sight also Figure 5.20, the graph of displacement for high wave load and wide grading, displayed a minor, almost negligible, distinction. While the displacement adjacent to the colour beams showed some higher values for an angle of 45°, a long stretch further away was to the advantage of a wave obliquity of 30°. As this part was integrated more often in order to determine the total longshore transport, the clear difference, as is shown in Figure 5.26, comes as no surprise.

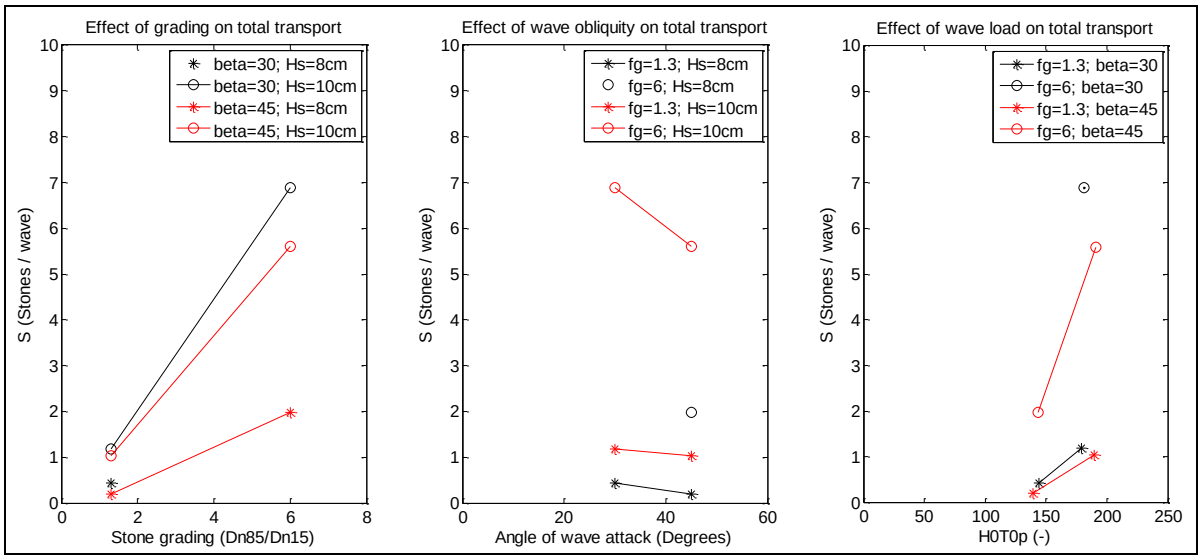

Figure 5.26: Corrected influence of grading, wave obliquity and wave load on longshore transport

According to the currently accepted models the larger the angle of incidence the larger the longshore current will be. In this case a maximum longshore transport would be expected at a wave obliquity of 45°. From the second graph, however, it is clearly visible that the value for an angle of 45° did not coincide with the maximum observed for longshore transport. Although the longshore current generated by oblique waves was larger, the impact and therefore load on the structure was less leading to a reduction in longshore stone transport.

In the third graph an increasing trend is visible for increasing H_0T_0. The rate of increase appears to be larger for the wider grading.

5.2.3 Comparison with commonly accepted formulas

The next step in the analysis of the longshore transport contains a comparison between the observed and computed values. From this analysis it is then possible to determine to what extent the currently accepted formulas predict the observed values. In section 2.4.1 several formulas were mentioned regarding the longshore transport. Most of these formulas were defined for berm breakwaters for which the equilibrium profile was reached after deformation. Additionally another important difference, compared to the current tests, can be mentioned: the grading used in the previous tests did not exceed $f_g = 2$ while for the current tests also a wide grading of $f_g = 6$ is used. As the existing relations do not take into account the influence of grading, no distinction can be made in the prediction between the two different gradings used. For this reason only the measured values of current tests with narrow grading can effectively be compared to values computed with the three most commonly accepted formulas. Nevertheless also the results of the tests with wide grading are included in the graphs displaying the relations as these will complete the insight in the current relations. In the graphs shown in this section also a distinction is made between reshaping and after-reshaping. Data points representing reshaping are portrayed in red, while data points portraying after-reshaping are black.
[TOMASICCHIO 2007] defined a formula to predict the longshore transport and used it to compute the transport not only after reshaping, but also during the reshaping process:

$$S_N = \frac{l_d}{D_{n50}} \frac{N_{od}}{N} \sin \psi_{kb} \qquad (2\text{-}50)$$

This formula is rather laborious in a sense that various additional parameters need to be defined before the actual computation can take place. In Figure 5.27 a comparison is made between the observed and computed transport. As only eight data points were generated during the current tests, also the data of previous tests were added to the comparison. Due to missing information regarding some of the additional parameters needed, computation of these test results was mostly difficult. Therefore in the computation estimates were used in case of unknown values. For the data set of [VAN DER MEER 1992] this meant that the following values

were assumed for the water depth and number of waves: $h = 8.6 - 9.6m$ and $N = 3000$. For the data set of [VAN HIJUM 1982] values had to be assumed for the mean wave period, nominal diameter and also the amount of waves. The values in the graph are calculated with the following assumptions: $T_m = {}^{T_s}/_{0.95}/_{1.15}$, $D_{n50} = 4.032mm$ and $N = 100000$.

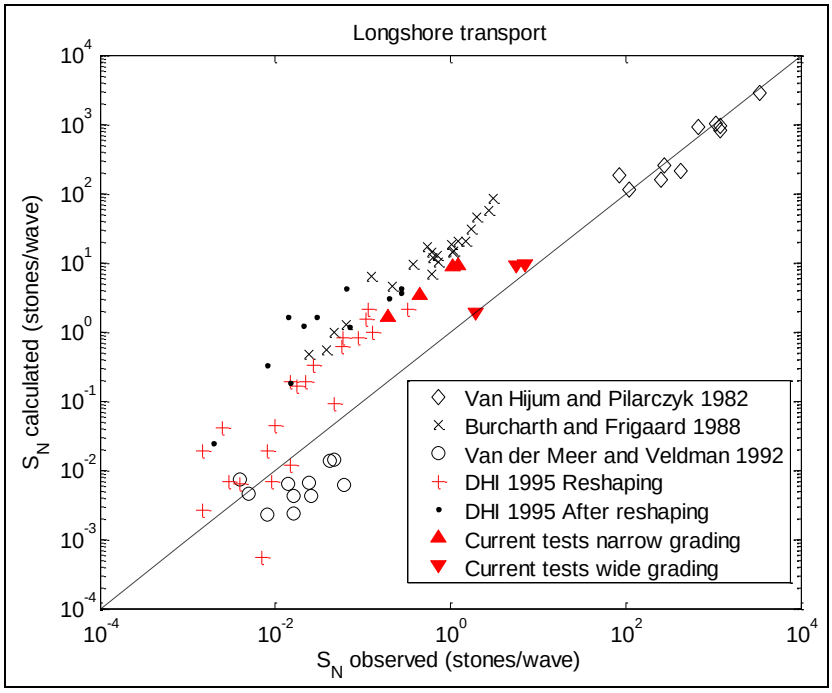

Figure 5.27: Comparison of test results with formula (2-50) of Tomasicchio

The data of the wide grading, aside from test W-30-8, seem to be fitted rather nicely by the relation. However for the data set of the current tests with narrow grading a large overestimation can be observed. This overestimation is roughly the same for each test and is in the order of magnitude 8. This is in line with data of tests during reshaping at DHI. For lower stability numbers $(H_0 = 2 - 2.5)$ the data of DHI is better fitted though the spreading is wider. However for data of tests after reshaping at DHI the overestimation is much higher. It appears that the effect of the number of waves in the relation is very dominant. As the reshaping tests consisted of 2 times the number of waves of the tests after reshaping, the overestimation of the latter is roughly 2 times higher. The same holds true for the comparison with Burcharth and Frigaard which give more or less the same overestimation. Still also these data sets fall nicely in line with the current data set for narrow grading. Finally the other two data sets are fitted even better by relation (2-50). Nonetheless they give a rather distorted image, as assumptions had to be made, especially for the number of waves, in order to carry out the calculations.

On the other hand the effect of obliquity in the computations is the same as observed from the current test data in the previous section. The longshore transport for 30° is higher than for 45° confirming observations done by Van der Meer and Tomasicchio in which maximum transport does not occur at 45° but at smaller angles.

When the observed longshore transport is plotted against the modified stability number the data of the current tests with narrow grading are nicely in line with the other datasets of berm breakwaters. Data of tests with wide grading do not fit in. Figure 5.28 shows this graph in which a distinction is made in three different regions. The first region, $2 < N_s^{**} < 6$, refers to berm breakwaters and the third to gravel beaches, $9 < N_s^{**} < 24$. The second region forms a transition region and can be referred to as rock and cobble beaches, $6 < N_s^{**} < 9$. No test data is yet available for this area.

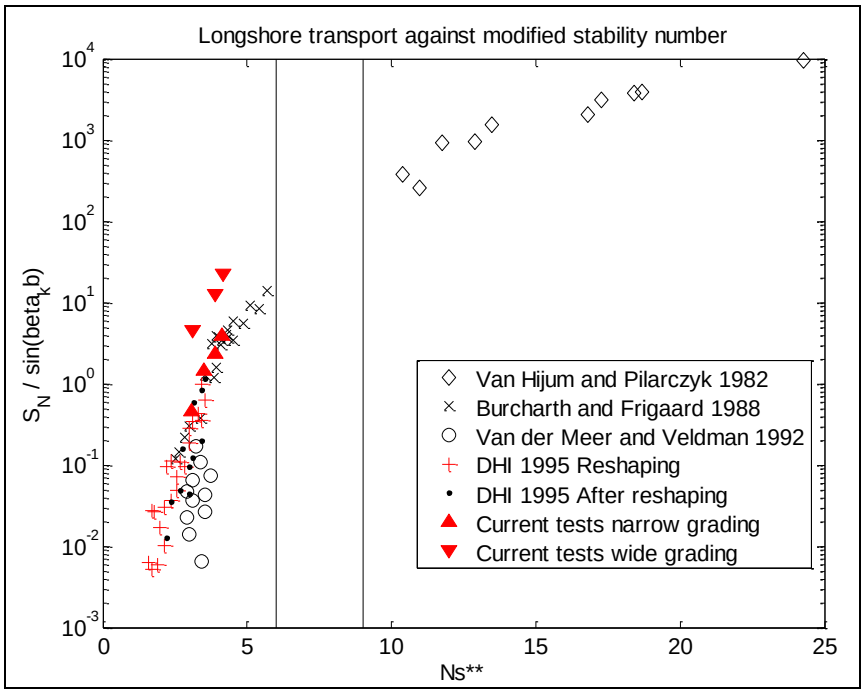

Figure 5.28: Longshore transport against modified stability number 'Ns'**

In Figure 5.29 this graph is plotted again, now with a double logarithmic scale. By means of curve fitting it is possible to draw a straight line through the data points. In this way a power function can be derived linking the longshore transport rate to the modified stability number. For the scaling component 'n' a value of 5.77 is found, which leads to the following relation:

$$S_N = 10.64 \cdot 10^{-5} \left(N_s^{**} \right)^{5.77} \qquad (5\text{-}1)$$

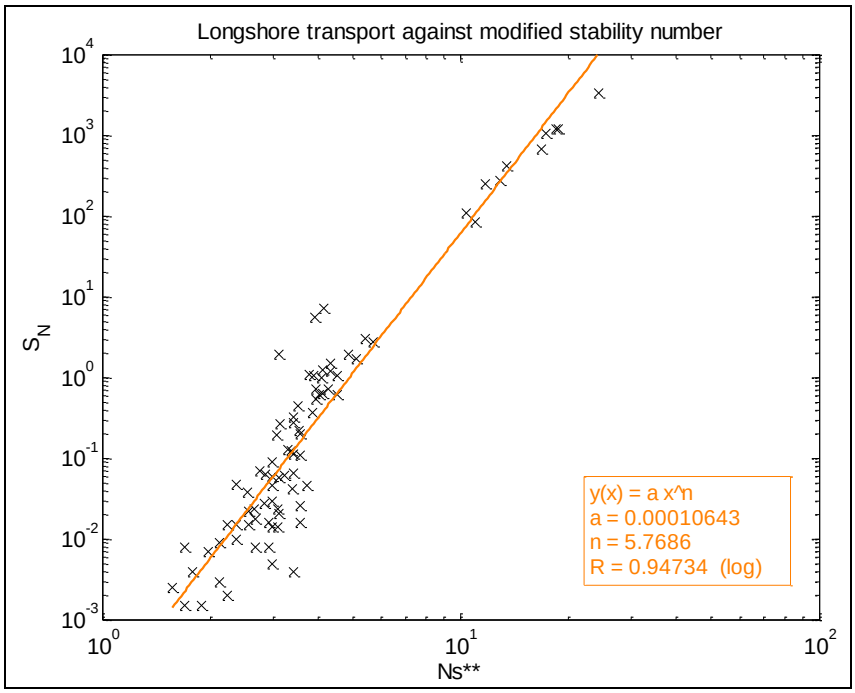

Figure 5.29: Curve fitting of relation between longshore transport and 'Ns'**

The second formula evaluated is the relation found by [ALIKHANI 1996] which predicts the longshore transport on already deformed profiles:

$$S_N = 0.8 \cdot 10^{-6} \sqrt{\cos\psi} \left(H_0 T_{0p} \sqrt{\sin 2\psi} - 75 \right)^2 \qquad (2\text{-}48)$$

The relation is written in the same format as the formulas for gravel beaches defined by Van Hijum and Pilarczyk and Van der Meer relating the longshore transport to the combined wave height-wave period parameter $H_0 T_{0p}$ and the angle of wave attack. As it concerns standard and easily determinable parameters the computation of the relation itself is easily accessible.

However when the predicted values are finally compared with the observed values, the analysis leads to unsatisfying results. The formula results in a very large underestimation which is on average in the order of magnitude 100, but varies considerably between 47 and 145. For data of tests with wide grading the underestimation is even larger.

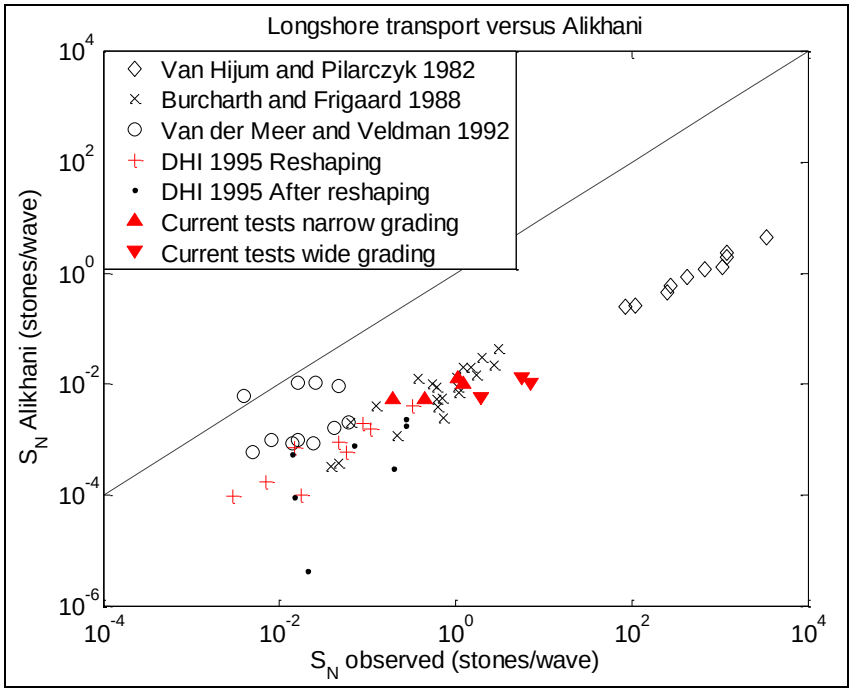

Figure 5.30: Comparison of test results with formula (2-48) of Alikhani

Moreover when previous test results are included in the comparison the similar conclusion can be drawn. This is clearly visible from Figure 5.30 where red points portray data from tests during reshaping and black from after reshaping. Even the test results of transport after reshaping at DHI, the same data set which was used to formulate the relation in the first place, lead to an underestimation largely in the same order of magnitude as for the current data set. Only in the comparison with tests of Van der Meer and Veldman with an obliquity of 50° a relatively nice fit is found.

Especially characteristic is the extreme underestimation for $H_0 T_{0p} \sqrt{\sin 2\psi} \approx 75 \rightarrow S_N \approx 0$. This is the threshold value for transport after reshaping and the computed values differ considerably from the observed values leading to an underestimation for some cases in the order of 10^4. Re-evaluation of this limit is therefore recommended.

Also the cooperation of the factors including the angle of wave attack, $\sqrt{\cos\psi}$ and $\sqrt{\sin 2\psi}$ do not appear to describe the influence of wave obliquity properly. Given $H_0 T_{0p} < 157$, the statement of zero transport for head-on waves does not hold true as this formula actually gives maximum transport for $\psi = 0$. Still under the threshold condition that $H_0 T_{0p} \sqrt{\sin 2\psi} > 75$, and $H_0 T_{0p} \sqrt{\sin 2\psi} > 50$ during reshaping, the maximum computed transport indeed occurs at an angle of wave attack of 45° with a decreasing tendency for both smaller and larger angles. However as in the previous section a different tendency was found, confirmed by

other preceding research, in which an angle of 30° results in a larger transport than at 45°, these factors should be adjusted.

To complete the picture a final comparison is made with the older formula of [VAN DER MEER 1992] from which the formula of Alikhani evolved. This formula does not include any effect of wave obliquity and was already described in section 2.4.1:

$$\begin{aligned} S_N(x) &= 0 && H_0T_0 < 105 \\ S_N(x) &= 0.00005\left(H_0T_0 - 105\right)^2 && H_0T_0 > 105 \end{aligned} \qquad (2\text{-}44)$$

In Figure 5.31 the observed values are again plotted against the computed values. Although the spreading is rather large the relation forms a relatively good fit with the different datasets, especially with the data of Burcharth and Frigaard and Van der Meer and Veldman under an angle of 25°. Data from the same tests with obliquity of 50° result in a large overestimation. Clearly high obliquity is of influence and its effect cannot be ignored.

Furthermore the transport during the reshaping phase appears higher than after reshaping. As the relation is formulated only for transport on the already deformed profile, values of tests during reshaping, including the current tests, are clearly underestimated. Therefore the formula is not suitable to describe the longshore transport during the reshaping process.

Also the very large underestimation of values near the threshold value, $H_0T_0 \approx 105$, is clearly visible. Generally speaking the closer around this threshold value the less accurate this formula becomes.

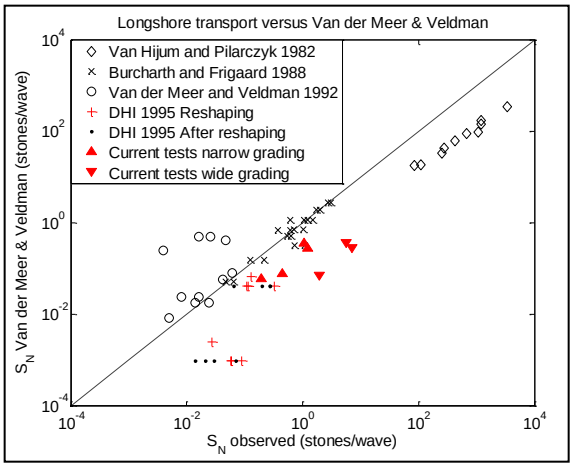

Figure 5.31: Comparison test results with formula (2-44) of Van der Meer

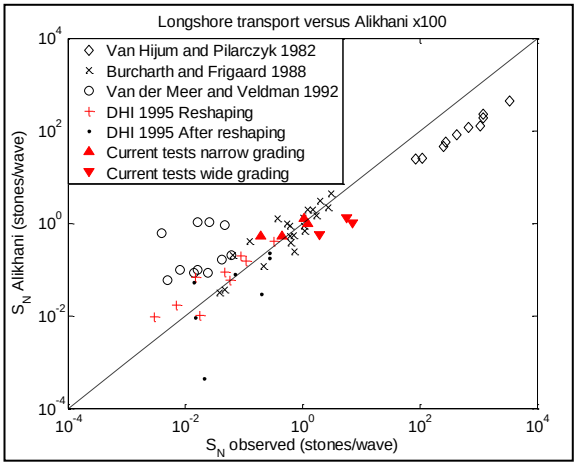

Figure 5.32: Comparison test results with formula (2-48) of Alikhani x100

Next to the graph in Figure 5.32 the same comparison of Figure 5.30 is given, but now the coefficient used in formula (2-48) is multiplied by a hundred. By doing this the new coefficient $\left(8\cdot10^{-5}\right)$ is of the same order of magnitude as the coefficient used earlier by [VAN DER MEER 1992] and [VRIJLING 1991], which leads to the following adjusted formula:

$$S_N = 8\cdot10^{-5}\sqrt{\cos\psi}\left(H_0T_{0p}\sqrt{\sin 2\psi} - 75\right)^2 \qquad (5\text{-}2)$$

Now a relatively nice fit is obtained with all data sets both during and after reshaping. When the new coefficient is checked with the research described in [ALIKHANI 1996] the same conclusion can be drawn as a far better fit is produced. This is clearly visible in Figure 5.33 and Figure 5.34 where the test results of respectively Burcharth and Frigaard and tests at DHI are compared with both formulas. Although it is not possible to give a clear explanation of what probably went wrong in the derivation of formula(2-48), it is likely that an error was

made. In appendix C5 the same comparisons are displayed, now also with the test results of other tests discussed.

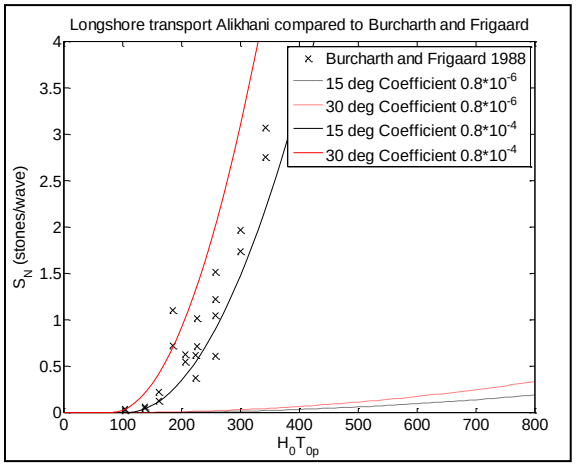

Figure 5.33: Comparison use different coefficients with Burcharth and Frigaard

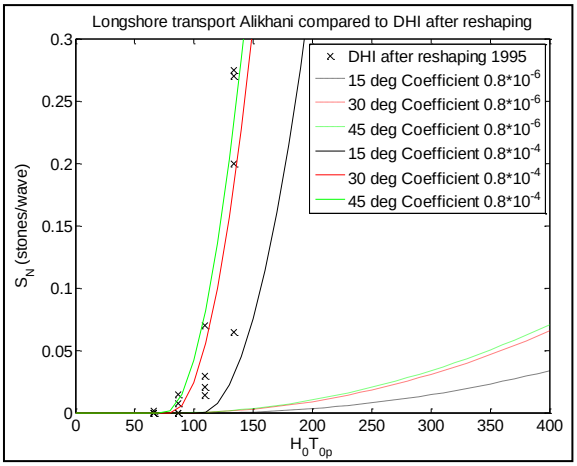

Figure 5.34: Comparison use different coefficients with DHI after reshaping

Compared to relation (2-44) of Van der Meer and Veldman the spreading of formula (5-2) is less and data of tests during reshaping are described better. This is however at the expense of the predictions of the tests of Van der Meer and Veldman for a wave obliquity of 50°. Nonetheless a first step in improving formula (2-48) is taken.

5.2.4 Longshore transport per stone fraction

As was visible in the previous sections, the longshore transport was more severe for the wide grading than for the narrow grading. On one occasion this difference was even ten times larger. The increase in volume transport however was not proportional as not all fractions were transported evenly. Mostly the finer fractions determine the total longshore transport in stones/wave while their contribution to the volume transport is far less.

In Table 5.1 again the total longshore transport rates are computed, but now per fraction. These values were acquired by deriving the exponential relations for every stone fraction separately. After that the separate relations were used to compute the longshore transport according to the method discussed in section 4.4.3. Compared to the previous computation, only some minor differences in the values of the longshore transport rate were found. These differences however are negligible and do not affect the trends found in the previous sections.

Table 5.1: Longshore transport per stone fraction

Sn (stone/wave)	**Narrow grading**	**Wide grading**					
	Total	*Total*	*4-8 mm*	*8-11 mm*	*11-16 mm*	*20-40 mm*	*30-60 mm*
30_8	0.445	0.578	0.205	0.186	0.161	0.022	0.0038
30_10	1.235	8.652	4.992	3.318	0.290	0.041	0.0108
45_8	0.196	1.937	1.338	0.444	0.135	0.017	0.0032
45_10	1.061	5.744	3.797	1.414	0.470	0.052	0.0100

Clearly visible are the rather low values for the transport of stone classes 4-8mm and 8-11mm during test W-30-8, while the transports of the coarser fractions was as expected. This observation confirms the explanation given in section 0, in which the deviant value for test W-30-8 was attributed to a deficit of the finer fractions. Apparently during this test the grading of the colour beams was narrower, making the test result not comparable to the other tests.

Furthermore for higher wave load it appears that the decreasing trend of the longshore transport for increasing angle of incidence, from 30° to 45°, could mostly be attributed to a decrease of transport of the finer two fractions. In fact the transport of fractions 11-16mm and 20-40mm even showed an opposite tendency. Probably the gradings of the colour beams during these two tests were not entirely comparable either, but in this case it is not possible to determine exactly which of the tests results show deviant behaviour in relation to the others.

By using the following formula, which was already mentioned in section 2.4.1, the longshore stone transport computed above can be converted into a volume transport:

$$S_V = \frac{S_N D_{n50}^3}{(1-n)T_m} \tag{2-51}$$

Table 5.2 shows the longshore volume transport for the current tests. When the nominal diameter of the whole mixture is used the volume transport will be overestimated greatly and the increase from narrow to wide grading ranges from a factor 5 to 9. Exception is the comparison between the tests with low wave load and obliquity of 30°, but this deviation was already mentioned and explained. When the nominal diameters of the different stone fractions are taken into account, the volume transports of the other three tests with wide grading are more or less a factor three smaller than when only one nominal diameter is used for the whole mixture. Now between tests with narrow grading and wide grading an increase of roughly a factor 2 is obtained.

Table 5.2: Longshore volume transport per stone fraction

Sv (mm3/s)	**Narrow grading**	**Wide grading**						**Over-estimate**
	Total	*Total*	*4-8 mm*	*8-11 mm*	*11-16 mm*	*20-40 mm*	*30-60 mm*	*Total*
30_8	1344.3	1437.4	76.2	103.6	438.5	361.4	457.7	1578.9
30_10	3429.1	5925.5	1707.6	1695.3	722.0	615.0	1185.6	21690.2
45_8	599.5	1778.3	502.7	249.3	369.9	272.7	383.7	5334.3
45_10	2901.1	4996.6	1281.1	712.7	1157.0	768.9	1076.8	14203.5

In contrast to the total amount of stones transported, the actual volume transport by the finer fractions was limited and relatively large contributions were given by the coarser fractions. The contributions of the coarsest fraction 30-60mm to the volume transport were; although slightly smaller; even in the same order of magnitude as the finest fraction 4-8mm. Except for the test result of test W-30-10 the same was also true for the contributions of the middle fraction 11-16mm. On the other hand this could not be said of the fractions in between as they constantly showed smaller transport values.

Looking to the distribution of the different fractions composing the widely graded mixture, a clear link can be found between the largest portion, 11-16m, and volume transport. However this link cannot be found in the comparison with both the finest and coarsest fractions. Apparently the higher instability of the fraction 30-60mm has led to a higher initial volume transport around the originating colour beams, while the mobility of the finest fraction contributed to large values for the volume transport on the long run.

6. Conclusions

6.1 Conclusions

Previous experiments were conducted to get a better understanding of the stability of dynamically stable berm breakwaters and gravel beaches. These researches resulted in several empirical formulas describing processes as two-dimensional deformation and longshore transport. While several governing parameters were investigated and included in the formulas; no or only minor attention was given to the effect of grading, not in the least the influence of wide to very wide grading.

As it turns out exposed breakwater cores under construction deform in more or less the same manner as berm breakwaters. However observations in the field have proved that this deformation is more severe, thereby complicating the predictions of available empirical formulas. Besides a smaller stone size the core material can also be characterized by a much wider grading than is used for the berm of berm breakwaters.

To investigate the influence of this wide grading on the two-dimensional deformation as well as the longshore transport new physical model tests were conducted, as described in this thesis. In total 12 tests were executed in which two different gradings were tested: a narrow grading $f_g = 1.3$ and wide grading $f_g = 6$. Other parameters varied were the wave spectrum, with a value for H_{m0} of 0.08m and 0.10m, and the angle of wave attack with values for ψ of 0°, 30° and 45°.

In general a clear distinction was found in the processes between tests with narrow grading and wide grading. Namely both the parameters describing the two-dimensional deformation and the longshore transport show an increase for wider grading. In the following sections the most important findings of the tests are discussed. Before the conclusions regarding the two-dimensional deformation and longshore transport are further elaborated, first of all the findings concerning the conceptual model are discussed.

6.1.1 Conceptual model stone transport

Stone movements during both reshaping phase and after reshaping

Although the tests were conducted for the main part during the reshaping phase, also some observations of stone displacements were done on the already deformed profile. As no quantitatively data of the outer profile and longshore stone displacements were obtained during the tests, it was not possible determine the point in time on which the equilibrium profile was reached. Nevertheless, some distinctions between both phases were clearly visible.

During the reshaping phase deformation was dominated by stones rolling down the slope due to instability created by wave attack and gravity. Because of this dominant transverse component, stones transported in longitudinal direction due to oblique wave attack were quickly overwhelmed. While the actual rate of the longshore transport was high the displacement length was rather short.

After reaching an equilibrium profile the crest kept slowly crumbling off at the impact of the highest waves of the wave spectrum. Also around the water line material continued to move in the direction of the incoming and reflected waves resulting in a transport along the breakwater in the case of oblique wave attack. Although the amount of stones transport was less than during the reshaping phase, the displacement length increased considerably. Stones kept being transported until the rear side of the breakwater was reached and further transport was prevented.

Segregation as a result of stone displacement

When the displacements of the different stone fractions are considered, it is concluded that through the differences in movement the widely graded mixture segregates in the transverse as well as the longitudinal

direction. Hereby the coarser fractions were transported mainly in a transverse direction until quickly a stable position was reached either at the foot of the breakwater or on the gentle slope after reshaping. While this transport was accompanied by only a minor displacement longshore, the finer fractions were transported much further along the trunk. As even after reshaping no stable situation was reached for the finer fractions, stones kept moving along the waterline in the direction of the up- and down-rush of the waves. The finer the material, the further this transport proceeded until finally at the rear side of the roundhead further movement was prevented.

6.1.2 Two-dimensional deformation

Profile measurements, taken after the tests, were processed into three-dimensional models which display the profile deformation clearly for each test. For the two-dimensional deformation the test results were compared to currently available formulas. Observed deformation parameters like l_c, l_s, h_c, h_s and Θ_3 were compared with relations derived by Van der Meer and Veldman and Merli, while predictions of formulas of Hall & Kao, Tørum and Merli were compared to the actual recession lengths, Rec.

Crest length 'lc'

While the angle of wave attack does not appear to have an influence on the crest length, l_c, the grading clearly does. Namely a wider grading results in a longer crest length as was already described by Merli. Formula (2-26) therefore produces a better fit describing the effect of grading rather well. Only for values of $f_g = 1.3$, which fall outside the range of grading tested by Merli, the values for l_c are underestimated and adjustment of this formula for very narrow gradings is recommended.

Step length 'ls'

Also for the step length, l_s, the effect of grading is evident; longer step lengths were observed for wider gradings. Accordingly formula (2-25) derived by Merli gives the best description. The effect of wave obliquity however appears ambiguous. While for narrow grading during the tests this effect neared the reduction factor, $\cos\psi$, for wide grading hardly any difference was found between the different angles of wave attack. This leads to the conclusion that the reduction factor might be grading dependent. As normally a clear distinction between the different angles is visible, this outcome was not expected. It is therefore recommended that the observed relations are investigated further in future model tests before the reduction factor is adjusted.

Crest height 'hc'

Whereas formula (2-13) of Van der Meer shows a clear distinction for different wave loads and angles of wave attack, no distinction was found in the values of the current test data. In fact all values found were equal to the initial freeboard of the breakwater model. Consequently all values for h_c were underestimated. The freeboard of the current breakwater model however was relatively high, while the relation was derived for berm breakwaters with the berm around still water level. It is assumed that the part of the outer slope above the initial deformation collapsed due to instability, partly because of the relatively steep slope. This process then continued, so that eventually the same value for h_c was acquired as the initial freeboard. Although the theory described here is comparable to dune erosion, it is rather new for the concept of breakwaters. Further research is required before it can be supported.

Step height 'hs'

For the step height, h_s, a more or less similar observation was done as for l_s during tests with wide grading: no effect was found regarding the angle of wave attack. However, now this observation was also done for tests with narrow grading. Apparently the effect of wave obliquity is not adequately described by the reduction factor, $\cos\psi$. Consequently for h_s it can even be suggested to omit the reduction factor entirely. As was already mentioned in this section regarding the crest height, the currently described outcome was unexpected. Therefore further research into this observed relation is recommended.

Regarding the effect of stone grading, the following can be concluded: h_s increases for wider grading. This effect however seems influenced by the angle of wave attack. The larger the angle of wave attack, the larger this increase from narrow to wide grading appears to be.

Slope below crest 'Θ_3'

In general formula (2-27) has the tendency to underestimate the values for Θ_3 observed from the tests. As the test results were directly related to the values of h_c, which showed a clear underestimation, this was expected. Regarding the different parameters tested, both a higher wave load and a wider grading lead to a lower value of Θ_3. The degree of decrease however differs slightly from the relation given. While the decrease of Θ_3 due to a wider grading tends to lag behind, the decrease of Θ_3 due to a higher wave load is actually more pronounced. No one-sided relation was found for the effect of wave obliquity.

Crest recession 'Rec'

Both a more severe wave load and wider grading result in a larger recession length, Rec. For the values of H_0T_0 and f_g used, the influence of the wider grading was even larger than was the case by increasing the wave load. Regarding wave obliquity, a larger angle of wave attack leads to a smaller value of Rec.

In the comparison with formulations derived by Tørum, Hall & Kao and Merli, the best description is given by formula (2-32) of Merli. Although all values were overestimated, again a result of the different relation observed for h_c, the linear trend described gives the best method of approach. Also here the narrow grading of 1.3 leads to a larger overestimation thereby reinforcing the conclusion given for l_c; that this grading falls outside the range of this formula. Adjustment of this formula is needed, especially for very narrow grading.

Another point of attention is the reduction factor, $\cos\psi$. Apart from the tests with wide grading and a wave obliquity of 45°, a general trend was visible for larger angles in which the overestimation became higher. This leads to the conclusion that the reduction factor for Rec should show an even faster reduction for increasing angle.

6.1.3 Longshore transport

For every test the stone displacement was measured, which was then used to determine the relation with the distance from origin. These relations were further analyzed to determine the influences of the parameters varied and the total longshore transport rates were computed through multiple integrations over the areas of uniform transport. Finally these transports were compared to the currently available formulas in order to determine their usability.

Stone displacement

For each test a clear exponential relation was found linking distance from origin and stone displacement (minimal value for R of 0.95). Furthermore an obvious influence of wave load and grading was found concerning the stone displacement of the entire stone samples. An increasing wave load leads to an increase in stone displacement and an extension of its area of influence. Directly around the colour beams and further away from the origin this influence diminishes until it is more or less levelled out. The same holds true for the effect of grading, although for this also the area directly around the colour beams was affected. Regarding the effect of wave obliquity however the relation is less evident. For this more or less the same conclusion can be drawn as for l_s and h_s, as no clear differences were found while currently available formulas indicate otherwise.

Total longshore transport

Regarding the longshore transport an increasing trend was observed for increasing wave load, H_0T_0, as well as wider grading. For the grading this increasing trend seems dependent on the wave load and obliquity. Both a higher wave load and the decrease in wave angle from 45° to 30° amplified the increase in longshore transport due to a wider grading. More of less the same is true for the increasing trend due to an increase in H_0T_0: the decrease in wave angle from 45° to 30° as well as a wider grading intensify the increase in longshore transport.

For the influence of wave attack a totally different relation was found. While the actual longshore current generated is expected to be maximal for a wave obliquity of 45°, the longshore stone transport is not. Between 30° and 45° a decreasing trend was observed, though this trend was far better visible for the wide grading of 6 than it was the case for the narrow grading. Apparently the impact on the structure due to oblique wave attack becomes less for wider angles leading to a decrease in transport for 30° to 45°. For the narrow grading of 1.3 the differences were rather small, an observation similar to ones done at the computations of l_s, h_s and the stone displacement.

Currently available formulas

In total three formulas were used in the comparison with the test data. Although constantly an overestimation was found in the order of magnitude 8, data concerning the tests with narrow grading produced a relatively nice fit with other test results when formula (2-50) of [TOMASICCHIO 2007] was used. This formula describes the decreasing trend between 45° and 30° well, but is rather laborious in the computation as multiple parameters have to be defined.

Formula (2-44) was derived by [VAN DER MEER 1992] for already deformed profiles under the same assumption as mentioned above. Nevertheless no influence of wave obliquity was included in the relation. In the comparison with all previous test results a relatively nice fit was produced, but the effect of neglecting wave obliquity was still visible, especially for a wave obliquity of 50°. Also data of tests during reshaping were consequently underestimated as well as the data of tests with a value of H_0T_0 close to the threshold value.

Unlike formula (2-44) the angle of wave attack is included in relation (2-48) which was formulated by [ALIKHANI 1996]. This formula however gives a different relation for the angle of wave attack which is in contrast to the relation found from the test results: increasing longshore transport for increasing obliquity with a maximum for 45°. In the comparison with previous test results a very large underestimation was found for most values. This leads to the conclusion that in the derivation of formula (2-48) probably some mistakes were made. By multiplying the coefficient with a factor 100, however, a rather nice fit was found, especially for the current test results with narrow grading. This new coefficient, $8 \cdot 10^{-5}$, is then also in the same order of magnitude as previous coefficients derived by [VRIJLING 1991] and [VAN DER MEER 1992] and leads to the following renewed version of formula (2-48):

$$S_N = 8 \cdot 10^{-5} \sqrt{\cos\psi} \left(H_0 T_{0p} \sqrt{\sin 2\psi} - 75 \right)^2 \qquad (5\text{-}2)$$

Finally through curve fitting also a new relation was found linking the modified stability number N_s^{**} to the longshore transport. This relation can be described with the following a power function:

$$S_N = 10.64 \cdot 10^{-5} \left(N_s^{**} \right)^{5.77} \qquad (5\text{-}1)$$

Volume transport

Whereas the transport rate in stones/wave was used to describe the longshore transport for the narrow grading with acceptable results, a rather distorted image was produced by the computation of the same rate for wide to very wide grading. This distortion becomes better visible when the transport rate is converted into a volume transport rate. Namely the increase in the volume transport from narrow to wide grading is not proportional to the longshore stone transport rate as not all fractions are transported evenly. While mostly the finer fractions determined the total longshore transport rate in stones/wave their contribution to the volume transport was far less. Accordingly a relatively large contribution was given by the coarser fractions.

Except for the middle fractions however no link was found between the contribution to the volume transport and distribution of the fractions inside the grading. The relatively large contributions by the finest and coarsest fractions were therefore attributed to either the higher mobility of the finest stones, even after reshaping, or the greater instability of the largest stones preceding deformation.

While the increase of the stone transport rate for the two gradings used varied between a factor 5 and 9, a factor 2 was found for the corresponding increase of the total volume transport rate. Accordingly when the damage due to longshore transport needs to be determined, the longshore volume transport is preferred above the stone transport.

6.2 Recommendations

Results of this study give a first insight in the behaviour of breakwater cores with very wide gradings regarding the reshaping process and longshore transport. These findings however are based on a relatively small amount of tests in which only a few parameters were varied. Bearing this in mind the following recommendations are formulated.

Adjust existing and new formulas using the current analysis of test data

Through analyses of the test results described in Chapter 5 some relations were found which were in conflict with the currently available formulas. Other outcomes resulted even in totally new relations. Accordingly the results of these analyses should be used to reformulate existing and new formulas:

- The observations regarding the deformation parameters can be used for adjustment of the relations of Merli and Van der Meer.
- The exponential relations of stone displacement derived in this thesis can further be elaborated so that the influence of grading, wave load and angle of wave attack are included separately.
- Formulas of the longshore transport should be adapted for both the previous and current data sets. For example formula (5-2) can be changed so that the influence of grading is included while the effect of wave obliquity is better described according to the relations found in this thesis.
- The power function (5-1) relating N_s^{**} to the longshore transport needs further improvement so that the effect of wave obliquity and grading is described.

Analyse test data not yet further analysed

Loads of test data, collected during the tests but not used in the analyses, still need further analyzing. Foremost a study into the deformation and longshore transport at the roundheads is recommended as elaboration of these roundheads fell outside the scope of this thesis. For this purpose also further investigation into the already created erosion models is advisable, which, according to the alternative method described in section 4.4.4, can also be used to determine the total longshore volume transport at the trunk. Other collected data include the spreading of the stones in longitudinal direction due to head-on waves and the segregation of material along the two-dimensional profile. Aside from the raw data also video recordings and photographs, taken both during and after the test, are available which can be used as a tool in all above-mentioned research.

Rerun currently described tests

Regarding the limited amount of tests executed, it is advised to obtain more test data. By repeating the tests the spread of the data can be better investigated. The same is valid for the sources of errors, described in paragraph 3.8, and their actual effects on the test results. Surprising outcomes, like the minimal distinction for some parameters observed between 30° and 45° and the newly found relation for h_c, can be checked and inaccurate data can be replaced. For example the results of test W-30-8 concerning the longshore transport did not give satisfying results, but also the stone displacement measurements of test W-45-8 and W-45-10 around the colour beams were inaccurate.

Expand test data for more values of grading, angle of wave attack and wave load

Another way to expand the data set is by conducting tests with different values for grading, angle of wave attack and wave conditions. It is therefore recommended to carry out experiments with both gradings in between the currently used gradings and wider gradings, so that relations can be derived which are valid for a wider range. Besides different gradings also additional tests with angles of wave attack in between 30° and 45° are advised as well as smaller angles for exact determination of the relations between wave obliquity and deformation, stone displacement and longshore transport.

Expand test data by investigating other parameters

Although the expansions of the data set, previous discussed, all involve research into the influence of the same parameters, already other parameters can be defined of which the effect on the described processes is also unknown. It is therefore recommended to expand the research also by investigating other parameters such as the height of the freeboard, the shape of the wave spectrum or the number of waves. By interrupting the new tests repeatedly on designated moments in time the time dependency of the deformation and longshore transport itself can be determined. From here a better insight can be acquired about the transition from reshaping to equilibrium state. Moreover the longshore transport can then better be investigated for the two different situations separately.

In this thesis only the two-dimensional deformation and longshore transport were studied. To increase the knowledge on the behaviour of exposed breakwater cores also other processes need to be investigated. Among other things this includes topics such as the relation between grading and porosity and the stability of the rear slope.

7. References

ALIKHANI, A., TOMASICCHIO, G.R. AND JUHL, J. (1996), "Berm breakwater trunk exposed to oblique waves"; *25th ICCE, ASCE*; *Orlando, USA*.

BURCHARTH, H. F., AND FRIGAARD, P. (1987), "On the stability of berm breakwater roundheads and trunk erosion in oblique waves"; *Seminar on unconventional rubble mound breakwaters, ASCE, Ottawa, Canada*.

BURCHARTH, H. F., AND FRIGAARD, P. (1988), "On 3-dimensional stability of reshaping breakwaters"; *21st ICCE, ASCE*; *Malaga, Spain*.

BURCHARTH, H. F., ZHOU, L., AND TROCH, P. (1999), "Scaling of core material in rubble mound breakwater model tests"; *5th COPEDEC*; *Cape Town, South Africa*.

CIRIA, CUR,, CETMEF (2007), "The Rock Manual; The use of rock in hydraulic engineering (2nd edition)", London, *C683, CIRIA*

HALL, K. R., AND KAO, J.S. (1991), "The influence of armour stone gradation on dynamically stable breakwaters"; *Coastal Engineering*, 15.

HOLTHUIJSEN, E. H. (2007), "Waves in oceanic and coastal waters", Cambridge, *Cambridge University Press*, 13 978-0-521-86028-4.

JOHNSON, D. (2007), "DIWASP, a directional wave spectra toolbox for MATLAB®: User Manual. Research Report WP1601-DJ(V1.1)"; *Centre for Water Research, University of Western Australia*,

JUHL, J., VAN DER MEER, J.W., BURCHARTH, H.F., D'ANGREMOND, K., SIGURDARSON, S., HOLMES, P., TØRUM, A. AND LAMBERTI, A. (1997), "Berm breakwater structures; Final report MAST contract MAS2-CT94-0087";

LAMBERTI, A., AND TOMASICCHIO, G.R. (1997), "Stone mobility and longshore transport at reshaping breakwaters"; *Coastal Engineering*, 29: pp.263-289.

LAMBERTI, A., TOMASICCHIO, G.R. AND GUIDUCCI, F. (1994), "Reshaping breakwaters in deep and shallow water conditions"; *24th ICCE, ASCE*; *Kobe, Japan*.

MERLI, D. (2009), "Stability of wide-graded rubble mounds"; *UNESCO-IHE, Delft*, MSc

PIANC (2003), "State of the art of designing and construction berm breakwaters"; *MarCom*; *Report of WG 40, 2003*, *International Navigation Association, Brussels, Belgium*, 2-87223-138-2.

TOMASICCHIO, G. R., ARCHETTI, R., D'ALESSANDRO, F. AND SLOTH, P. (2007), "Long shore transport at berm breakwaters and gravel beaches"; *5th Coastal Structures International Conference CST07*; *Venice, Italy*.

TOMASICCHIO, G. R., LAMBERTI, A. AND GUIDUCCI, F. (1994), "Stone movement on a reshaped profile"; *24th ICCE, ASCE*; *Kobe, Japan*.

VAN DER MEER, J. W. (1988), "Rock slopes and gravel beaches under wave attack"; *Delft University of Technology, Delft*, PhD

VAN DER MEER, J. W. (1992), "Stability of the seaward slope of berm breakwaters"; *Coastal Engineering*, 16: 205-234.

VAN DER MEER, J. W., AND VELDMAN, J.J. (1992), "Singular points at berm breakwaters: scale effects, rear, roundhead and longshore transport"; *Elsevier, Coastal Engineering*, 17: pp.153-171.

VAN HIJUM, E., AND PILARCZYK, K.W. (1982), "Equilibrium profile and longshore transport of coarse material under regular and irregular wave attack"; *Delft Hydraulics*, 274

VANLISHOUT, V. (2008), "Oblique wave transmission through rough impermeable rubble mound submerged breakwaters"; *Delft University of Technology, Delft*, MSc

VRIJLING, J. K., SMIT, E.S.P. AND DE SWART, P.F. (1991), "Berm breakwater design - the longshore transport case: a probabilistic approach"; *Coastal structures and breakwaters, ICCE*; *London, U.K.* , Thomas Telford.